

# Microfissures et délaminations des composites stratifiés soumis à des chargements quasi-statiques et cycliques

Hiba Ben Kahla

▶ **To cite this version:**

Hiba Ben Kahla. Microfissures et délaminations des composites stratifiés soumis à des chargements quasi-statiques et cycliques. Science des matériaux [cond-mat.mtrl-sci]. Université de Lorraine; Université de technologie de Luleå (Suède), 2019. Français. NNT : 2019LORR0333 . tel-02929449

**HAL Id: tel-02929449**

**https://hal.univ-lorraine.fr/tel-02929449**

Submitted on 3 Sep 2020

**HAL** is a multi-disciplinary open access archive for the deposit and dissemination of scientific research documents, whether they are published or not. The documents may come from teaching and research institutions in France or abroad, or from public or private research centers.

L'archive ouverte pluridisciplinaire **HAL**, est destinée au dépôt et à la diffusion de documents scientifiques de niveau recherche, publiés ou non, émanant des établissements d'enseignement et de recherche français ou étrangers, des laboratoires publics ou privés.

AVERTISSEMENT

Ce document est le fruit d'un long travail approuvé par le jury de soutenance et mis à disposition de l'ensemble de la communauté universitaire élargie.

Il est soumis à la propriété intellectuelle de l'auteur. Ceci implique une obligation de citation et de référencement lors de l'utilisation de ce document.

D'autre part, toute contrefaçon, plagiat, reproduction illicite encourt une poursuite pénale.

Contact : ddoc-theses-contact@univ-lorraine.fr

LIENS

Code de la Propriété Intellectuelle. articles L 122. 4
Code de la Propriété Intellectuelle. articles L 335.2- L 335.10
http://www.cfcopies.com/V2/leg/leg_droi.php
http://www.culture.gouv.fr/culture/infos-pratiques/droits/protection.htm

# THÈSE

**Pour l'obtention du titre de**

**DOCTEUR de L'UNIVERSITÉ DE LORRAINE**

**Spécialité: Science des Matériaux**

**Présentée par:**

**Hiba BEN KAHLA**

---

# Microfissures et délaminations des composites stratifiés soumis à des chargements quasi-statiques et cycliques

---

**Thèse soutenue publiquement le 4 Juin 2019 à Luleå (Suède) devant le jury suivant :**

| | | |
|---|---|---|
| **Prof. Per GRADIN** | **Mid Sweden University, Suède** | **Examinateur** |
| **Prof. Yves BERTHAUD** | **Université Pierre et Marie Curie, France** | **Rapporteur** |
| **Prof. Federica DAGHIA** | **Ecole Normale supérieure Paris-Saclay, France** | **Rapporteur** |
| **Prof. Zoubir AYADI** | **Université de Lorraine, France** | **Directeur de thèse** |
| **Prof. Janis VARNA** | **Luleå University of Technology, Suède** | **Directeur de thèse** |

**Institut Jean Lamour –UMR 7198- Département SI2M – Equipe 304 Université de Lorraine**

**Pôle M4: matière, matériaux, métallurgie, mécanique**

**Résumé :**

L'industrie aéronautique concentre ses efforts sur l'amélioration de la performance de ses avions, tout en réduisant leur poids et limitant l'impact environnemental. Une partie de cet objectif est assurée par l'utilisation des matériaux composites stratifiés à fibres longues. Les fissures matricielles, dans les plis où les fibres ont des orientations éloignées de la direction principale du chargement, sont le premier mode d'endommagement observable dans un stratifié. Tandis que ces fissures se propagent dans des tunnels et augmentent en nombre, deux proches fissures matricielles de deux plis voisins peuvent se croiser formant une enveloppe avec le bord libre. Des délaminations locales peuvent y être générées. L'évolution et l'interaction de ces deux modes d'endommagement ainsi que l'accumulation de l'endommagement sous des sollicitations spécifiques sont des informations cruciales pour bien comprendre les mécanismes et prévoir avec exactitude la dégradation des propriétés mécaniques du matériau endommagé. Ce mémoire aborde l'initiation et l'évolution des fissures matricielles et des délaminations inter-couches des matériaux stratifiés.

Dans la première partie (Paper A et Paper B), des essais mécaniques en statique et en fatigue sont menés sur des stratifiés NCF (Non Crimp Fabric) quasi-isotropes $[45/90/-45/0]_s$ Epoxy/ fibres de carbone.

L'objectif du **Paper A** est de développer une méthodologie efficiente pour déterminer l'évolution de l'endommagement sous chargement cyclique tout en économisant le temps et le coût des tests et de la caractérisation.

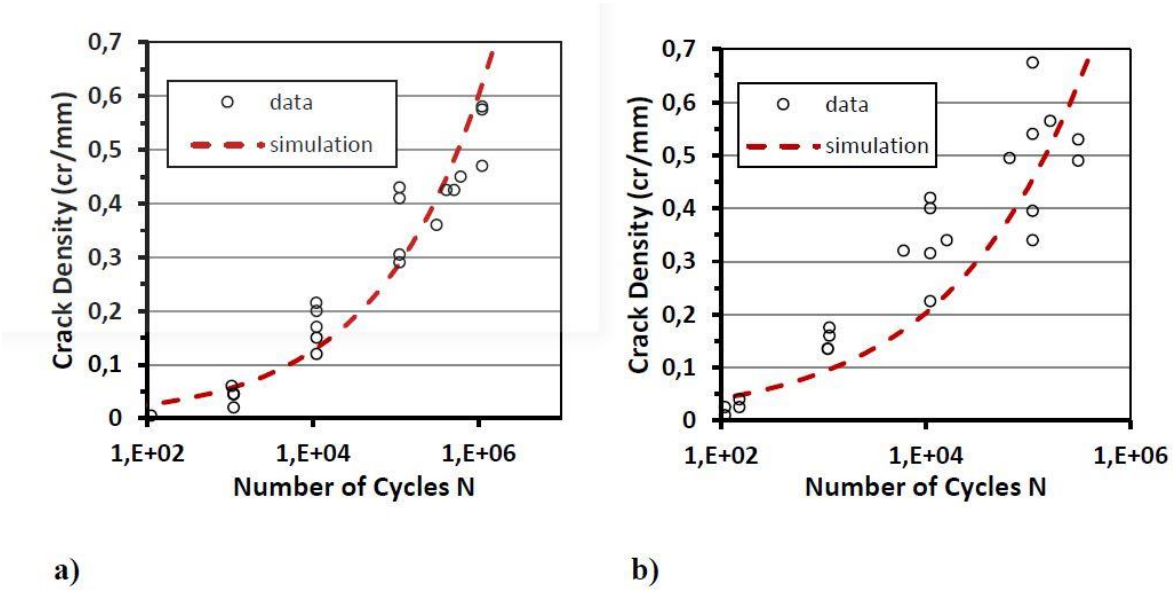



***Figure 1: Densité des fissures dans les plis à 90° du stratifié $[-45/90/+45/0]_s$ en fonction du nombre de cycles a) 0.5%; b) 0.6% de déformation appliquée en chargement cyclique***

Un model simple basé sur la distribution de Weibull permet de prévoir la densité des fissures matricielles. Une partie des paramètres du model est déterminée par de simples tests quasi statiques et l'autre partie est déterminée grâce à un nombre limité des essais cycliques. La comparaison entre la simulation de la densité des fissures et les résultats expérimentaux montre une cohérence (Figure 1) et le modèle est validé pour les niveaux de chargement bas en fatigue. En augmentant la déformation appliquée en fatigue, une interaction aura lieu entre les différents mécanismes d´endommagement: les fissures matricielles dans les différents plis, et les delaminations locales qui se sont créées à cause d'un état de contraintes élevées dans les régions où des fissures matricielles croisent le bord de l´échantillon. Les mécanismes de croissance de ces modes d'endommagement, ainsi que leurs interactions à des chargements élevés appliqués en fatigue sont différents du cas où le chargement est statique. Mieux comprendre les phénomènes d´endommagement en fatigue dans le cas de ces stratifiés NCF est l ´objet du **Paper B**. L'objectif est d´étudier le développement des fissurations intralaminaires dans les couches du stratifié, leur interaction avec le bord du spécimen et son effet sur les délaminations induites et d´estimer la contribution de différents modes d'endommagement sur la dégradation de la rigidité axiale. Après chaque étape cyclique, le module axial a été déterminé, et des répliques de bord ont été prises pour caractériser l'état d'endommagement ultérieurement à l´aide d´une analyse de microscopie optique.

L'effet des paramètres du chargement appliqué sur la longueur moyenne de délaminations est caractérisé et lié ensuite à la perte de rigidité résultante est présente sur la figure 2.

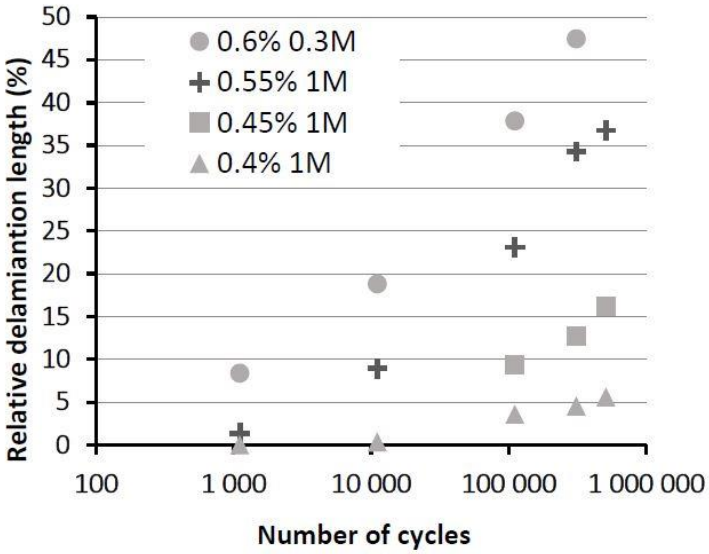



***Figure 2: L'évolution avec le nombre de cylces (%) du rapport de la longueur de délaminage mesurée aux bords sur une distance L pour de différentes déformations maximales appliquées en fatigue***

Les délaminations à l'interface 45 ° / 0 ° étaient petites et détectées uniquement à des charges très élevées ; ils n'ont pas été quantifiées dans ce travail. Les delaminations qui ne sont pas liées à des fissures matricielles sont rarement observées.

Pour les essais cycliques à faible contrainte maximale appliquée, un nombre très élevé de cycles est nécessaire pour observer la délamination locale et celle-ci est confinée au bord. Alors que, soumis à des essais cycliques sous contrainte maximale appliquée élevée, un nombre limité de cycles est suffisant pour induire une délamination qui se propage plus rapidement à l'intérieur du composite (20% de l'interface dans la zone centrale de l'échantillon peut être délaminée). Pour une raison actuellement inconnue, la délamination à l'interface (-45 ° / 90 °) est significativement plus grande que celle observée à l'interface (90 ° / + 45 °). Le motif de point du NCF combiné avec l'état de fissuration intra-laminaire aux bords et l'interaction entre les modes d´endommagements existants peuvent être la raison la différence signalée. Malgré cette différence, la longueur de délaminage entre les deux interfaces a les mêmes caractéristiques de croissance le long de l'interface de la région de bord à l'intérieur du stratifié. Figure 3 montre cette variation par rapport à la distance y qui sépare le plan d´observation et le bord.

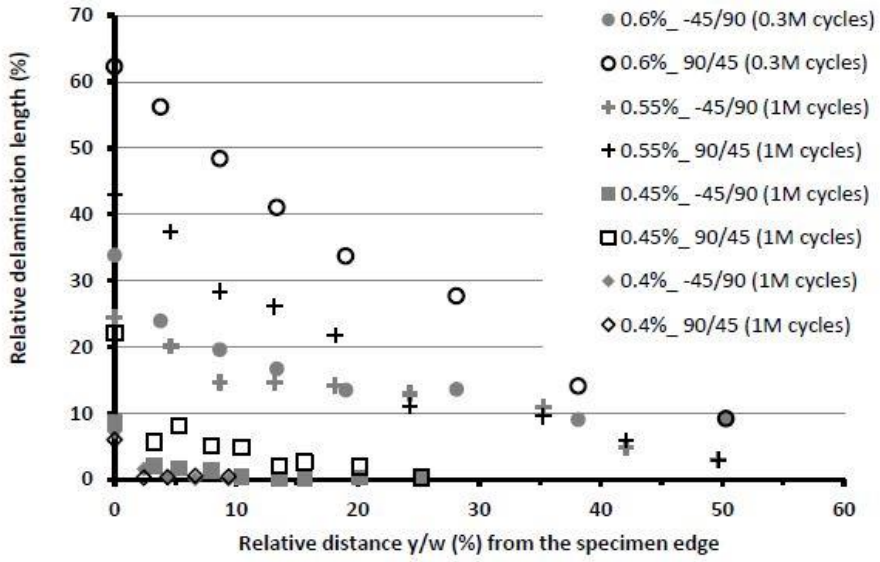



***Figure 3: L´évolution du pourcentage de la longeur délaminée aux interfaces -45°/90° and 90°/45° du bord à l'intérieur du stratifié en fonction de la distance y par rapport au bord ( W : largeur de l´échantillon)***

L'observation expérimentale montre que la délamination initiée aux pointes des fissures et les fissures matricielles dans les plis adjacents à ±45° apparaissent simultanément. Dans le cas d'un chargement cyclique, la région délaminée et le nombre des fissures dans les plis à +45 ainsi que leur longueur croissent avec le nombre des fissures matricielles dans les plis à 90. La délamination initiée aux pointes des fissures matricielles fait augmenter l'ouverture moyenne

des lèvres de ces fissures ce qui conduit à une réduction plus importante de la rigidité du matériau composite stratifié. Par conséquent, la contribution de chaque mode d'endommagement dans la réduction de la constante élastique axiale apparente est difficile à estimer. De toute évidence, les larges délaminations développées lorsque le matériau stratifié est soumis à un chargement cyclique sous forte contrainte contribuent le plus à la dégradation de la rigidité. Figure 4 présente l´évolution de la constante élastique axiale apparente du stratifié avec la longueur de la délamination observée au bord et montre une relation assez linéaire.

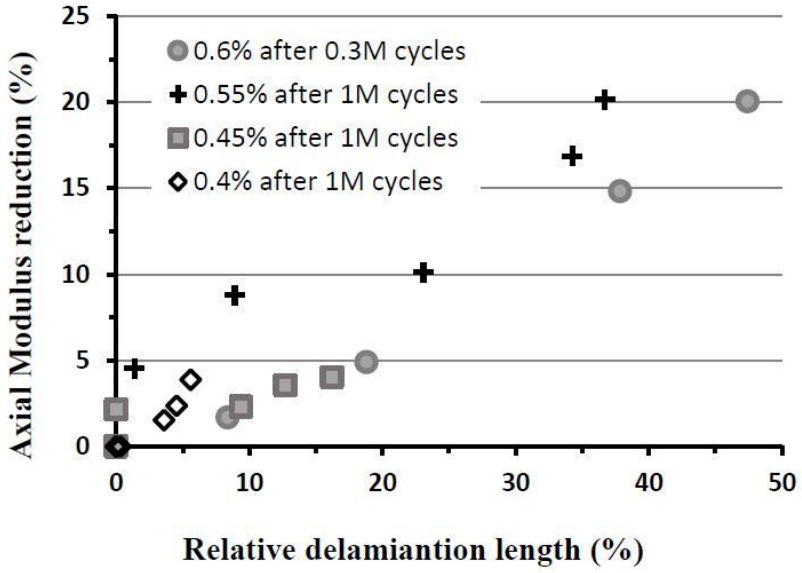



***Figure 4: L´évolution de la réduction de la constante élastique axiale apparente du stratifié avec le pourcentage de la longueur de la délamination observée au bord par rapport à la longueur du bord***

Dans **la deuxième partie**, la présence du délaminage local et son effet sur la rigidité du composite stratifié sont examinés à l'aide d'une analyse numérique par éléments finis et l´approche Glob-Loc. Cette approche permet d'obtenir l'ensemble des constantes thermo-élastiques du composite ayant des fissures matricielles, en liant la réduction des constantes élastiques, la rigidité en particulier à l'ouverture moyenne des lèvres des fissures matricielles (COD), normalisées par rapport à la contrainte appliquée. L´approche est généralisée pour le cas où il y a des délaminations locales dont la présence fait augmenter l´ouverture moyenne des fissures (COD).

Dans **Paper C**, la simulation est réalisée en traction unidirectionnelle pour composites stratifiés à plis croisés CF / EP et GF / EP : $[90/0]_s$, $[90_2/0]_s$, $[90_2/0_2]_s$ , $[0/90]_s$, $[0/90_2]_s$, $[90_2/0_2]_s$ ; avec des longueurs de délaminage différentes pour différentes densités de fissures matricielles, afin d'étudier l'influence de la progression des délaminations sur l'ouverture moyenne des lèvres des fissures matricielles (COD) et la réduction de la rigidité axiale.

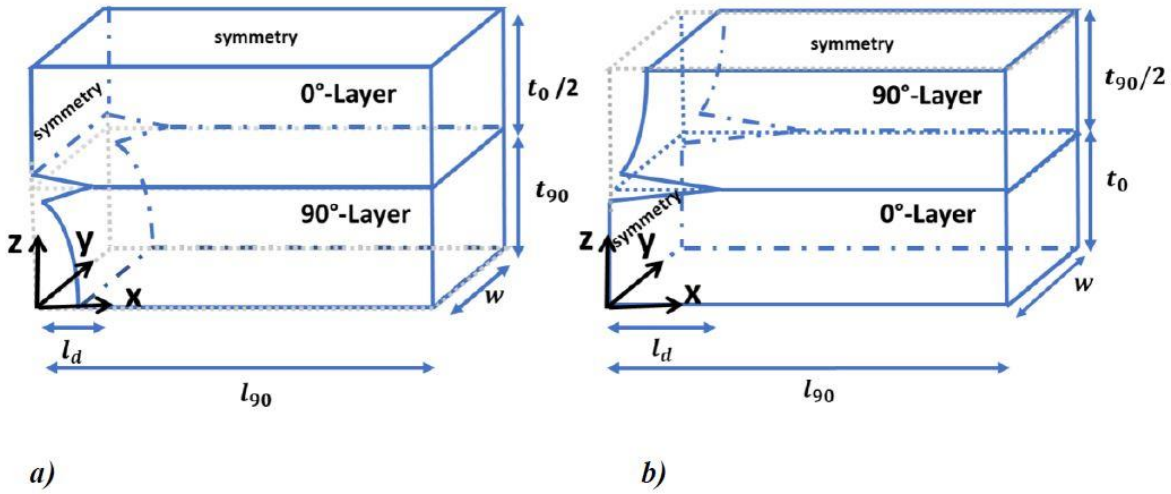



***Figure 5**: **Représentation du volume élémentaire utilisé pour la modélisation par éléments finis a) cas de de fissure à la surface, b) cas de fissure interne***

Premièrement, la rigidité dans le plan du stratifié croisé endommagé a été calculée de deux manières : (1) en utilisant le modèle FEM de l'élément de volume représentatif (RVE) comme le montre Figure 5 et (2) en utilisant l'approche analytique GLOB-LOC basée sur COD. Seul le module efficace transversal de la couche endommagée dépend de la densité des fissures. Cette dépendance est montrée dans la Figure 6. Les valeurs obtenues pour le coefficient de poisson ainsi que pour le coefficient de dilatation thermique à partir des deux méthodes coïncident presque pour toutes les densités de fissures : Figure 7 présente les résultats pour le coefficient de poisson pour un composite GF/EP $[0/90]_s$ à fissures internes dont densité est $\rho_{90n} = 0.1$. Une fonction d'ajustement est proposée.

Les derniers résultats sont utilisés dans **Paper D** pour simuler le comportement du composite dans le cas de flexion 4-points, comme le présente Figure 7.

Des Stratifiés à plis croisés CF / EP et GF / EP : $[90/0]_s$, $[90_2/0]_s$, $[90_2/0_2]_s$ ont été étudiés.

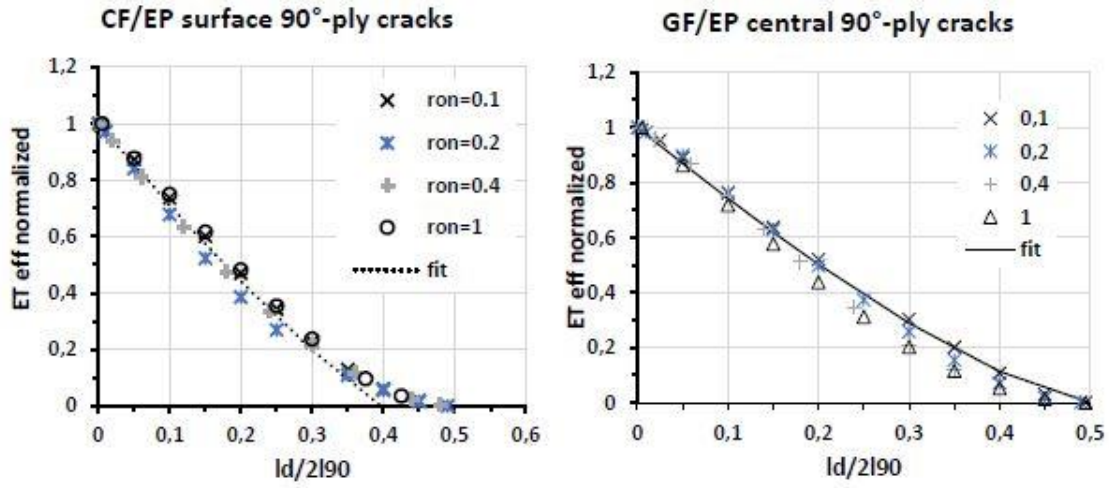



***Figure 6: L'évolution en fonction de la longueur délaminée du module efficace transversal de la couche endommagée normalisé par rapport à sa valeur dans le cas d'absence de délamination pour la même densité de fissures matricielles ; ron est la densité des fissures matricielles***

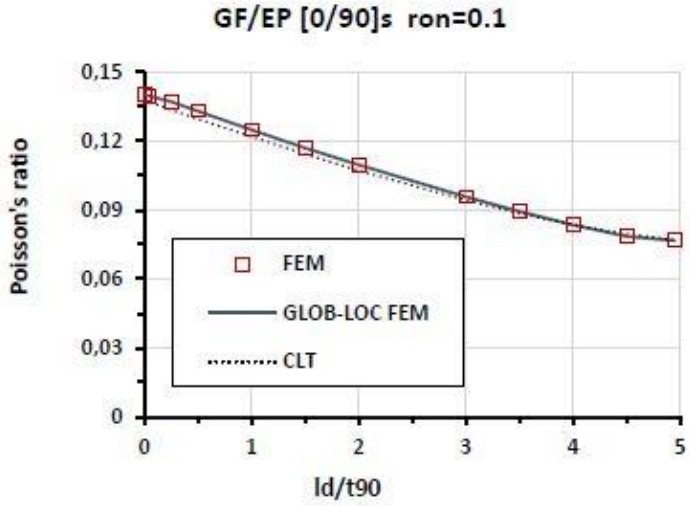



***Figure 7: L´évolution du coefficient de Poisson avec la longeur délaminée ( $l_d/t_{90}$ ). Symbols represent FEM solution; GLOB-LOC has COD from FEM; the dotted line is by using fitting equation and CLT***

Une simple approche basée sur théorie classique des stratifies (CLT) et la rigidité effective du pli endommagé est proposée pour déterminer la rigidité de flexion pour un stratifié endommagé ayant des fissures matricielles ainsi que des delaminations induites de ces fissures. La rigidité de flexion est considérablement réduite par les fissures matricielles accompagnées de délaminations. La matrice de rigidité effective obtenue est alors une fonction de la densité des

fissures matricielles dans les plis et de la longueur de délamination développée entre les plis du stratifié.

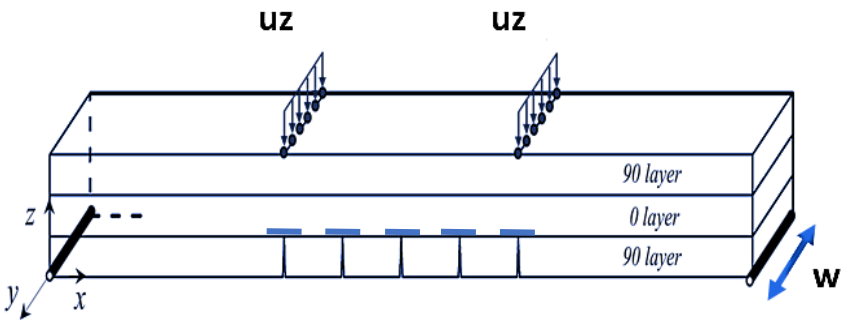



***Figure 8: Représentation d'un modèle FEM de flexion 4-points***

Dans cette approche, le pli ayant des fissures intralaminaires et éventuellement avec des délaminations initiés aux pointes de ces fissures est remplacé par un pli non endommagé ayant une rigidité effective du pli endommagé. La rigidité effective est utilisée pour déterminer la rigidité de flexion pour le stratifié endommagé et sa dépendance de la longueur de délamination pour différentes densités de fissures. Figure 9 présente quelques exemples.

Des simulations FEM ont été effectuées pour un essai de flexion en 4 points ( tel est présenté par Figure 7). De toute évidence, la résistance à la flexion du stratifié avec des fissures est en outre réduite par la présence de délaminations développées en points des fissures. Indéniablement, plus les délaminations sont longues, plus la réduction est importante

L'approche de rigidité effective avec des calculs de rigidité effectives basés sur FEM ou sur GLOB-LOC donne une précision acceptable pour la réponse de flexion du stratifié endommagé: la courbature ainsi calculée est en bon accord avec celle obtenue par une modélisation 3D FEM dans le cas de la flexion 4-points où il y a les deux modes d'endommagement.

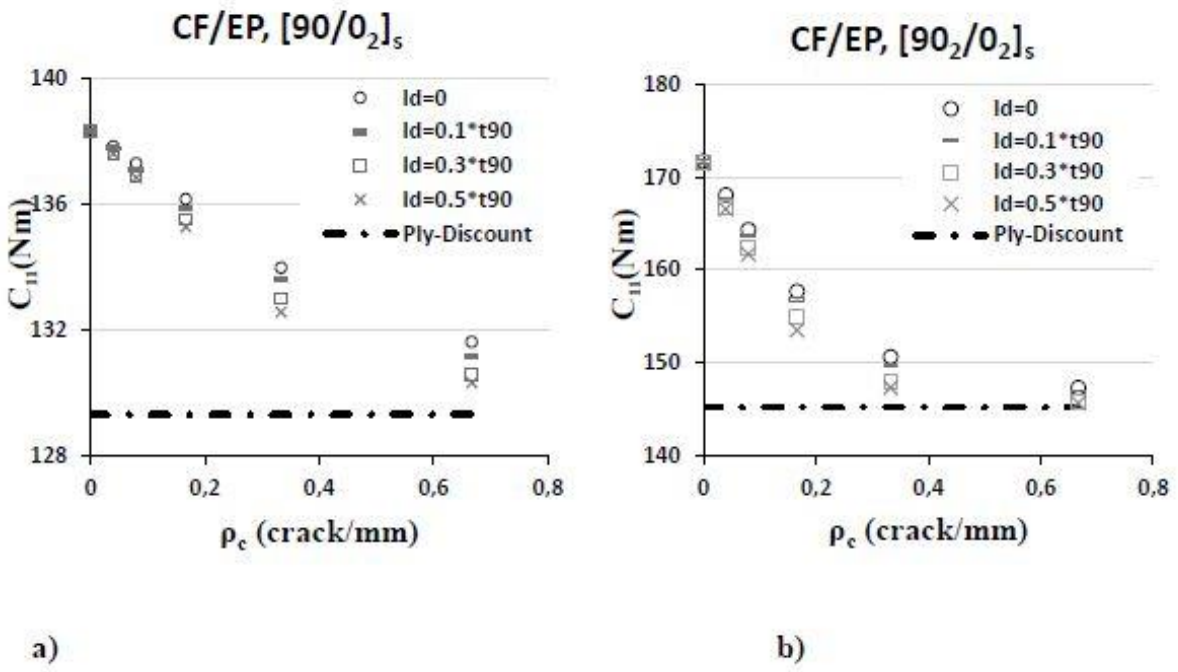



***Figure 9: L'effet de la delamination sur la rigidité en flexion pour des composites à plis croisés CF/EP avec des fissures matricielles au plis 90°***

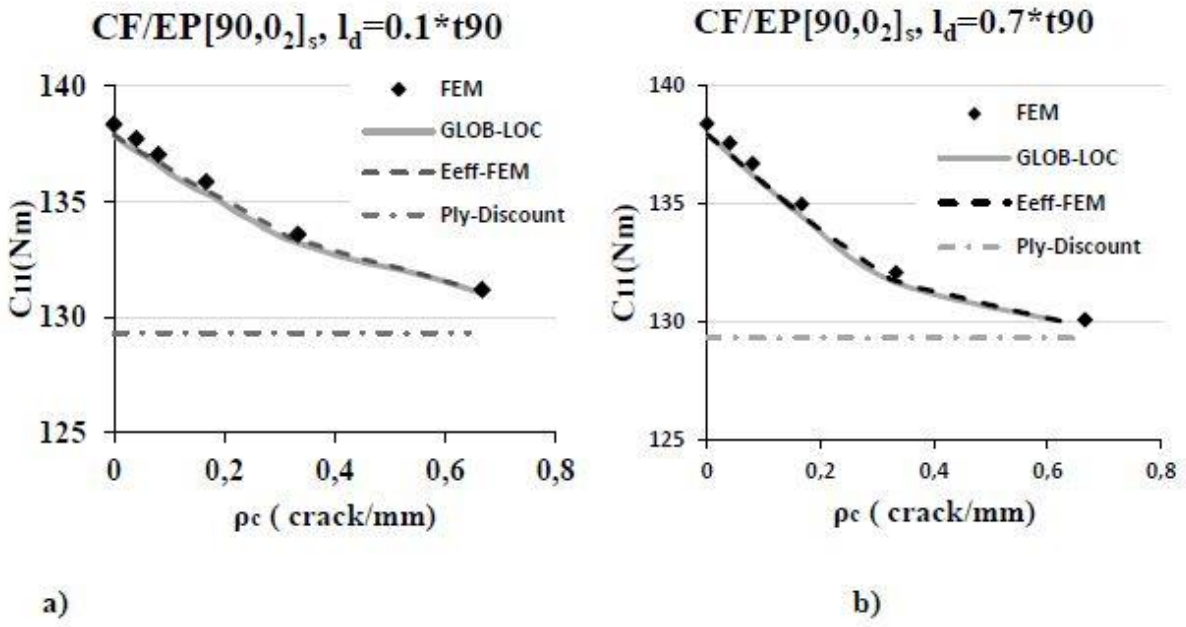



***Figure 10: Comparaison entre les résultats obtenus en utilisant une simulation 3-D FEM et ceux obtenus à partir des modèles basés sur l'approche de rigidité effective pour deux longueurs de délaminations***

# Micro-cracking and delaminations of composite laminates under tensile quasi-static and cyclic loading

DOCTORAL THESIS

**Hiba Ben Kahla**

Division of Materials Science
Department of Engineering Sciences and Mathematics
Luleå University of Technology
SE-971 87 Luleå, Sweden

June 2019

# Dedication

*I would like to dedicate my work to:*

*My parents, I had been missing you every single day of the seven years I spent far from you.*

*My Daddy, who constantly encouraged me and pulled me up when I would be down and under, Daddy this is for you,*

*My mother, who has been a source of motivation and strength during moments of despair and discouragement. Your motherly care, support and prayer have been shown in incredible ways recently. Summer far away from you is as cold as Luleå´s winter, and winter far from our Home is even colder,*

*The loving memory of my grandmother Zbaida, you are no longer around but your presence never left my side. I even hear your voice in my head guiding me. Life is crazy but it's crazier without you,*

*My beloved brothers and sisters: Dhia, Dorra, Emna, Imene, Mariam and Wajdi: your kindness and extensive support, your never-failing empathy, sympathy and encouragement have been always present; I admire your magical touch to cheer me up, to make me smile and how do we share "my dreams" with open eyes. Without you, the road would have been a lonely place,*

*Thank you for being my rock, my inspiration and my biggest support system. I cannot wait to see where the road takes us next, hand in hand, moving forward together,*

*Everyone and anyone who ever believed in me and could see beyond the simple appearances,*

*Those many versions of "me" who I met during the last few years. It was such a unique experience meeting "you", getting to "you" and becoming "one",*

*I love you people, forever and a day, to the moon and back,*

*Your daughter, granddaughter, sister and friend Hiba.*

# Preface

The work presented in this thesis has been carried out in the Division of Materials Science at Luleå University of Technology (LTU) in Sweden and in the Division of Mechanics of Materials (SI2M) in Jean Lamour Institute in France during the period from October 2014 to June 2019.

Many people have significant contribution during the accomplishment of the work presented in this thesis, in one way or another, and all of them deserve my sincere gratitude.

First, I would like to thank my supervisors Professor Janis Varna and Professor Zoubir Ayadi for their unswerving support and precious guidance. There is no way I can ever thank you for generously sharing your knowledge and experience. I would have never did it without you.

I am deeply grateful to all members of the committes for agreeing to read the manuscript and to participate in the defense of this thesis.

I also want to express my sincere appreciation towards all my colleagues, friends and administration staff within the Division of Materials Science in LTU for the nice working environment. Special thanks for Professor Roberts Joffe, Professor Lennart Wallström, Dr Mohamed Loukil, Dr. Andrejs Pupurs, Nawress Al-Ramahi and Lucas Di Stasio for their kind help and fruitful discussions.

I also want to thank my friends and the amazing people I met both in Sweden. I appreciate the time we spent together and the memories we shared.

I want to thank my friends and colleagues in Nancy, especially those I met during Doctoriales 2016: Dorra, Enaam Hiba, Hichem, Israa, Sofia, Rana … Admisitration staff at Université de Lorraine and at EEIGM, Madame Christine Sartori in particular: Thanks all of you to be welcoming me each time I was back Nancy, you gave me the impression I am back home!

It is a pleasure to thank the Joint European Doctoral Program in Material Science and Engineering (DocMASE) for financing the three first years of my PhD studies.

I thank every and each one who took part in making this thesis possible... I owe you a huge debt of gratitude.

Luleå, June 2019



Hiba BEN KAHLA

# Abstract

Aerospace industry is devoted to improving the aircraft performance while reducing its weight and limiting the emissions. Part of this objective can be accomplished with the use of high-performance long fibre reinforced polymer laminated composites. Being the first mode of damage under loading, intralaminar cracks initiate at the free edge of the off-axis plies and propagate along the respective fibre orientation. While these cracks grow as tunnels and increase in number, at some point two close cracks in plies of different off-axis orientation could intersect forming an envelope with the free edge. As loading continues, local delamination is expected within this envelope. The evolution and interactions of the different damage modes and the accumulation of damage under a specific loading (Tensile quasi-static, Compression, Bending, Fatigue…) are crucial to study in order to have a good understanding of the mechanisms and hence an accurate prediction of the mechanical properties' degradation.

The current thesis consists of four papers devoted to the initiation and evolution of intralaminar cracking in plies and interlayer delamination in composite laminates.

In the first paper, the intralaminar cracking in plies of carbon fibre /epoxy non-crimp fabric (NCF) composite quasi-isotropic laminates is studied experimentally in a quasi-static and tension-tension cyclic loading. The results are intralaminar crack density in different plies as a function of the applied strain in quasi-static tests and as a function of the number of cycles in fatigue loading. Methodology is developed to minimize the experimental effort for the characterization of this type of damage in cyclic loading: part of the statistical parameters is obtained in quasi-static test and, therefore, only a limited number of time-consuming cyclic tests is necessary. This methodology is based on the generalization of the Weibull statistical strength theory assuming that the shape parameter in this distribution depends on non-uniformity of fibre distribution in the composite and, therefore, it is the same in fatigue as in the quasi-static loading. The scale parameter in the distribution is assumed to degrade with the number of cycles. It is shown, that the scale parameter degradation follows a power law with respect to the number of cycles. Hence, cyclic tests at only two stress values are required to full identification of the model. Interesting phenomena were found for cracks in off-axis plies adjacent to the cracked 90-plies: systems of short cracks are generated in these layers in local stress concentration zones close to existing cracks in 90-plies.

In the second paper, the effect of intralaminar cracking in plies on inter-ply delaminations was studied. In a position where intralaminar cracks meet the specimen edge, local delaminations initiate due to the high 3D stress state. The delamination is further assisted by cracks in other

off-axis plies which usually link them. These trends in cyclic loading are confirmed, characterized and explained. The average delamination length dependence on loading parameters is characterized and linked with the extent of the laminate stiffness reduction, using a simple ply-discount analysis delaminations are shown to be the main reason for very large axial modulus reduction. The growth of delaminations away from edges towards the central region is characterized by specimen grinding and careful edge optical observations.

In the third paper, local delaminations and their effect on laminate stiffness are analysed using FEM. A modelling approach, known as GLOB-LOC, is used for data analyses. In this approach, exact expressions for stiffness matrix of a damaged arbitrary symmetric laminate are used, however, their use requires FEM information about the shape of the deformed crack and its opening displacement (COD). Expressions for the COD for cracks without delaminations have been obtained previously after performing careful FEM analysis. In this paper, a similar analysis is performed for intralaminar crack case with local delaminations starting from the intralaminar crack. The delamination length is used as a parameter and studies are performed for different materials. A strong effect of delaminations on COD and on the axial modulus of the laminate is found. The effect of delaminations on COD is described in terms of reduced stiffness of the damaged ply. Simple and accurate fitting function for effective transverse modulus is presented and validated with FEM calculations.

Finally, the findings of the previous paper are used to simulate the damaged composite laminate behaviour in 4-point bending test in the fourth paper. The bending stiffness of the laminate is significantly reduced by intralaminar cracks with delaminations. An approach, using the concept of the effective stiffness of the damaged ply is adopted, back-calculating it from the differences in the extensional stiffness matrix of the undamaged and damaged (FEM, GLOB-LOC) laminate using Classical laminate theory (CLT). The obtained effective stiffness matrix is a function of intralaminar crack density in the ply and the delamination length. The effective stiffness is used (CLT) to calculate the bending stiffness of the damaged laminate. The laminate curvature calculated in this way is in a very good agreement with the curvature obtained in 3-D FEM simulations of the test with explicitly included cracks and delaminations in the model.

# List of appended papers

## Paper A

"Statistical model for initiation governed intralaminar cracking in composite laminates during tensile quasi-static and cyclic tests". Ben Kahla, H., Ayadi, Z., Edgren, F., Pupurs, A., & Varna, J. (2018). *International Journal of Fatigue*, *116*, 1-12.

## Paper B

"Intralaminar cracking and specimen edge interaction induced local delaminations in quasi-isotropic CF/ EP NCF composites in Fatigue". Ben Kahla, H., Ayadi, Z., & Varna, J. *submitted to Mechanics of Composite Materials*

## Paper C

"Effect of intralaminar cracking induced local delaminations on laminate stiffness". Ben Kahla, H., Ayadi, Z., & Varna, J. *To be Submitted*

## Paper D

"Effective stiffness concept in bending modeling of laminates with damage in surface 90-layers". Pupurs, A., Varna, J., Loukil, M., Kahla, H. B., & Mattsson, D. (2016). *Composites Part A: Applied Science and Manufacturing, 82, 244-252.*

# Contents

Dedication ..... i
Preface ..... iii
Abstract ..... v
List of appended papers ..... vii
Contents ..... ix
1. Introduction ..... 1
1.1 Fibre reinforced composites ..... 1
1.1.1 Background ..... 1
1.1.2 NCF composites ..... 2
1.2 Damage modes and stiffness reduction ..... 5
1.2.1 Damage features under tensile loading ..... 5
1.2.2 Distribution parameters for initiation strength ..... 6
1.2.3 Reduction of Stiffness due to microcracking ..... 8
2. Objectives and methodologies ..... 16
2.1 Objectives ..... 16
2.2 Experimental Procedure for the performed mechanical testing: ..... 16
2.2.1 Quasi-static tensile loading ..... 17
2.2.2 Cyclic tensile loading ..... 17
2.2.3 Quantification methods of intra- and inter-laminar cracking ..... 17
2.3 Modelling using FEM ..... 19
3. Summary of appended papers ..... 21
3.1 Paper A ..... 21
3.2 Paper B ..... 24
3.3 Paper C ..... 27
3.4 Paper D ..... 30
References ..... 33
Paper A ..... 41
Paper B ..... 73
Paper C ..... 97
Paper D ..... 127

# 1. Introduction

## 1.1 Fibre reinforced composites

### 1.1.1 Background

Composite materials are widely used in high performance applications such as aerospace and marine industry due to their strength and stiffness to weight ratios. Composite materials could be classified, based on the geometry of the reinforcement, into two main categories: particle and fibre reinforced composites, where the particle is approximately equiaxed and the fibre has larger length compared with its cross-sectional dimensions.

Composites for highly demanding structural applications usually have continuous fibres that may be made of carbon, glass, or Kevlar depending on the application structural requirements. Continuous fibre reinforcement is embedded in the matrix in form of uniformly dispersed fibres or in form of bundles. In the case of the first form, laminated composites are manufactured from unidirectional fibre-oriented layers of pre-impregnated tapes (prepregs), with a partially cured resin, stacked in a specified sequence. The high fibre volume fraction that could be obtained and the good fibre alignment lead to excellent in-plane stiffness and strength strongly required for performant structures. However, the prepreg composite laminate is highly sensitive to out-of-plane loading due to poor interlaminar fracture toughness. Another disadvantage of prepreg composites is that they require high manufacturing and storing costs (for example because of the need for freezers providing low temperatures to prevent curing of the polymer matrix during storage). As an alternative to conventional prepreg laminates, the use of a textile technology processes, e.g. weaving, stitching knitting, braiding, etc… with resin infiltration just before curing helps to avoid these disadvantages.

Woven reinforcement is produced by interlacing fibre bundles of two different orientations (or more) in a regular pattern or a weave style. The multi-axial fabric's integrity is insured by the mechanical interlocking of the fibres. In fact, the high waviness of the layers introduced in the fibre bundles in the out-of-plane direction improves the interlaminar fracture toughness and reduces the important in-plane properties compared to prepreg laminates. Depending on the application- structure-requirements, prepreg or woven composites are used as **Figure 1** shows. Based on the advantages and disadvantages of prepreg and woven composites a new class of

reinforcement -combining the advantages of the two previously mentioned reinforcement types and overcoming their drawbacks- appeared. This material, called Non-Crimp Fabric (NCF) composite, has attracted the attention of the composite industry and its use is increasing rapidly [1].

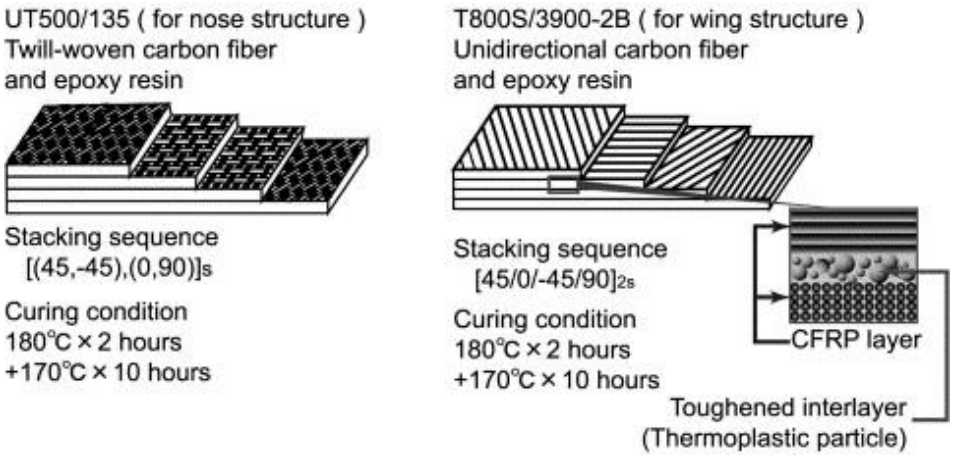



***Figure 1: Two kinds of quasi-isotropic CFRP laminates for aircraft applications [2]***

The individual unidirectional plies of parallel dry fibre tows are arranged in various orientations and held together by stitching yarns forming a multi-axial fabric that depends on the desired composite structure properties. The fabric preform is later infiltrated with a liquid resin; thus, creating a composite material after curing. The interlacing-yarn-structure, characterizing the woven composites, is avoided in these reinforcement-type composites which have ideally no crimp and, therefore, they are called Non-Crimp Fabrics (NCFs).

## 1.1.2 NCF composites

### a) Generalities:

NCF are generally identified with the number of reinforcement yarn directions inserted into the binding structure: biaxial, triaxial and quadriaxial fabrics are the main commercially available fabrics.

The dry perform could be used in manufacturing complicated shapes before being consolidated to final composite by resin transfer moulding (RTM). Depending on the desired properties of a specific application, several layers are stacked in different directions, particular nature of the fibre (Glass, Carbon ...) is used and specific stitching / bindings systems are created.

As a compromise between prepreg and woven composites, NCF composites became an attractive alternative for aerospace, marine and automotive applications [3]. They were first manufactured in 1983 for the marine industry and their use has been increasing since then. Some examples of applications that used NCF reinforced composites are: a floor pan of a car made of carbon fibre NCF; a six-metre diameter pressure bulkhead of an A380 aircraft made of carbon fibre NCF and a sixty-metre-long blade of a wind turbine made of glass fibre NCF [4].

## b) Structure and mechanical properties

Due to the knitting and the fibre bundle structure, NCF composites present three levels of heterogeneity:

- Micro-scale level: At this scale NCF are similar to prepreg laminates: each bundle can be described as a unidirectional (UD) composite, the fibre tows can be regarded as transversely isotropic and the mechanical properties can be determined using micromechanics´ expressions of classical UD long fibre composites [5].
- Meso-scale level: Each layer consists of impregnated fibre bundles with resin region between them. Despite the name non crimp, a certain degree of fibre crimp is present in the dry fibre tows and in the final composite after curing. This waviness is induced by both stitching and composite manufacturing processes with different proportions. In fact, the stitching thread causes compression at extremities of the fibre tows. **Figure 2** shows the internal structure of a quasi-isotropic NCF composite.

  The heterogeneity of NCF at this scale is caused by the different degrees of waviness (in-plane and out-of-plane) of the fibre tows as well as from the rich resin regions separating the fibre bundles. The bundle content and the fibre content in the bundle are the main geometrical characteristics of the mesoscale level for the composite material.
- Macro-scale level: The heterogeneity comes from the different fiber orientations of the layers constituting the NCF composite.

Although the heterogeneity of NCF composites at the macroscale level does not differ from prepreg laminates heterogeneity, the mechanical properties are affected by the geometrical parameters of the micro/ meso-structure. Resin rich regions separating the fibre tows affect the properties and the behaviour of NCF composites. Generally, the tensile strength of NCF is

lower than the one of an equivalent prepreg laminates due to the local damage and fibre misalignment induced by the stitching process [6,7].

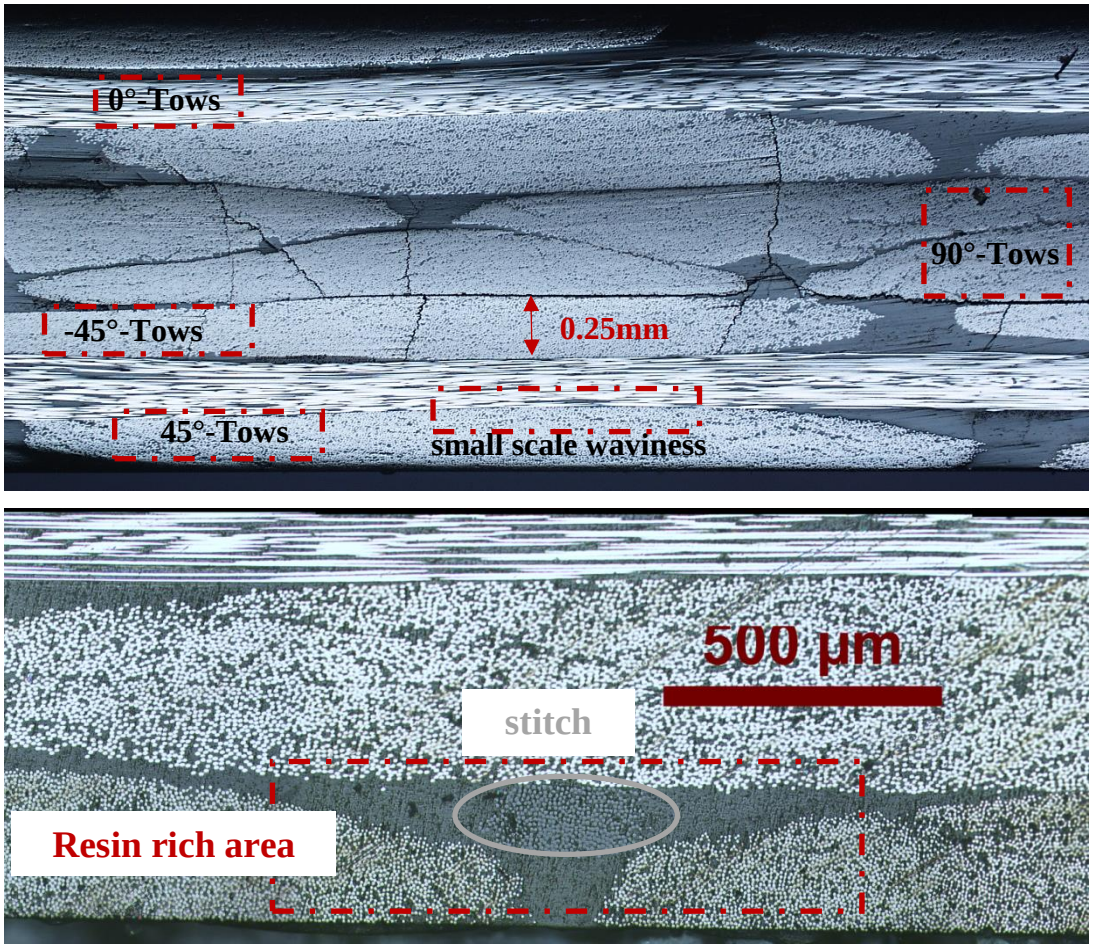



***Figure 2: Internal mesoscopic structure of a quasi-isotropic Non-Crimp-Fabric laminate***

Several researchers studied the effect of stitching on the mechanical properties of NCF composites. The results were contradictory. Considering the in-plane properties, some found that stitching is improving them [8,9] where others found the opposite [7]. Others reported no effect of stitching on in-plane properties [10–12]. The origin of this contradiction, for the same type of fibres, resin and volume fraction, is mainly the stitching conditions such as stitch pattern type of thread, stitch density, stitch tension, etc [11]. However, NCF laminates are generally considered to have lower tensile strength compared to an equivalent prepreg laminate. This reduction can be attributed to the damage and the misalignment generated in the fibres by the knitting process. Compressive strength of NCFs was found lower comparing to prepreg laminates. This difference in both compressive and tensile strength is not always an effect of the NCF structure: in several research works, the difference is attributed to different fibre volume fraction leading to non-valid comparison [7,13].

# 1.2 Damage modes and stiffness reduction

Extensive research has been conducted to study damage initiation and propagation of damage in laminates; a high percentage of those studies were focusing on cross-ply laminates consisting of plies in the 0°- and the 90°- direction. In this work, both cross-ply prepreg and quasi-isotropic NCF laminates were a subject of interest.

## 1.2.1 Damage features under tensile loading

When a composite is loaded in tension with increasing load, three main different damage modes can be observed before the final failure of the laminate:

### a) Matrix cracks or transverse cracking:

The first damage mode during tensile loading for prepreg laminates (cross-ply or multidirectional) is the cracking of matrix in layers with off-axis orientations with respect to the load direction [14]. This occurs because the stiffness, the failure strain and the strength of long fibre reinforced composites are lower in the transverse than in the longitudinal direction (the fibres are stiffer than the matrix). The same damage feature is observed in NCF composites; however, two differences compared to prepreg laminates could be mentioned: the first is related to their initiation load and the second to the location where the matrix cracks appear. Fibre waviness and rich resin regions separating bundles cause stress concentration and lead to premature failure. Moreover, the stitching material generally presents lower properties than the properties of the layers and they exhibit lower stress to be damaged. Therefore, two matrix crack types are observed within a layer: matrix cracks in the bundle and stitch related matrix cracks. It was demonstrated that there is a relationship between the stitching and the damage pattern [15]. The bundle structure and the undulation of neighbouring plies influence the bundles´ transverse failure initiation stress in the laminate and affect the position where the cracks initiate and the angle at which they grow [16]. Mikhaluk and al. [15] among others found that matrix cracks detected in NCF composites at an early stage are related to the resin rich zones created by stitches. Several research works [3,17] studying the dependence of the damage accumulation on the stitching process found that the in-plane matrix cracks form preferably on the stitching sites.

### b) Delamination

When excessive out-of-plane or interlaminar stresses are generated at the interface between adjacent plies, cracks in the interfacial plane develop leading to the separation of the layers. It may arise where a local discontinuity creates out-of-plane stresses: from manufacturing defects, at the edges where high interlaminar stresses exist at the boundaries [18] or at the matrix crack tips. The onset and growth of delamination affect considerably the capacity of the laminate to support further loads and indirectly lead to the final failure of the structure.

### c) Fibre Breaking

The breaking of fibres generally comes at the latest stage for multidirectional long fibre reinforced composites. In unidirectional composite subjected to tensile loading, fibres fail at their weakest position, which can affect other neighbouring fibres and break more of them.

The difference between the NCF composites and prepreg composites in the mesoscale structure leads to diverse mechanical behaviour under loading. Subjected to tensile loading, NCF composites show different failure mechanisms than prepreg laminates; however, the main damage modes are similar. A micrograph of some damage modes examples observed in quasi-isotropic NCF composite is presented in **Figure 3.**

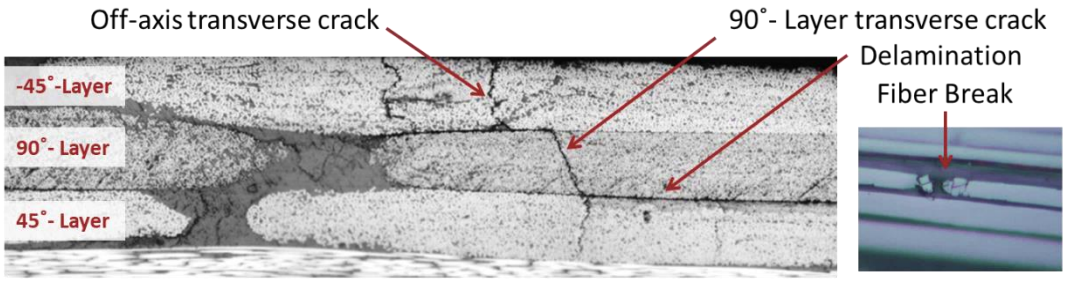



***Figure 3: Damage in quasi-isotropic NCF laminate***

## 1.2.2 Distribution parameters for initiation strength

The crack density in a damaged K-th layer is denoted $\rho_k$ (cracks/mm). It is defined as the inverse to the average distance between two consecutive cracks $\rho_k = \frac{1}{2l_k}$. If the distance

between cracks is less than $5t_k$,where $t_k$ is the thickness of the layer, the induced stress perturbations can overlap and cracks are considered interactive.

First, multiple irregularly-spaced intralaminar cracks in the 90°-layers initiate from the locations of defects such as resin rich areas, voids or stitches (in case of NCFs). When the loading increases, the stress transfer occurs from high damage regions to low damage regions and with increasing the distance from the cracks the transverse and the in-plane shear stresses in the damaged layer recover approaching the Classical Laminate Theory (CLT) far-field value. As the applied load or the number of cycles increases, more cracks appear due to the stress recovery mechanism. When the crack density increases, the tensile stress between cracks is reduced and a higher load is required to create new cracks. As the load increases a saturation region can be reached characterized by a strong crack interaction where the spacing between cracks is approximately equal to the thickness of the damaged layer.

The development of each crack has two stages: initiation and propagation. The initiation is usually independent of meso-scale geometrical parameters, hence the use of approaches with in-situ strength. A large meso-scale damage is created from the fibre/resin scale failure process when energy conditions are satisfied. A certain level of stress is required so the cracks are growing in tunnels along the fibres. Linear Elastic Fracture Mechanics (LFEM) using the concept of released potential energy is used for crack growth analysis.

At the present, the initiation stress required to create a possibly growing defect can not be determined using micromechanics analysis. It is a distribution depending on the statistical nature of failure properties in the layer due to the non-uniform distribution of fibres. There are weak positions, where the fibre/matrix interface and resin failure properties are lower, which are promising for first crack initiation. Larger load is required to initiate cracks in stronger positions. An approach, defining the initiation stress as a necessary material-system dependent stress level to initiate a large-enough- defect to grow unstably in the thickness direction, is used.

The transverse cracking initiation stress, $\sigma_{in}$, is assumed to have a statistical distribution along the layer transverse direction. The damaged layer is assumed to be divided in its transverse direction into many small elements sharing the same elastic properties. A specific intralaminar cracking-initiation stress corresponds to each element. Weibull strength distribution is considered in several research works to describe the variation in $\sigma_{in}$ between elements whose

geometrical positions are random. The Weibull initiation stress distribution is written as following:

$$P_{in} = 1 - \exp\left[-\frac{V}{V_0}\left(\frac{\sigma_T}{\sigma_{in0}}\right)^m\right], \text{ where:} \quad (1)$$

$P_{in}$ is the probability of crack initiation when the element´s transverse tensile stress is $\sigma_T$; $m$ and $\sigma_{in0}$ are the shape and the scale parameters obtained in tests with reference specimens of the element volume $V_0$, $V$is the volume of the considered element.

The element length is linked to the maximum possible crack density. Based on experimental observations and stress analysis, the maximum crack density in the damaged layer is inversely proportional to the layer thickness. Each element is assumed to have no more than one crack that once it exists in one element does not influence the stress state in the neighbouring elements. The element length is taken equal to the ply thickness $t_k$. To avoid crack interaction, the studied crack densities should be at least 2 to 3 times lower than $\rho_{kmax}$.

The number of elements in a layer over a length L is :

$$M = L/t_k = L.\rho_{kmax} \quad (2)$$

The probability of crack initiation at a specific stress $P_{in}(\sigma_{T0})$ is defined as the ratio of the number of elements with initiated cracks to the number of elements M in the layer.

$$P_{in} = M_{cr}/M = \rho_k(\sigma_{T0})/\rho_{kmax} \quad (2)$$

CLT is used to calculate the transverse stress from the applied load and from the difference of temperature between the manufacturing and testing conditions.

$$\sigma_{T0} = \sigma_{T0}^{mech} + \sigma_{T0}^{thermal} \quad (3)$$

When the experimental probability of failure data follows the Weibull distribution, a linear dependence of $ln(-\ln(1 - P_{in}))$ on $\ln(\sigma_{T0})$ is expected and the Weibull parameters $m$ and $\sigma_{in0}$ are determined from the linear fitting function.

## 1.2.3 Reduction of Stiffness due to microcracking

An obvious effect of ply cracking is reducing the thermo-elastic properties of the laminate. The evolution of the stiffness as well as other material mechanical properties with the damage

development is of extensive interest since the 1970s [19]. Earlier, the ply discount model, assuming that a cracked ply is unable to carry any load, was used by changing the stiffness matrix of the damaged layer to zero. Experimental work confirmed that the ply is still able to sustain a part of the load and the model over-estimates the mechanical properties reduction. Ply discount model does not take into account the crack density evolution and it is more valid at high crack density. Two main subfields were developed over the years to address the problem of the reduction of the thermo-elastic properties: Micro-damage mechanics and macro-damage mechanics. The first studies the damage directly at the scale of cracks formation, while the macro-damage mechanics´ approach- also referred to in the literature as Continuum Damage Mechanics (CDM)- is based on the overall response at the macroscale. CDM can be used to predict the reduction on the stiffness of laminates with intralaminar cracks in off-axis plies of any fibre orientation. Talreja developed in 1985 a CDM approach. Its drawback was that it is based on parameters that have to be experimentally found or determined using FE analysis for each material and each laminate configuration [20].

## a) Micro-damage mechanics

In this subfield, a wide range of approaches have been developed: Shear lag model, variational approach, crack opening displacement (COD) based models and computational methods. The focus is on the local stress state determination between two cracks. The simplest approximate solutions are those based on Shear lag model or on variational principles. The shear lag model, applied initially for damaged 90°-layer in cross ply laminates in 1977 [21], was based on one-dimensional stress analysis. Although minor modification to correct the contraction due to Poisson´s effect was applied to these models in order to develop "two-dimensional" shear lag models in [22-25], the modified models still suffer from the one-dimensionality deficiency of the approach [25].

An improved 2-D stress analysis (**variational method**) can be achieved based on the principle of minimum complementary energy. This variational method developed first by Hashin in 1985 [26,27] was based on the assumption that normal ply stresses in load direction are constant over the ply thickness. Although the model is more complex comparing to shear lag model, the resulting expressions can be simply used. More sophisticated variational models were established in [28,29].

Comparisons between the shear lag and the variational analyses performed in [30] confirmed that variational analyses stiffness reduction predictions are better than those obtained using shear lag models and are closer to FE result predictions. The main deficiency of shear lag models is their one-dimensionality of the stress field.

**McCartney** [31] developed a theory of stress transfer between 0°- and 90°- layers while all relevant stress and strain components are maintained. This approach is similar to that of Hashin. Meanwhile, the difference lies in the fact that the latter uses a stress formulation where the former uses a displacement formulation (generalised plain strain analysis model). The model was applied to doubly cracked cross ply laminates (the laminate presents a double periodicity along both x- and y- axes and it is constituted by repeating unit cells limited by two pairs of consecutive cracks in 0°- and 90°- plies.).

Most of the analytical solutions of the previous models are applicable only to cross-ply laminates while higher accuracy imposes more complex models [32,33].

An alternative way to view the elastic response change caused by the presence of cracks is to consider the crack surface displacements of those cracks: crack opening displacement (COD) and crack sliding displacement (CSD). **COD based Models,** first suggested by Gudmundson [34,35], use COD and CSD for stiffness prediction. The derived expressions for 3-D laminate thermo-elastic constants are exact assuming a homogenisation procedure. However, the unknown average COD and CSD have to be determined from a local problem, which can be solved only numerically. Gudmundson and al. [34] suggested some assumptions to determine these parameters from a known analytical solution for a periodic system of cracks, however, despite the assumptions used in COD determination, the method is still quite complex and difficult to implement numerically. Nuismer and al. [22] pointed out that the results overestimate significantly the laminate compliance change.

Lundmark and Varna, using a homogenization similar to the one of Gudmundson approach in the framework of the classical laminate theory, developed **GLOB-LOC** approach: exact expressions for stiffness matrix, compliance matrix and thermal expansion coefficients of an arbitrary damaged laminate were derived. These relationships contain thermo-elastic constants of the UD laminate, geometrical properties of the lay-up, crack density and they are based on normalised average COD and CSD with respect to the ply CLT stress numerically obtained

from FEM simulations. Varna showed that COD and CSD are proportional to the average value of the stress perturbation [36].

**The computational methods** such as finite element method (**FEM)**, finite difference method (FDM) and boundary element method (BEM) have been used to simulate the damage effect in composite laminates. FEM is the most common numerical approach for modelling and simulations, it is extensively used in the industry and academia to solve various mechanical problems (Stress and strain analysis, mechanical properties determination, failure and fracture prediction...) based on the theories of continuum mechanics. This method is a powerful tool to represent virtually any type of geometry. One of the main concerns of FEM (as well as for all numerical methods) is dealing with the compromise between modelling accuracy and computational cost, especially that every time the geometry, boundary conditions, or material properties change, simulation has to be carried afresh. The first step in FE modelling is to define a geometrical model of the damaged laminate. Generally, a representative unit cell is generated assuming periodic array of similar cracks. For cross-ply laminates, a reduction to two-dimensional plane stress or plane strain model is possible. Additionally, the symmetry of the resulting boundary value problem can decrease the size of the modelled unit cell. For example, damaged $[90/0]_s$ can be reduced using a quarter of a representative unit cell as shown in **Figure 4**.

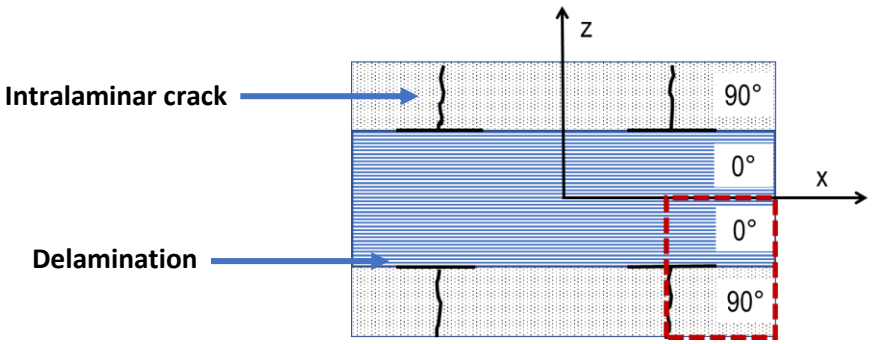



***Figure 4: Representative Volume Element for a damaged $[90/0]_s$***

Once the FE results are computed, the overall stiffness properties of the damaged laminate are determined by the volume averaging of stresses and strains inside the representative unit cell. Examples of numerical studies relating damage state to the stiffness of the damaged laminates can be found in [37–41].

## b) Bending stiffness reduction Modelling

Composite structures are generally subjected to combinations of in-plane loading as well as torsional and bending moments. However, most of the studies have focused on the laminate behaviour under in-plane loads only, mainly under uniaxial loading. Studying damaged laminates subjected to bending has begun only in the end of the 90s. Experimental investigations in this area have been reported in [42,43].

In the previous section, some of the main concepts and methods used to evaluate the effect of cracking on the response of composite materials were summarised. Those approaches can be used to treat the case where the laminate is subjected to bending loading.

A one-dimensional analysis of a cross-ply laminate, containing cracks in the transverse plies and subjected to flexure was presented in [44,45]. Simple bending theory combined with a shear-lag analysis is used to determine the flexural modulus of the laminate through the reduced transverse modulus of a cracked transverse ply.

Kuriakose and al. [46] studied general cross-ply laminates subjected to out-of-plane bending and biaxial in-plane loading. They developed a variational model for predicting stress transfer due to ply cracking using the principle of minimum complementary energy. The model is based on an assumption similar to the one used by Hashin [26] in the case of tensile test.

One more advanced analytical method in bended laminates with transverse cracks was the method developed by McCartney and al. [47] that provides approximate solutions to the stress state. In this approach, a ply refinement technique was used dividing each ply into several sublayers in the thickness direction and the 2-D elasticity equations for each layer with the appropriate interface and boundary conditions were considered (plane strain condition). The effective thermo-elastic constants relevant to bending are predicted from the stress and displacement distributions. The accuracy of the results can be improved by increasing the number of layer subdivisions. The model is limited to one curvature, the study is extended to orthogonal bending in [48]. The disadvantage of this work is that it requires complex numerical calculations to find the stress state for each change on the damage state, the boundary conditions, the elastic parameters of the layers and the geometrical parameters of the laminate.

An analytical constitutive model to predict the transverse crack initiation, the evolution of crack density versus applied strain and the bending stiffness degradation is the subject of [49]. The

stiffness reduction of the bended laminate was computed via (COD) based approach developed in [50] and the generalization to multiple cracking laminates is made via continuum damage mechanics (CDM) concept.
A more comprehensive review of the bending modelling methods can be found in [51].

## 1.2.4 Tension-tension cyclic loading

As a gradual process, Fatigue can be invisible for a long period in the life of a structure before leading to its catastrophic failure. Crashes of the Comet aeroplanes in the 1950s are one famous example of fatigue failure in aeronautics history. On the early 1970s, Boller [52] has published one of the earliest works on the fatigue response of fibre reinforced composites, followed by Owen and his collaborators [53].

### a) Fatigue damage mechanisms

When subjected to fatigue loading, the modes of damage and the sequence of their appearance are quite close to the ones observed under quasi-static loading: the damage develops in quasi-static loading when load increases and in fatigue loading with the progression of fatigue cycles. Several studies confirmed that the observed damage mechanisms are the same under quasi-static and fatigue loadings. These mechanisms were described by Talreja in [54] and summarized in **Figure 5**.

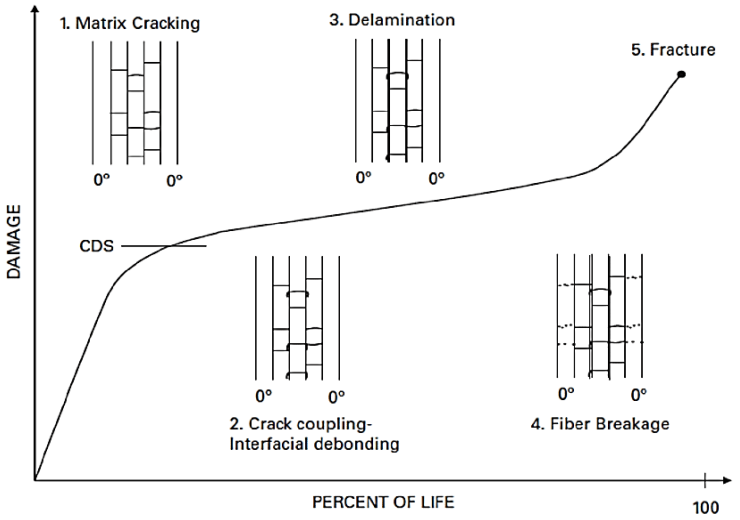



***Figure 5: Damage mechanisms in laminates under cyclic loading [54]***

When the number of cycles increases, fibre-matrix debonding and matrix microcracks lead to the initiation and propagation of intralaminar cracks in the damaged layer until they reach the ply interface, where they can lead themselves to interlaminar cracks. The individual delaminations grow and merge together. Once the matrix is damaged, it can not transfer loads between fibres in the same way as before being damaged. The redistribution of loads makes some fibres more loaded than others which causes progressive fibre failure and rapidly result in the loss of the material integrity and the total failure.

Despite the similarity in the observed damage mechanisms under quasi-static and cyclic loadings, the damage evolution laws are different and the damage threshold during quasi-static is obviously higher than the fatigue damage threshold [55–57].

In recent years, in order to better understand the fatigue response and behaviour of composites at various load levels, frequencies, material properties and geometric parameters [58–61], a comprehensive amount of investigations has been carried out. Glass fibre reinforced polymer (GFRP) laminates are most commonly investigated, since it is possible to visually observe the crack formation within the matrix thanks to the partial transparency of the specimens. Carbon fibre reinforced laminates are equally of considerable interest in research especially because of their wide use in high-performance applications owing to their mechanical properties.

## b) Damage Fatigue Models

Composite fatigue modelling is required in order to limit the number of tests for predicting the composite failure. The challenge is that different composites do not show the same behaviour under the same test conditions due to the different material configurations that they could present a multitude of parameters (fibres, matrices, constituent volume fractions, fibre orientations, stacking sequences, manufacturing methods…). This fact hinders the development of a general approach/ model describing the composites behaviour covering all the variances and explaining the vast number of the developed fatigue models that are often limited to a specific composite and/or a particular stacking sequence. In this section only few models are cited, however good review papers have been published [62–64] on the fatigue behaviour of fibre reinforced composites.

Composite fatigue Models can be divided into three main groups: fatigue life models, phenomenological models and progressive damage models.

Fatigue life modelling is based on failure criterion combined with S-N curve as input. Several fatigue life models are available in the literature [63,65–67] in order to predict the number of cycles to failure. Some of the disadvantages of these models: they do not consider the damage accumulation and they depend on a large amount of experimental input for each lay-up, material properties and loading conditions [68].

Phenomenological models use experimental observations describing the loss of one specific composite property such as residual strength or residual stiffness. Several research studies have successfully developed and used this model [69–72]. The main advantage of the residual stiffness model over the strength model is that only the stiffness is required for material characterisation.

Progressive damage models are currently the most advanced models, able to predict both the number of cycles to failure and the damage progression. These models can be divided into two groups: Models predicting damage growth [73,74] and Models predicting residual mechanical properties [75–77]. Obviously, damage growth must be correlated with residual mechanical properties degradation, which is proved by Shokrieh and al. [75] who developed a more generalised approach integrating residual strength and stiffness theory, failure criteria for different mechanisms and constant life analysis.

One drawback of stiffness and strength degradation theories is that they do not take into account multiaxial property degradation [78]. They spotlight the mechanical properties in the principal loading direction. Recently, there have been research works focusing on the development of models that take into account the degradation of the Poisson's ratio, the transverse stiffness and other material elastic constants. The strength degradation theories were used also together with phenomenological modelling to estimate the material properties during fatigue loading.

In spite of the extensive research in this domain, the challenge of developing models with a more generalized applicability in terms of loading conditions and materials used persists.

# 2. Objectives and methodologies

## 2.1 Objectives

Matrix crack formation can initiate mechanical properties reduction of the laminate and may induce other damage forms such as delaminations; hence, influencing the whole structure performance. Therefore, prediction of matrix cracking in laminated composites is a crucial issue that has been investigated in several studies.

The micro structural mechanisms of damage accumulation cited previously can occur independently or interactively. Depending on the materials variables and the testing conditions, the distribution of the present damage features and their predominance can be strongly different affecting the interactions that could take place. The main objectives of this work are:

- Understand the mechanisms of the tensile fatigue damage in NCF laminates, as well as find procedures to predict the development and the accumulation of damage of the studied material.
- Analyse local delaminations and their effect on laminate stiffness for cross ply laminates under tensile loading.

The performed Experimental work and FEM modelling carried out to achieve the objectives are described in the next sections.

## 2.2 Experimental Procedure for the performed mechanical testing:

In Papers A and B, the fatigue behaviour of a quasi-isotropic NCF CF/EP composite laminates was investigated. The findings were based on experimental analyses. Two types of mechanical testing were performed: Quasi-static and cyclic loading tests. A quantitative and qualitative study of intra- and inter-laminar cracks was carried out.

## 2.2.1 Quasi-static tensile loading

An Instron 3366 universal testing machine with 10 KN load cell and pneumatic grips is used to perform the needed quasi-static tests. Several loading-unloading ramps with a displacement rate of 2 mm/min were carried out while increasing each time the maximum strain level.

## 2.2.2 Cyclic tensile loading

Stress controlled cyclic loading at a frequency of 5Hz and with a ratio R =0.1 of the minimum to the maximum stress in the cycle using ElectroPuls$^{TM}$E10000 Linear Torsion machine with 10 KN Load cell. Cyclic testing was carried out for five different maximum strain levels. The test is stopped after each block of cycles ($\Delta N = 1, 10, 10^2, 10^3, 10^4,...$).

In research, most composite testing was traditionally conducted until $10^6$ cycles, which correspond to the fatigue limit of steel materials. For composite materials, this limit is not easily determined but could reach 10 million cycles in case of carbon fibre wind turbine structures.

## 2.2.3 Quantification methods of intra- and inter-laminar cracking

Several experimental methods can be useful to characterise the damage state. Few of them are cited concisely below.

For transparent materials, such as Glass Fibre composites, counting can be made on the tested specimen edge or on the surface without taking it out from the testing machine, using transduced light. The characterisation gets harder with decreasing the layer thickness or when more than one layer is damaged which reduces the visibility of the cracks and the ability to distinguish between them, especially at high crack densities.

Using **X-ray Technique,** it is difficult to distinguish between cracks in the top and in the bottom damaged layer of the laminate if there is more than one damaged layer. Another drawback of this method is that it uses a penetrant liquid which must enter the crack in order to be seen. This means that the method provides information only about surface layer cracks or cracks connected with the specimen edge.

**Acoustic emission (AE)** has been used for damage characterization for almost all kinds of materials and systems. Often the energy released during crack propagation is larger than required to create a new crack surface. Part of the excess of the energy is dissipated in the form of acoustic signal which can be heard as a noise in the frequency region of 10 to 100 kHz. A transducer is fixed on the surface of the specimen under test to record those signals as a function of time. The applied strain dependence of time is simultaneously recorded which allows to obtain the crack density evolution as a function of the reached level of strain. This method has issues identifying and registering cracks at high crack densities since the signals are less distinguishable comparing to signals in the initial stage of cracking. One more drawback is that this method can not be used to distinguish between different co-existent damage modes nor quantify them.

**X-ray computed tomography (CT)** [79,80] is getting more importance among the non-destructive inspection techniques for applications where the three-dimensional (3D) assessment is required, or where the evolution of critical features is of importance, either during manufacturing or under in-service conditions. The heterogeneity of the architecture of composite materials, as well as the complex mechanisms of the nucleation and the evolution of damage, explain the significant growth of popularity of this method in the field of composites over the last decade. X-ray CT relies on the computational reconstruction of projections acquired from different angles of illumination. The image contrast relies on differences in the attenuation of X-rays paths through the studied object. Although X-ray CT provides detailed information through the whole components, from fibre tows to the individual fibre level, the poor phase contrast and long acquisition times among other drawbacks are limiting the applications of the X-ray CT to the study of composites.

The most suitable method of intralaminar cracking/ delamination quantification differs according to the material, the damage state, the accuracy required, available equipment, etc. For Carbon Fibre materials used in this research work, the simplest and most suitable method is **optical microscopy** which does not require sophisticated and expensive equipment. The damage state after increasing the strain level or after each block of cycles was characterized using optical microscopy (Nikon Eclipse MA200 equipped with DS-U3camera control unit). Specimens are removed from the tensile machine in order to be inspected. The microscopy observation of interlaminar cracks on the specimen edge when it is not loaded is very difficult because the delamination cracks are usually not opened and the accuracy of a quantitative

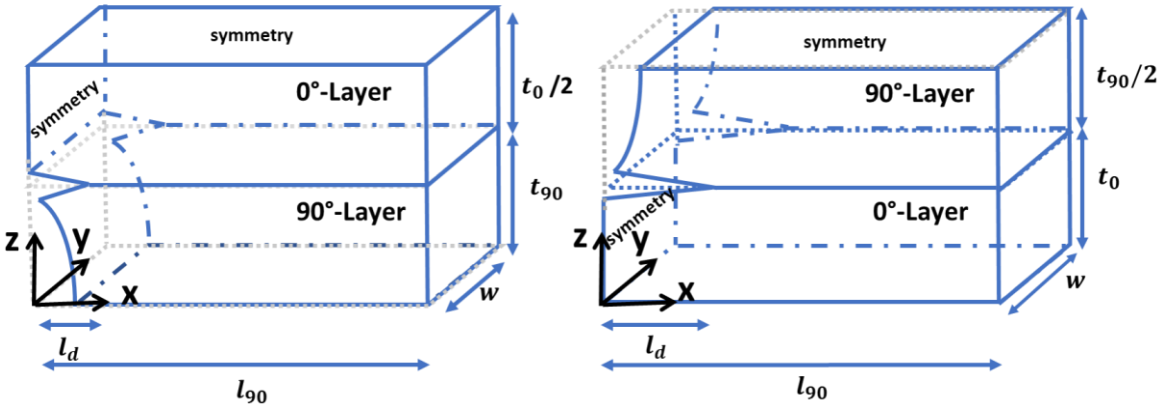
evolution of interlaminar cracks is then doubtful. The edge replicas method (a “print” of the crack on a rubber film) is often used to solve most of the problem. Taken in slightly loaded state when the cracks are open, replicas are analysed in a microscope after the mechanical test. That also avoids removing the specimen from the machine which increases the reliability of the results. In fact, after removing and putting back the specimen in the machine once it is damaged, the specimen alignment may not be the same.

The defects observed at the surface could be not developing into the specimen and therefore not representative for the damage state inside of the specimen. The difference can be very significant for secondary damage like delaminations. Thus, the minimum requirement during calibration stage is to check if the damage state is the same for specimens’ both edges; there may be more or less or exactly the same amount of cracks seen on the edges. In order to obtain a close image of the full 3D pattern of the damage, cross-sectioning of the sample has to be performed. The edge is grinded then polished to remove all scratches. The polished surface is examined under the optical microscope. This procedure is repeated reducing at each step a small distance from the width of the specimen to examine the damage state at different distances from the edges of the specimen and to evaluate the damage propagation inwards from the sample edges.

## 2.3 Modelling using FEM

FEM is used in Papers C and D to analyse the effect of the delamination length on the normalised average crack opening displacement for different intralaminar crack densities in cross-ply laminates subjected to uniform uniaxial tensile loading. The 3-D model assumes uniform intralaminar crack distributions which means the distance separating two cracks is constant and they grow the same in size and shape. The delaminations are modelled symmetric with respect to the intralaminar crack planes. In reality, the variation in crack spacing and growth can be considerable, particularly at low crack densities or when different damage mechanisms are interfering.

**Figure 6** shows a schematic representation of the representative volume element model used in FEM. $t_{90}$ and $t_o$ are respectively the 90°-layer and the 0°-layer thicknesses. $l_{90}$ is the half distance between two intralaminar cracks and $l_d$ is the half length of delamination. FE simulations were carried out for Carbon Fibre/ Epoxy (CF/EP) and Glass Fibre/ Epoxy (GF/EP) laminates.




*a)* *b)*

***Figure 6: Schematic representation of the representative volume element used for finite element analyses Model a) in the case of surface crack, b) inside crack***

In paper D, FEM is used to simulate 4-point bending test for cross-ply laminate, where peak stresses along an extended region in the middle of the material are produced, by applying constant displacement $u_z$ on the top surface points and adding simple supports at the extremities. Delaminations are assumed to be symmetrical with respect to the intralaminar crack plane. **Figure 7** shows a schematic presentation of the 3-D model used.

In all FEM calculations, the commercial code Ansys was used.

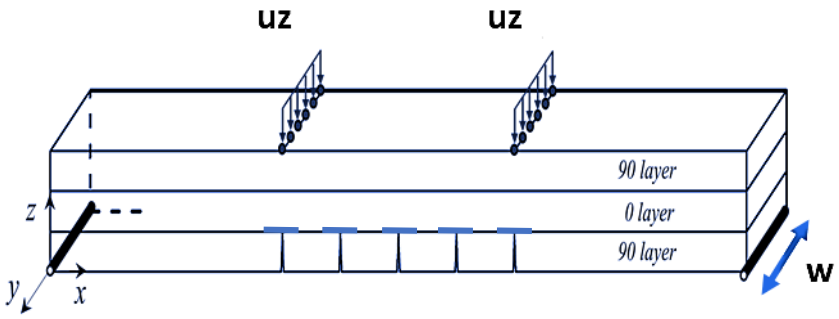


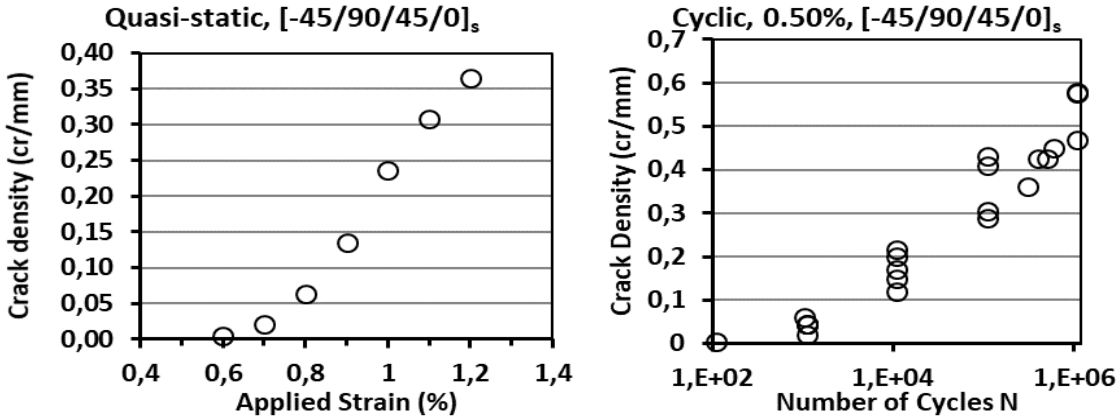

***Figure 7: Schematic representation of 4-point bending FEM model***

# 3. Summary of appended papers

## 3.1 Paper A

Intralaminar cracking in 90°-layer of HTS/RTM6 $[45/90/-45/0]_s$ carbon Fibre/ Epoxy NCF laminate is studied experimentally under tension -tension cyclic loading. The NCF UD ply used consists of 12K fibre bundles. The average layer thickness is 0.25 mm and the average bundles width is 3.5 mm. The fibre content in the laminate is 55%.

The 90°-layer intralaminar crack density growth during cyclic loadings is similar to its growth observed during quasi-static loading (**Figure 8**). The objective of this paper is to suggest and validate an efficient testing methodology for statistical 90°-layer intralaminar cracking evolution prediction in cyclic loading.




**a)** **b)**

***Figure 8: Intralaminar crack density in 90°-layers of $[-45/90/+45/0]_s$ laminate: a) as a function of the applied strain in quasi-static tensile loading; b) as a function of the number of cycles under 0.5% strain cyclic loading.***

A methodology, based on modified Weibull distribution and adjusted for cyclic loading effects, is suggested based on two main assumptions:

- The weakest position in the layer favourable for crack initiation is influenced by the non-uniform distribution of fibres and is the same independently of the loading nature

whether quasi-static or cyclic. Then, Weibull shape parameter for cyclic loading remains the same as in quasi-static, measuring the layer fibre distribution non-uniformity.

- The resistance of the damaged layer to transverse failure initiation is reduced in the case of cyclic loading. The shape parameter $\sigma_{in0}$ is then a monotonously decreasing function of the number of cycles and the cycling stress level. The function n in Weibull analysis describing the number of defects per volume unit initiating at a stress level $\sigma$, depends on the number of cycles and can be described by a power law function as following:

$$n(\sigma_T) = f(N)\left(\frac{\sigma_T}{\sigma_{in0}}\right)^m = N^n\left(\frac{\sigma_T}{\sigma_{in0}}\right)^m \quad (4)$$

For cracking analysis in a cyclic loading test $\sigma_T = \sigma_T^{fat}$ , and expression (1) is adjusted as following:

$$P_{in} = \frac{\rho_k(\sigma_T^{fat}, N)}{\rho_{kmax}} = 1 - exp\left[-\frac{V}{V_0}N^n\left(\frac{\left(\sigma_T^{fat}\right)^{1+\gamma}}{\sigma_{F0}^{\gamma}\sigma_0}\right)^m\right] \quad (5)$$

Replacing $\sigma_{F0}^{\gamma}\sigma_0$by $\sigma_{00}^{1+\gamma}$, the intralaminar cracking evolution in cyclic loading becomes:

$$\frac{\rho_k(\sigma_T^{fat}, N)}{\rho_{kmax}} = 1 - exp\left[-\frac{V}{V_0}N^n\left(\frac{\sigma_T^{fat}}{\sigma_{00}}\right)^{m(1+\gamma)}\right] \quad (6)$$

It is clear that the shape parameter for the equation (6) $m^* = m(1+\gamma)$ is larger in cyclic loading than in quasi-static loading. Nevertheless, performing cyclic loading, it was found that $\gamma$ can be neglected since $\gamma$<<1 and its effect can not be separated from the measurement error. That leads to the following expression:

$$P_{in} = \frac{\rho_k(\sigma_T^{fat}, N)}{\rho_{kmax}} = 1 - exp\left[-\frac{V}{V_0}N^n\left(\frac{\sigma_T^{fat}}{\sigma_{00}}\right)^m\right] \quad (7)$$

The shape parameter m is determined from crack density evolution with strain in quasi-static loading. Then, using one representative load level, in cyclic loading n and $\sigma_{00}$ are determined.

The damage state after increasing stress/strain level in the quasi-static tensile test was characterized and the crack density data as a function of applied stress was obtained. Presenting the experimental probability of failure as $ln(-\ln(1-P_{in}))$ (using the collected data and equation (1)) versus $\ln(\sigma_{T0})$, the relationship is found linear following Weibull distribution, as

presented in Figure 9. The Weibull parameters $m$ and $\sigma_{in0}$ are determined from the linear fitting function: $m = 7.11$ *and* $\sigma_{in0}$ =187.5 MPa.

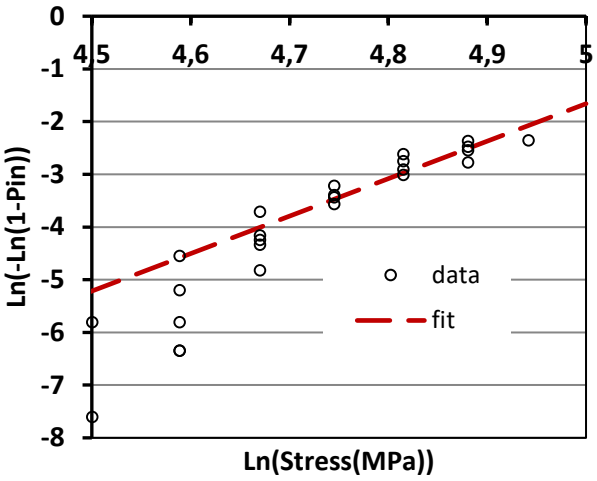



***Figure 9: Weibull analysis of the crack density in the 90°-layers of [-45/90/+45/0]$_s$ specimens***

Assuming the scale parameter m for fatigue loading case is the same as in quasi-static tests, the two remaining parameters are determined using equation (7). **Figure 10** shows the fatigue test data for some load levels presented with the predictions based on the Weibull parameters.

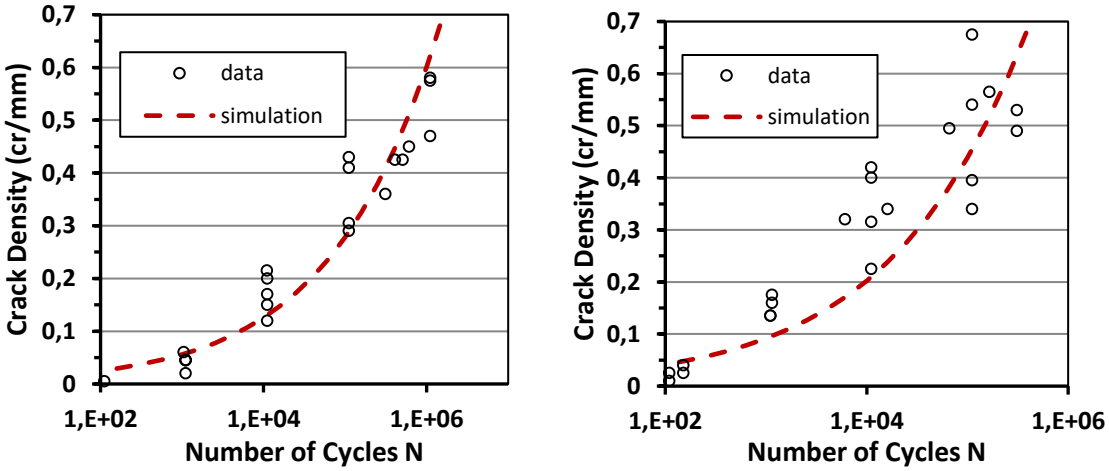



***Figure 10: Crack density growth with the number of cycles, (m=7.11, n=0.35, σ0=215): a) 0.5%; b) 0.6% strain cyclic tests.***

The validity of the methodology is proven for a case where $\varepsilon_{x,max} = 0.2\%$. The model calculation has a good agreement with the crack density quantified experimentally. Using this

methodology, is useful for laminates with thick damaged layers where crack initiation governs the number of tunnelling cracks. Cyclic tests at only one representative load level and quasi-static tests are proven sufficient for this material to determine the 90-layer intralaminar crack evolution in cyclic loading. If this methodology is proven correct for other material variables (geometry, lay-up, material properties…), it can be used to develop a time-efficient testing methodology where a smaller amount of time-consuming cyclic tests is required.

Regarding intralaminar cracks in ±45°-layer, the prediction of their evolution based on statistics of the 90°-layer is not accurate. A proper stress concentration analysis is needed since the initiation of these cracks occurs in stress concentration zones close to cracks in the neighbouring 90°-layers.

## 3.2 Paper B

In the previous paper, a methodology to predict the crack density in the 90°-layer of Quasi-isotropic CF/EP NCF laminates was suggested and validated. The intralaminar cracking, generating interlaminar stresses at the crack tips, especially at the edges, promotes the initiation of local delamination at the interface with ±45°-layers. The stress magnification in the neighbouring layers triggers short cracks in the adjacent off-axis layers. The damage mechanisms (intralaminar cracking, interlaminar cracking, fibre breaking…) have different characteristics depending on the material properties and the geometric parameters. Interaction among multiple cracks from the same category and/or interaction between different mechanisms complicate the damage analysis. The objective of this paper is to better understand the matrix related fatigue phenomena in the case of NCF laminates: the intralaminar cracking development in the laminate layers, their interaction with specimen edge and its effect on induced delaminations are studied and the contribution of different damage modes on the axial stiffness degradation are estimated. The material used is the same as described in Paper A. After each cyclic step, the axial modulus was determined, and edge replicas were taken to characterise the damage state later using optical microscopy analysis.

The delamination length is defined as the total length of all local delaminations observed on one interface and measured over a distance L. The relative delamination extent (%) is the ratio of the delamination length measured to L. Delaminations at 45°/0° interface were small and detected only at very high loading; they were not quantified in this work.

Delaminations that are not linked to intralaminar cracks are seldom observed.

**Figure 11** shows the growth of the edge relative delamination length with the number of cycles at different fatigue strain levels.

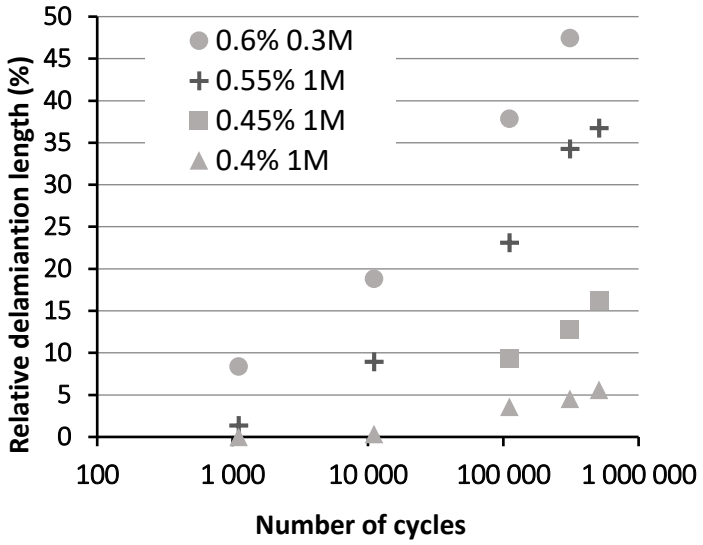



***Figure 11: Relative delamination growth on the edge: average over both interfaces***

For low maximum stress level cyclic tests, very high number of cycles is required to observe edge delamination which are confined to the edge. Whereas, when subjected to high stress cyclic tests, smaller number of cycles is sufficient to induce delamination that grow faster inside of the composite (20% of the interface in the central zone of the specimen can be delaminated). For a currently unknown reason, the delamination extent at the -45°/90° interface is significantly larger than the extent observed at the 90°/+45° interface. The stitch pattern combined with the intralaminar cracking state at the edge and the interaction between the existing damage modes can be the reason for the clear difference reported. Despite this difference, the delamination length between both interfaces has the same growth features along the interface from the edge region to the inside of the laminate. Grinding the edges of tested specimens and observing the delamination extent after polishing show two behaviour patterns dependent on the fatigue stress level. For low cyclic strain levels (under 0.45% of strain), even at high number of cycles, the intralaminar crack induced delaminations at the edge do not grow deeper inside of the laminate. For high cyclic strain levels, the zone with delamination is partially growing through the whole width of the specimens. The higher the cyclic stress is, the deeper the delamination develops inside of the material. **Figure 12** shows this variation with respect to the depth coordinate.

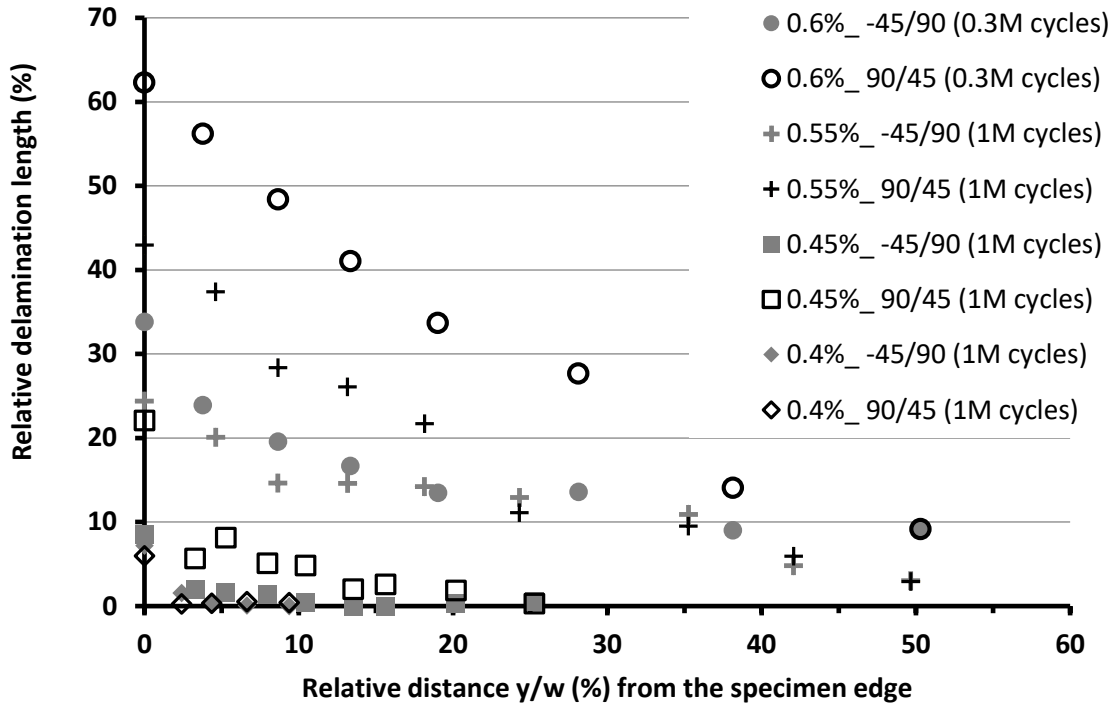



***Figure 12: Relative delamination length at the -45°/90° and 90°/45° interfaces as a function of the distance from the edge***

Axial Modulus reduction:

Experimental testing shows that induced delamination and intralaminar cracking in the off-axis layers start almost simultaneously; and during cyclic loading, both the delaminated area and the length of off-axis layer cracks grow with the number of 90°-layer intralaminar cracks. Local delamination increases the intralaminar crack opening displacement leading to higher stiffness reduction. Therefore, the contribution of each damage mode to the axial stiffness reduction is difficult to be estimated. Obviously, large delaminations at high stress cyclic loading contribute the most to the stiffness degradation. **Figure 13** presents the axial modulus variation with respect to the edge relative delamination extent and shows a rather linear relationship. The reduction due to delamination can be evaluated using the ply-discount model depending on the damage state, e.g. for regions which are fully separated from the laminate, not only the transverse and shear modulus are reduced due to cracking, but the longitudinal modulus is assumed null, too.

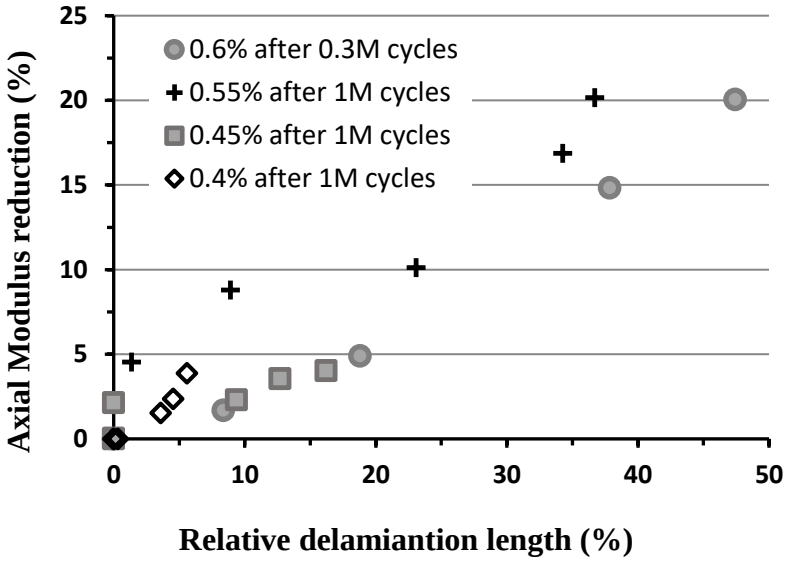



***Figure 13: Axial modulus reduction versus the relative delamination lengths averaged over both interfaces***

# 3.3 Paper C

The simultaneous growth of several damage modes and their interaction observed for NCFs in Paper B make it difficult to assess the effect of each individual damage mode on the stiffness reduction. Although the damage modes are the same for both NCF and prepreg tape laminates, the damage analysis and prediction are more complex due to the stitching pattern and heterogonous meso-structure. Prepreg and cross-plies are more used in research for their relative simplicity, hence, the choice to study cross-plies. CF/EP and GF/EP cross-plies with layups: $[90/0]_s$, $[90_2/0]_s$, $[90/0_2]_s$, $[0/90]_s$, $[0/90_2]_s$ and $[0_2/90]_s$ were investigated in this paper.

The stiffness reduction in cross-ply laminates with intralaminar crack induced delaminations is analysed using GLOB-LOC approach based on the definition of crack opening and crack sliding displacements denoted respectively (COD) and (CSD). FEM analysis was performed to evaluate the COD dependency on the delamination length for different intralaminar crack densities in both internal and surface 90°-layers of cross-ply laminates. In the model the intralaminar cracks have a uniform distribution and delaminations are symmetric with respect to the intralaminar crack plane. **Figure 6** is a schematic representation of the representative volume element used for finite element analyses model.

Results show that several geometrical parameters and elastic constants affect the COD and simple fitting functions accurately describing these effects in the presence of delaminations

were not found at the present. However, analysis confirm that the delaminations sliding and opening do not affect the stiffness degradation explicitly. They affect the stiffness via increasing the COD of intralaminar cracks. Thus, the numerical COD value corresponding to the delamination present and the COD based GLOB-LOC model are used for the case with delaminations to predict all thermoelastic constants (axial modulus, $E_{xlam}$, for example) of the damaged laminate. The obtained results are identical with values from direct FEM analysis. The effective transverse modulus (EFTM) of the damaged ply is back-calculated using the numerical COD and the obtained damaged laminate constants. For all investigated crack densities and delamination lengths, the effect of the surrounding plies (thickness and elastic constants) on the EFTM is found negligible. This non-significant effect allows the introduction of simple fitting expression describing the EFTM dependence on the intralaminar crack density and on the delamination length. The dependence of EFTM on the delamination length is more linear in the case of CF/EP than in the case of GF/EP.

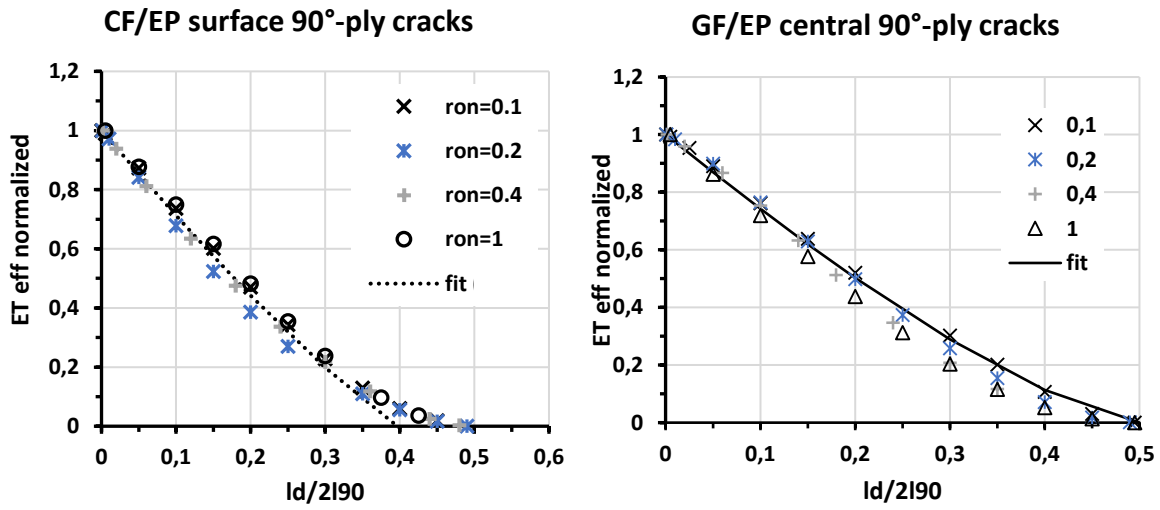



***Figure 14: Effective transverse modulus of a damaged central 90-ply in cross-ply laminates normalized with respect to its' value at the same crack density at zero delamination length. Dependence on relative delamination length (defined as $l_d/2l_{90}$) for different values of $\rho_{90n}$ demoted as ron.***

**Figure 14** shows the delamination length normalised with the distance between two consecutive intralaminar cracks ($2l_{90}$) on the EFTM normalized with respect to the effective modulus for this crack density but with zero delamination.

Comparison of thermo-elastic constants (axial Modulus, Poisson´s ratio, axial thermal expansion) obtained by FEM solution or using CLT, those determined based on GLOB-LOC predictions using the numerical obtained value of COD and those predicted based on effective stiffness used together with the Classical Laminate Theory shows a good agreement (**Figure 15**). Thus, the effective stiffness approach is proved to have good accuracy.

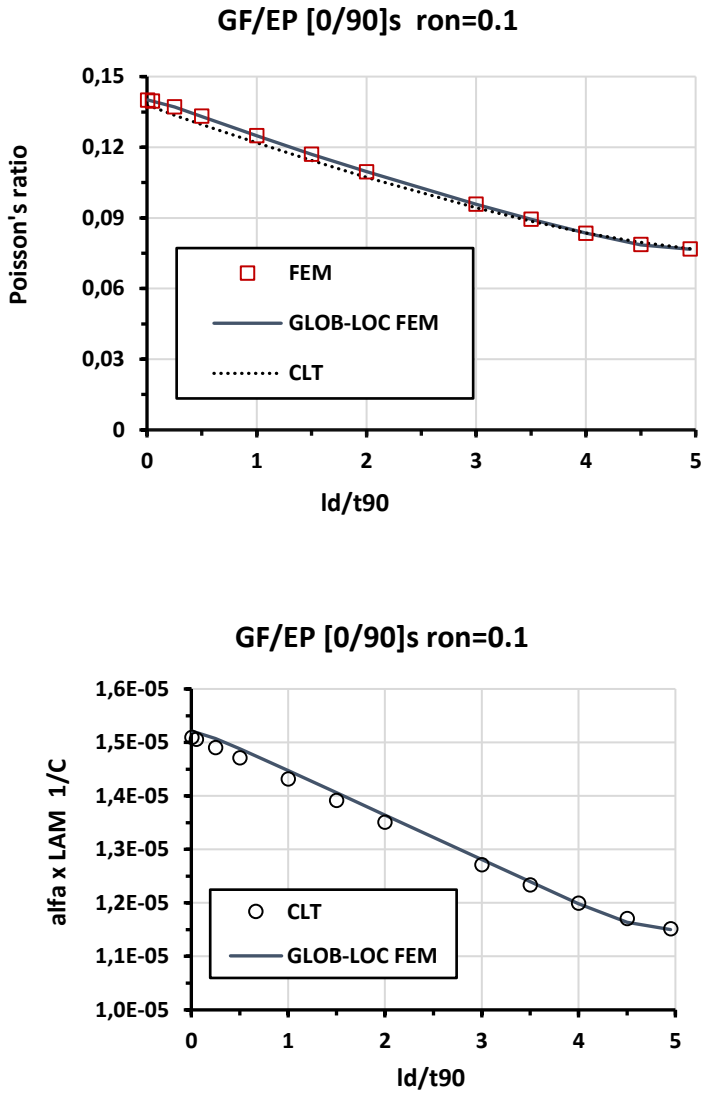
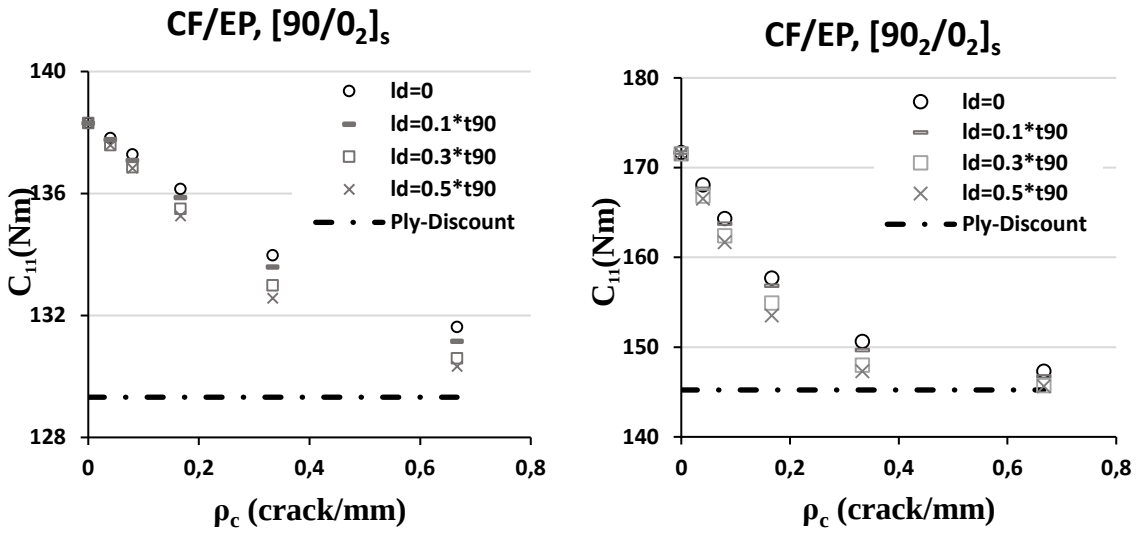



***Figure 15: Poisson's ratio of two cross-ply laminate with damaged central 90°ply. Dependence on relative delamination length (defined as $l_d/t_{90}$ ) for $\rho_{90n} = 0.1$. Symbols represent FEM solution; GLOB-LOC has COD from FEM; the dotted line is by using fitting equation and CLT.***

# 3.4 Paper D

A simple approach based on Classical Laminate Theory (CLT) and effective stiffness of damaged layer is suggested for bending stiffness determination of laminate with intralaminar cracks in surface 90°-layers and matrix crack induced delaminations. In this approach, the layer with intralaminar cracks and possibly with interlaminar cracks initiating from the intralaminar crack tips is replaced with an undamaged layer with effective stiffness of the damaged layer. CF/EP and GF/EP cross-plies with layups: $[90/0]_s$, $[90_2/0]_s$, $[90_2/0_2]_s$ were investigated in this paper. First, the in-plane stiffness of the damaged cross-ply laminate was calculated in two ways: (1) using FEM model of representative volume element (RVE) as shows **Figure 6.a** and (2) using the analytical GLOB-LOC approach based on COD. The obtained values from both methods are almost coinciding for all crack densities. Only the transverse effective modulus of the damaged layer depends on the crack density.

The crack opening displacement values depend on intralaminar crack density $\rho_c$ and are strongly affected by the presence of delaminations and their growth; hence, the dependence of the laminate stiffness on the delamination length $l_d$. The obtained effective stiffness was used to determine the laminate bending stiffness dependency on the delamination length for different crack densities. **Figure 16** shows this effect for CF/EP, $[90/0_2]_s$ and $[90_2/0_2]_s$ respectively for different crack densities on bending stiffness parameter ($C_{11}$). $C_{11}$ is the proportionality coefficient between the applied moment and the curvature. The bending stiffness tends towards the ply-discount value at high crack density.




**a)** **b)**

***Figure 16: Delamination effect on bending stiffness of CF/EP laminates with cracks in 90°-layer for two different Lay-ups***

FEM simulations were performed for 4-point bending test. The model used is presented in **Figure 7**. Obviously, the bending resistance of the laminate with cracks is additionally reduced by the presence of transverse crack induced delaminations. Undeniably, the longer the delaminations are, the larger the reduction is.

Finally, **Figure 17** shows an excellent agreement between 3-D FEM simulations of a 4-point bending test ( denoted as "FEM") and the CLT results with effective stiffness for CF/EP $[90,0_2]_s$ laminate with cracks in the bottom 90°-layer and for delamination lengths, $l_d = 0.1 * t_{90}$ and $l_d = 0.7 * t_{90}$ respectively. Significant effect of local delamination on bending stiffness was found, whether simulating 4-point bending test or using the effective stiffness approach.

The effective stiffness approach with effective stiffness calculations based on FEM (denoted as Eeff-FEM in **Figure 17**) or on GLOB-LOC gives acceptable accuracy for damaged laminate bending response.

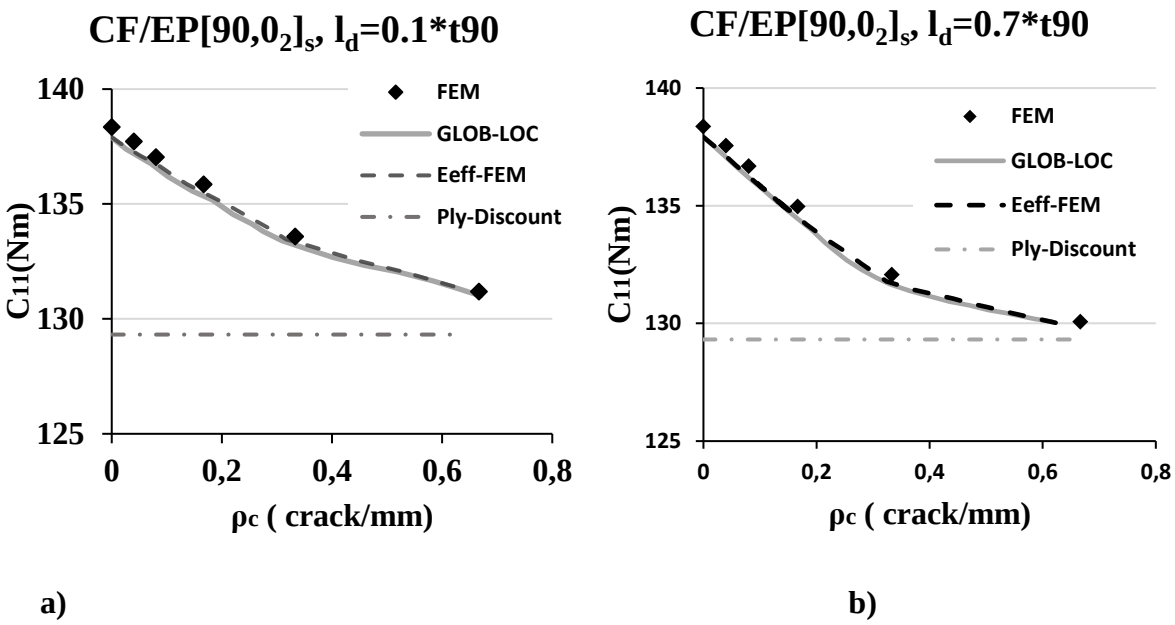



***Figure 17: Comparison between direct 3-D FEM simulation results and models based on effective stiffness***

# References


1. Chi, T. T., Lomov, S. V., & Verpoest, I. (2002). The mechanical properties of multi-axial multi-ply carbon fabric reinforced epoxy composites. In *Proc. ECCM-10, 10th European Conference on Composite Materials* (pp. 1-7).
2. Miyano, Y., Nakada, M., & Nishigaki, K. (2006). Prediction of long-term fatigue life of quasi-isotropic CFRP laminates for aircraft use. *International journal of fatigue*, *28*(10), 1217-1225.
3. Mattsson, D., Joffe, R., & Varna, J. (2007). Methodology for characterization of internal structure parameters governing performance in NCF composites. *Composites Part B: Engineering*, *38*(1), 44-57.
4. Lomov, S. V. (Ed.). (2011). *Non-crimp fabric composites: manufacturing, properties and applications*. Elsevier.
5. Cox, B. N., & Flanagan, G. (1997). Handbook of analytical methods for textile composites.
6. Wang, Y., Li, J., & Do, P. B. (1995). Properties of composite laminates reinforced with E-glass multiaxial non-crimp fabrics. *Journal of composite materials*, *29*(17), 2317-2333.
7. Bibo, G. A., Hogg, P. J., & Kemp, M. (1997). Mechanical characterisation of glass-and carbon-fibre-reinforced composites made with non-crimp fabrics. *Composites science and technology*, *57*(9-10), 1221-1241.
8. Mouritz, A. P., Leong, K. H., & Herszberg, I. (1997). A review of the effect of stitching on the in-plane mechanical properties of fibre-reinforced polymer composites. *Composites Part A: applied science and manufacturing*, *28*(12), 979-991.
9. Mouritz, A. P., & Cox, B. N. (2000). A mechanistic approach to the properties of stitched laminates. *Composites part A: applied science and manufacturing*, *31*(1), 1-27.
10. Godbehere, A. P., Mills, A. R., & Irving, P. (1994). Non crimped fabrics versus prepreg CFRP composites- A comparison of mechanical performance. In *FRC'94-International Conference on Fibre Reinforced Composites, 6 th, Univ. of Newcastle upon Tyne, United Kingdom* (p. 6).
11. Asp, L. E., Edgren, F., & Sjögren, A. (2004). Effects of stitch pattern on the mechanical properties of non-crimp fabric composites. *Proceeding of the 11 ECCM*, 31-05.

12. Heß, H., & Himmel, N. (2011). Structurally stitched NCF CFRP laminates. Part 1: Experimental characterization of in-plane and out-of-plane properties. *Composites Science and Technology*, *71*(5), 549-568.
13. Dexter, H. B., & Hasko, G. H. (1996). Mechanical properties and damage tolerance of multiaxial warp-knit composites. *Composites science and technology*, *56*(3), 367-380.
14. Nairn, J. A. (2000). Matrix microcracking in composites. *Polymer matrix composites*, *2*, 403-432.
15. Mikhaluk, D. S., Truong, T. C., Borovkov, A. I., Lomov, S. V., & Verpoest, I. (2008). Experimental observations and finite element modelling of damage initiation and evolution in carbon/epoxy non-crimp fabric composites. *Engineering Fracture Mechanics*, *75*(9), 2751-2766.
16. Marklund, E., Asp, L. E., & Olsson, R. (2014). Transverse strength of unidirectional non-crimp fabric composites: Multiscale modelling. *Composites Part B: Engineering*, *65*, 47-56.
17. Truong, T. C., Vettori, M., Lomov, S., & Verpoest, I. (2005). Carbon composites based on multi-axial multi-ply stitched preforms. Part 4. Mechanical properties of composites and damage observation. *Composites Part A: applied science and manufacturing*, *36*(9), 1207-1221.
18. Pipes, R. B., & Pagano, N. J. (1970). Interlaminar Stresses in Composite Laminates Under Uniform Axial Extension. *Journal of Composite Materials*, *4*(4), 538-548.
19. Highsmith, A. L., & Reifsnider, K. L. (1982). Stiffness-Reduction Mechanisms in Composite Laminates. *Damage in Composite Materials*, *775*, 103-117.
20. Talreja, R. (1985). Transverse cracking and stiffness reduction in composite laminates. *Journal of composite materials*, *19*(4), 355-375.
21. Garrett, K. W., & Bailey, J. E. (1977). Multiple transverse fracture in 90 cross-ply laminates of a glass fibre-reinforced polyester. *Journal of materials science*, *12*(1), 157-168.
22. Nuismer, R. J., & Tan, S. C. (1988). Constitutive relations of a cracked composite lamina. *Journal of Composite Materials*, *22*(4), 306-321.
23. Tan, S. C., & Nuismer, R. J. (1989). A theory for progressive matrix cracking in composite laminates. *Journal of Composite Materials*, *23*(10), 1029-1047.
24. Flaggs, D. L. (1985). Prediction of tensile matrix failure in composite laminates. *Journal of Composite Materials*, *19*(1), 29-50.
25. Nairn, J. A., & Hu, S. (1994). Micromechanics of damage: A case study of matrix cracking. *Damage Mechanics of Composite Materials*, 187-243.

26. Hashin, Z. (1985). Analysis of cracked laminates: a variational approach. *Mechanics of materials*, *4*(2), 121-136.
27. Hashin, Z. (1987). Analysis of orthogonally cracked laminates under tension. *Journal of Applied Mechanics*, *54*(4), 872-879.
28. Varna, J., & Berglund, L. A. (1994). Thermo-elastic properties of composite laminates with transverse cracks. *Journal of Composites, Technology and Research*, *16*(1), 77-87.
29. Varna, J., & Berglund, L. (1991). Multiple transverse cracking and stiffness reduction in cross-ply laminates. *Journal of Composites, Technology and Research*, *13*(2), 97-106.
30. Joffe, R., & Varna, J. (1999). Analytical modeling of stiffness reduction in symmetric and balanced laminates due to cracks in 90 layers. *Composites Science and Technology*, *59*(11), 1641-1652.
31. McCartney, L. N. (1992). Theory of stress transfer in a 0°—90°—0° cross-ply laminate containing a parallel array of transverse cracks. *Journal of the Mechanics and Physics of Solids*, *40*(1), 27-68.
32. McCartney, L. N., Schoeppner, G. A., & Becker, W. (2000). Comparison of models for transverse ply cracks in composite laminates. *Composites Science and Technology*, *60*(12-13), 2347-2359.
33. Hajikazemi, M., & McCartney, L. N. (2018). Comparison of Variational and Generalized Plane Strain approaches for matrix cracking in general symmetric laminates. *International Journal of Damage Mechanics*, *27*(4), 507-540.
34. Gudmundson, P., & Östlund, S. (1992). First order analysis of stiffness reduction due to matrix cracking. *Journal of composite materials*, *26*(7), 1009-1030.
35. Gudmundson, P., & Weilin, Z. (1993). An analytic model for thermoelastic properties of composite laminates containing transverse matrix cracks. *International Journal of Solids and Structures*, *30*(23), 3211-3231.
36. Varna, J. (2015). Strategies for stiffness analysis of laminates with microdamage: combining average stress and crack face displacement based methods. *ZAMM-Journal of Applied Mathematics and Mechanics/Zeitschrift für Angewandte Mathematik und Mechanik*, *95*(10), 1081-1097.
37. Srirengan, K., & Whitcomb, J. D. (1998). Finite element based degradation model for composites with transverse matrix cracks. *Journal of Thermoplastic Composite Materials*, *11*(2), 113-123.

38. Li, S. (1999). On the unit cell for micromechanical analysis of fibre-reinforced composites. *Proceedings of the Royal Society of London. Series A: Mathematical, Physical and Engineering Sciences*, *455*(1983), 815-838.
39. Li, S. (2001). General unit cells for micromechanical analyses of unidirectional composites. *Composites Part A: applied science and manufacturing*, *32*(6), 815-826.
40. Noh, J., & Whitcomb, J. (2001). Effect of various parameters on the effective properties of a cracked ply. *Journal of composite materials*, *35*(8), 689-712.
41. Li, S., Singh, C. V., & Talreja, R. (2009). A representative volume element based on translational symmetries for FE analysis of cracked laminates with two arrays of cracks. *International Journal of Solids and Structures*, *46*(7-8), 1793-1804.
42. Echaabi, J., Trochu, F., Pham, X. T., & Ouellet, M. (1996). Theoretical and experimental investigation of failure and damage progression of graphite-epoxy composites in flexural bending test. *Journal of reinforced plastics and composites*, *15*(7), 740-755.
43. Adolfsson, E., & Gudmundson, P. (1999). Matrix crack initiation and progression in compositelaminatessubjected to bending and extension. *International journal of Solids and Structures*, *36*(21), 3131-3169.
44. Smith, P. A., & Ogin, S. L. (1999). On transverse matrix cracking in cross-ply laminates loaded in simple bending. *Composites Part A: Applied Science and Manufacturing*, *30*(8), 1003-1008.
45. Smith, P. A., Ogin, S. L., & Faulks, G. Matrix cracking in a (0/90) 2s GFRP laminate loaded in flexure.
46. Kuriakose, S., & Talreja, R. (2004). Variational solutions to stresses in cracked cross-ply laminates under bending. *International journal of solids and structures*, *41*(9-10), 2331-2347.
47. McCartney, L. N., & Pierse, C. (1997). Stress transfer mechanics for multiple ply laminates subject to bending. *National Physical Laboratory Reports(UK)*, *55*, 41.
48. McCartney, L. N. (2001, April). Stress transfer mechanics for multiple ply cross-ply laminates subject to bending. In *summary in Proceedings of 6th International Conference on the Deformation and Fracture of Composites, Manchester* (pp. 57-66).
49. Adumitroaie, A., & Barbero, E. J. (2015). Intralaminar damage model for laminates subjected to membrane and flexural deformations. *Mechanics of Advanced Materials and Structures*, *22*(9), 705-716.

50. Adolfsson, E., & Gudmundson, P. (1997). Thermoelastic properties in combined bending and extension of thin composite laminates with transverse matrix cracks. *International Journal of Solids and Structures*, *34*(16), 2035-2060.
51. Hajikazemi, M., Sadr, M. H., & Talreja, R. (2015). Variational analysis of cracked general cross-ply laminates under bending and biaxial extension. *International Journal of Damage Mechanics*, *24*(4), 582-624.
52. Boller, K. H. (1970, January). Some fatigue characteristics of glass-reinforced composite laminates. In *DESIGN NEWS* (Vol. 25, No. 9, p. 123)
53. Owen, M. J., & Howe, R. J. (1972). The accumulation of damage in a glass-reinforced plastic under tensile and fatigue loading. *Journal of Physics D: Applied Physics*, *5*(9), 1637.
54. Talreja, R. (1986). Stiffness properties of composite laminates with matrix cracking and interior delamination. *Engineering Fracture Mechanics*, *25*(5-6), 751-762.
55. Berthelot, J. M., & Le Corre, J. F. (1999). Modelling the transverse cracking in cross-ply laminates: application to fatigue. *Composites Part B: Engineering*, *30*(6), 569-577.
56. Lafarie-Frenot, M. C., Henaff-Gardin, C., & Gamby, D. (2001). Matrix cracking induced by cyclic ply stresses in composite laminates. *Composites science and technology*, *61*(15), 2327-2336.
57. Berthelot, J. M. (2003). Transverse cracking and delamination in cross-ply glass-fiber and carbon-fiber reinforced plastic laminates: static and fatigue loading. *Applied Mechanics Reviews*, *56*(1), 111-147.
58. Mouritz, A. P., & Cox, B. N. (2000). A mechanistic approach to the properties of stitched laminates. *Composites part A: applied science and manufacturing*, *31*(1), 1-27.
59. Caous, D., Bois, C., Wahl, J. C., Palin-Luc, T., & Valette, J. (2017). A method to determine composite material residual tensile strength in the fibre direction as a function of the matrix damage state after fatigue loading. *Composites Part B: Engineering*, *127*, 15-25.
60. Shahzad, A., & Nasir, S. U. (2018). Validation of fatigue damage model for composites made of various fiber types and configurations. *Journal of Composite Materials*, *52*(9), 1183-1191.
61. Lingxiao, J., Penghu, D., Yi, W., Dan, L., & Zaixing, Z. (2018). Fatigue failure characterization of multi-axial warp-knitted composites under cyclic uniaxial tensile loading. *The Journal of The Textile Institute*, 1-7.
62. Reifsnider, K. L. (Ed.). (1991) Fatigue of composite materials, Elsevier.
63. Degrieck, J., & Van Paepegem, W. (2001). Fatigue damage modeling of fibre-reinforced composite materials. *Applied mechanics reviews*, *54*(4), 279-300.

64. Wicaksono, S., & Chai, G. B. (2013). A review of advances in fatigue and life prediction of fiber-reinforced composites. *Proceedings of the Institution of Mechanical Engineers, Part L: Journal of Materials: Design and Applications*, *227*(3), 179-195.
65. Fawaz, Z., & Ellyin, F. (1994). Fatigue failure model for fibre-reinforced materials under general loading conditions. *Journal of composite materials*, *28*(15), 1432-1451.
66. Jen, M. H., & Lee, C. H. (1998). Strength and life in thermoplastic composite laminates under static and fatigue loads. Part I: Experimental. *International journal of fatigue*, *20*(9), 605-615.
67. Paramonov, Y. M., Kleinhof, M. A., & Paramonova, A. Y. (2002). A probabilistic model of the fatigue life of composite materials for fatigue-curve approximations. *Mechanics of composite materials*, *38*(6), 485-492.
68. Schaff, J. R., & Davidson, B. D. (1997). Life prediction methodology for composite structures. Part I—Constant amplitude and two-stress level fatigue. *Journal of composite materials*, *31*(2), 128-157.
69. Diao, X., Ye, L., & Mai, Y. W. (1995). A statistical model of residual strength and fatigue life of composite laminates. *Composites science and technology*, *54*(3), 329-336.
70. Whitworth, H. A. (1997). A stiffness degradation model for composite laminates under fatigue loading. *Composite structures*, *40*(2), 95-101.
71. Wen, C., & Yazdani, S. (2008). Anisotropic damage model for woven fabric composites during tension–tension fatigue. *Composite structures*, *82*(1), 127-131.
72. Epaarachchi, J. A., & Clausen, P. D. (2003). An empirical model for fatigue behavior prediction of glass fibre-reinforced plastic composites for various stress ratios and test frequencies. *Composites Part A: Applied science and manufacturing*, *34*(4), 313-326.
73. Biner, S. B., & Yuhas, V. C. (1989). Growth of short fatigue cracks at notches in woven fiber glass reinforced polymeric composites. *Journal of engineering materials and technology*, *111*(4), 363-367.
74. Dahlen, C., & Springer, G. S. (1994). Delamination growth in composites under cyclic loads. *Journal of Composite Materials*, *28*(8), 732-781.
75. Shokrieh, M. M., & Lessard, L. B. (1997). Multiaxial fatigue behaviour of unidirectional plies based on uniaxial fatigue experiments—I. Modelling. *International journal of fatigue*, *19*(3), 201-207.
76. Shokrieh, M. M., & Lessard, L. B. (2000). Progressive fatigue damage modeling of composite materials, Part II: Material characterization and model verification. *Journal of Composite Materials*, *34*(13), 1081-1116.

77. Shokrieh, M. M., & Lessard, L. B. (2000). Progressive fatigue damage modeling of composite materials, Part I: Modeling. *Journal of composite materials*, *34*(13), 1056-1080.
78. Vassilopoulos, A. (Ed.). (2010). *Fatigue life prediction of composites and composite structures*. Elsevier.
79. Maire, E., & Withers, P. J. (2014). Quantitative X-ray tomography. International materials reviews, 59(1), 1-43.
80. Garcea, S. C., Wang, Y., & Withers, P. J. (2018). X-ray computed tomography of polymer composites. Composites Science and Techno *Composites Science and Technology*, *156*, 305-319.

# Paper A

# Statistical model for initiation governed intralaminar cracking in composite laminates during tensile quasi-static and cyclic tests

H. Ben Kahla[1,2] , Z. Ayadi[1] , F. Edgren[3] , A. Pupurs[1]and J. Varna[1*]

[(1)] Department of Engineering Sciences and Mathematics, Luleå University of Technology, SE-97187,Luleå,Sweden

[(2)] Institut Jean Lamour, SI2M, Université de Lorraine, EEIGM 6 Rue Bastien Lepage, F-54010 Nancy, France

[(3)]GKN Aerospace, SE-46181, Sweden

* Corresponding author (Janis.Varna@LTU.SE)

## Abstract

A simple model for predicting intralaminar cracking in laminates under cyclic loads is proposed and validated. The model is limited to low stresses and low crack density and is based on the assumption that the non-uniformity of the fiber distribution is the main reason for the observed large variation of cracking resistance along the transverse direction of the layer. Hence, the resistance variation in quasi-static and in cyclic loading can be described by the same parameter. At low crack density the failure resistance variation is more significant than the variation of the stress state in the specimen, the latter becoming dominant at high crack density. At low crack density the Weibull distribution for probability of intralaminar cracking is used for crack density growth simulation during cyclic loading. Assuming the non-uniformity of the fiber distribution as the cause for variation of cracking resistance, the Weibull shape parameter in cyclic loading is the same as in quasi-static loading case while the scale parameter is assumed to degrade with the applied number of cycles and this dependence is described by a power function. Thus, the determination of parameters is partially done using quasi-static tests and partially using cyclic tests, significantly reducing the necessary testing time. The predictions of dependency of the cracking on the stress and number of cycles are validated against experimental observations of cracking in the 90-plies of quasi-isotropic non-crimp fabric (NCF) laminates as well as in tape based cross-ply laminates.

**Key words**: Intralaminar cracking, Quasi-static loading, Cyclic loading, Weibull distribution, Crack density

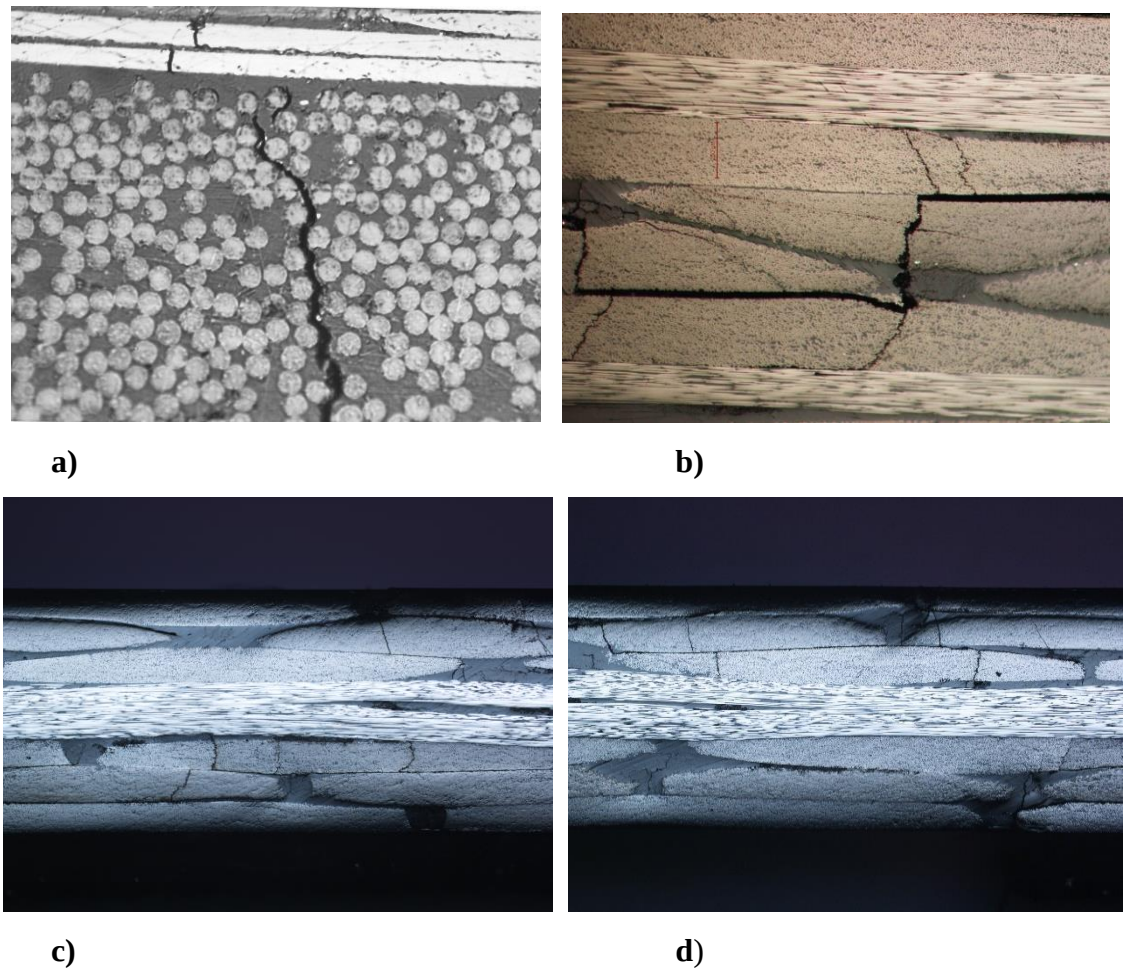
# 1. Introduction

Fiber orientation in layers of laminated composite structures is usually optimized with respect to the expected service loads. Depending on the application, the final failure of a structure is defined as a loss of structural integrity or as a limit of stiffness degradation. The most typical modes of final failure in composites are longitudinal failure of the critical ply **[1]** or large delaminations between plies **[2]**. Both these modes are severely affected (or sometimes even triggered) by multiple intralaminar cracking in plies with off-axis orientation with respect to the main loading direction. These cracks are caused by common action of the transverse tensile stress and the in-plane shear stress **[3,4]**. In quasi-static loading the crack density grows with the increasing load level whereas in cyclic loading the number of cracks increases with the number of the applied load cycles.

Intralaminar cracks usually do not break the fibers, they run parallel to the fiber direction in the ply and the crack plane is perpendicular to the laminate middle-plane (x-y plane). These cracks often cover the whole thickness of the ply creating well defined tunnels, growing over the whole width of the specimen, see **Figure.1**. Intralaminar cracks may significantly impair the effective thermo-elastic constants of the laminate **[5-7]**. They also initiate other damage modes, such as local delaminations starting at the intralaminar crack tips **[8]**, and fiber breaks in the neighboring plies, see **Figure 1 a** and **b**.

To understand the suggested methodology, two major stages have to be recognized in the development of each intralaminar crack: initiation and propagation. The crack initiation is a process on the fiber/matrix scale (microscale), which leads to development of a mesoscale damage entity (defect, flaw) the growth of which is analysed in a homogenized ply using the stress and the available energy conditions. The sequence of the events during the initiation stage is known: depending on the interface and the matrix properties it is a combination of the failure of the interface leading to prolonged debonds **[9-12]** and/or the matrix failure followed by the coalescence of these small damage entities into a larger damage entity **[10,13,14**], which, after reaching the critical size, grows unstably in the ply thickness direction **[15]**. The growth is arrested when the crack approaches the interface with the neighbouring ply. In this paper, the stress in the ply required for crack initiation is called the “initiation strength” and it is calculated using the Classical Laminate theory (CLT).

In quasi-static loading, the growth of an intralaminar crack along the fibers, i.e., the propagation, is usually analysed in a homogenized ply using energy considerations, calculating the potential energy before and after the crack propagation and comparing the change with the fracture toughness **[5,16-18,19]:** the available potential energy has to be equal to or larger than the work required for creating a new crack surface. Since for the fiber-reinforced composites the Mode I fracture toughness $G_{IC}$ is usually significantly lower than the Mode II fracture toughness $G_{IIC}$ , the main driving force for crack propagation is the transverse tensile stresses in the ply. Large in-plane shear stresses, if present, would contribute to the propagation and hence, a mixed mode crack propagation would take place **[20].**



**a)** **b)**

**c)** **d**)

***Figure 1: Damage modes in laminates: a) fiber breaks in 0- ply close to intralaminar crack tip ; b) large delaminations linking intralaminar cracks in NCF [45/0/-45/90]$_s$ laminate; c and d) intralaminar cracks in off-axis layers of the [-45/90/+45/0]$_s$ quasi-isotropic laminate.***

The energy release rate (ERR) in Mode I is proportional to the square of the in-plane transverse stress in the layer and to the thickness of the cracked layer. Therefore, equalizing it with $G_{IC}$ ,

the stress level $\sigma_{prop}$ for the propagation has the well known $1/\sqrt{t_k}$ dependence on the ply thickness $t_k$**[3]**. Crack propagation in Mode II has the same ply thickness dependence **[20]**. The stress for propagation, $\sigma_{prop}$ in thin ply laminates is higher than the initiation strength and hence, the intralaminar cracking is controlled by the propagation stress. If the ply is sufficiently thick, the stress level for propagation is lower than the stress for initiation, and the initiated cracks grow in an unstable manner. Of course, in this case a crack initiated in a local stress concentration region will cross this region and it will stop when entering a region with lower stresses.

In a stress-controlled cyclic loading a certain number of cycles is required for crack initiation and a different number of cycles is required for its propagation through the width of the specimen. In this paper the focus is on cases when the initiation requires significantly more cycles than the propagation.

In tension-tension cyclic loading the growth of an individual off-axis ply crack was studied in **[4],** measuring the crack length growth rate in plies with different orientations and thicknesses at several applied stress levels. The energy release rate was calculated using FEM. It was shown that the crack growth rate has a power function dependence on the total energy release rate.

Nairn et al **[21, 22]** proposed to use a phenomenological relationship, where the crack density growth rate and not the individual crack length is a power function of the energy release rate change during one cycle, when the stress changes from the highest to lowest value. In **[21,22]** the energy release due to formation of a new crack between the two existing cracks was calculated using Hashin's model **[23].** It was shown that for many cross-ply laminates made of the same material, linear relationship exists between the logarithm of the experimental crack density and the logarithm of the calculated energy release rate. In [**24]** the same propagation criterion was used together with a more sophisticated stress analysis, where each ply in the numerical model was divided in several sublayers using the Hashin's simplified stress assumptions in each of them. The used calculation scheme is the same as in **[25]** and in **[26],** where an extremely high accuracy of the stress analysis was demonstrated. In **[24]**, using their own fatigue test data for $[\theta/0]_s$ and $[0/\theta]_s$ laminates, the authors proved that the power law is applicable.

In spite of the demonstrated good ability to predict the crack density growth in cycling loading, the Paris law type of behaviour of the crack density, has not been confirmed theoretically. This model also has a difficulty to explain the crack density increase with the number of cycles at

low stresses. There are no cracks in the beginning of a low stress fatigue test and the cracks start to appear one by one. The crack density is low, the stress perturbations caused by the cracks are not overlapping and large regions with CLT stress exist between the cracks. Since the stress distribution between the cracks has a large plateau region, the deterministic power law for crack density would predict not a single first crack but many cracks to appear at the same number of cycles. However, experiments **[5, 27-31]** show that in quasi-static tests the first crack appears at a certain strain but the next crack requires a higher strain. In cyclic loading the next cracks appear after a larger number of cycles than the first crack **[2,4,32-34],** both loading cases resulting in a monotonous increase in crack density. This case has a practical significance because it is the first crucial step from "zero damage" design philosophy to "controlled damage" design.

We claim that the described feature of cracking at low stresses has its origin in the non-uniformity of the fiber distribution in the ply, which leads to different positions having difference resistance to failure. The Weibull distribution is widely used for analysis of initiation strength controlled intralaminar cracking in tensile quasi-static loading, where the crack density increase with the applied strain is slow in the beginning **[5,27, 28]**.

In the crack density region, where the stress perturbations are interacting, the statistical strength distribution approach is not in a contradiction with the described deterministic power law approach. At high crack density the stress distribution has a distinct maximum and the probability to have the crack at the maximum point is not significantly affected by the strength variation along the ply. In fact, since the weakest positions already have cracks, there are many positions with similar strength and the stress state defines the position of the next crack.

One of the first attempts to generalize the statistical approach to cyclic loading was made in **[4,30]**. In the approach presented in this paper we assume that because of the material non-uniformity the weakest position in quasi-static loading is also the weakest in cyclic loading. We assume the same about the second weakest position, and so on. However, the "initiation strength" in each position is assumed to degrade with the number of cycles. If so, we can describe the probability of the appearance of an intralaminar crack by Weibull distribution and the shape parameter in this distribution would be the same as in quasi-static case. The scale parameter is a monotonously decreasing function of the number of cycles. In the beginning of the fatigue test the growth rate of the crack density depends on the probability density of the failure properties. When due to cracking in weakest positions the crack density increases, many

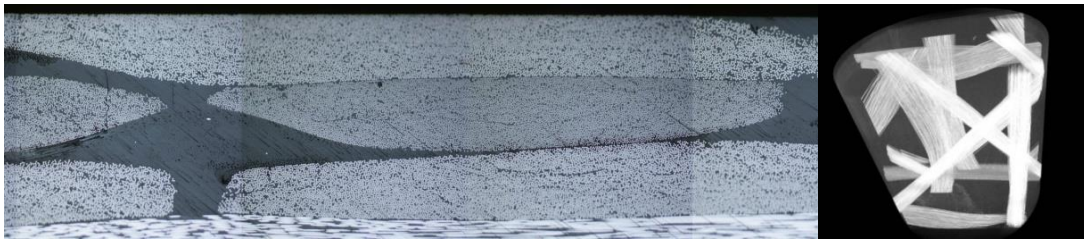
positions have similar failure properties and the stress state between the cracks controls the cracking. The cracking rate decreases due to crack interaction and also because the remaining positions have higher failure resistance.

In this paper we will analyse the type of composite, in which the intralaminar cracks after their initiation almost immediately propagate as long tunnels. Cracking in this case is often a dynamic process accompanied by acoustic emission signal and a small load drop registered in a displacement-controlled test **[27,35]**. In a uniform stress field the crack would cross the whole width of the specimen but if it is initiated in a stress concentration region its propagation will slow down when it exits the stress concentration zone.

The objective of this paper is to present a simple probabilistic model describing the intralaminar cracking in low stress cyclic loading at low crack density. Its applicability and the sensitivity of results with respect to experimental inaccuracies are investigated. Since part of the model parameters are obtained from quasi-static tests, this methodology requires much less cyclic testing than the traditional testing with many stress levels and large number of cycles. The methodology will be evaluated on intralaminar cracking in 90-plies of quasi-isotropic laminates made of carbon fiber/epoxy NCF layers with bundle meso-structure. Some results for tape based thin ply TR50S/EP composite cross-ply laminates, supporting this approach, will also be presented.

## 2. Materials and characterization

Resin Transfer Molding with curing temperature 180 ℃ was used to produce quasi-isotropic laminates with $[-45/90/+45/0]_s$ lay-up by stacking plies of unidirectional (UD) NCF carbon fiber HTS40/RTM6 composite. Each UD ply consisted of 12K fiber bundles held together by orthogonal stitching yarns along the fibers and transverse to them, see the pattern of stitching yarns in **Figure 2**. Plies in the laminate were not stitched together. The average bundle (ply) thickness in the laminate was 0.25 mm and the bundle width was 3.5mm. Since the width to thickness ratio of the bundle is large, assumption was made that in the bulk part of the bundle the stress is the same as in a layered laminate and the CLT is applicable for stress analysis. One crack in the 90-bundle close to the matrix region is also visible in **Figure 2a**. The fiber content in the composite was 55%.



**a)** **b**)

***Figure 2: Upper part of the [-45/90/45/0]$_s$ quasi-isotropic laminate: a) optical micrograph of the edge view; b) spacial distribution of stitch yarns obtained from micro computed tomography.***

The following thermo-elastic constants for a UD layer were measured

$E_L = 120\ GPa$ $E_T = 9.18\ GPa$ $G_{LT} = 3.94\ GPa$ $\nu_{LT} = 0.311$

$\alpha_T = 31.6 \cdot 10^{-6} 1/℃$ $\alpha_L = 0.32 \cdot 10^{-6} 1/℃$

Using these data and the CLT, the elastic constants of the quasi-isotropic laminate were calculated as $E_x^{LAM} = 46.23\ GPa$ and $\nu_{xy} = 0.32$. These values are in a good agreement with the experimental data 46.3 GPa and 0.32. Thermal residual stresses in all layers of a quasi-isotropic laminates are equal. The shear component of the thermal stress is zero. The thermal transverse stress at room temperature calculated using the CLT is rather high, $\sigma_T^{th} = 40.1\ MPa$.

Rectangular specimens with dimensions 200 mm x 16 mm were made and reinforced with glass fiber/epoxy end tabs. The gauge length between the tabs was 100 mm. Two types of mechanical testing to introduce intralaminar cracking were performed: a) quasi-static tensile tests of specimens with 100 mm gauge length with displacement rate 2 mm/min; b) tension- tension cyclic tests with 5 Hz frequency and load ratio R=0.1.

The quasi-static tests were performed on Instron 3366 universal testing machine equipped with a load cell of 10 kN and pneumatic grips. The axial strain was measured with a dynamic Instron surface-mounted extensometer with 50 mm gauge length and a travel of ±5mm. This extensometer is suitable for tensile, compressive & fatigue testing. Several loading-unloading ramps were performed inspecting the specimen for damage under an optical microscope after each ramp. The maximum strain in each following ramp was higher than in the previous ramp. In this way the crack density in layers was characterized as a function of the applied maximum strain in the ramp. The number of ramps for each specimen was small and, therefore, fatigue effects in these tests were assumed as negligible.

Fatigue testing was performed using the Instron ElectroPulsTM E10000 Linear-Torsion machine with load cell of 10 kN in a load controlled mode. The dynamic extensometer with 50 mm gauge length was used. In Section 4.2 the crack density increase with the number of cycles is presented for several applied maximum strain levels. This means that first for each specimen the elastic modulus was determined and then this value was used to calculate the necessary applied maximum load corresponding to the selected maximum strain $\varepsilon_{x,max}$. The test results are referred to as data for strain level $\varepsilon_{x,max}$. Such "strain representation" of results was found to be more informative than representation with respect to the applied macroscopic stress, which depends on the laminate lay-up. However, the CLT transverse stress level in a ply, which contains thermal as well as mechanical part, is an even better alternative for use in the data reduction in Section 4.2. The cyclic tension-tension tests were interrupted after a certain number of cycles and specimens were inspected for damage under an optical microscope. To confirm the observed trends, also a small number of tape based thin ply TR50S 15k CF, LY556/HY917/DY070 composite cross-ply laminates was tested as described above.

The intralaminar crack density in plies was characterized using an optical microscope Nikon Eclipse MA200 equipped with DS-U3 camera control unit and the NIS-Elements software, and in some cases using also X-ray micro computed tomography (CT) equipment Xradia 510 Versa from Zeiss. For favorable optical inspections, the specimen edges were carefully polished prior to testing using SiC papers (P240, P600, P1200, P2500, P4000) followed by polishing in liquid diamond slurry (from 9 μm to 0.25 μm).

The optical microscopy was used in two approaches: a) direct specimen edge observations; b) analyzing images obtained from flexible fast-curing silicon rubber replicas of the specimen edges. Repliset-T3 silicon rubber-based compound with working life of 3 minutes and curing time of 10 min at 25 ºC was used. During the direct edge observations the specimen was taken out from the testing machine for optical microscopy inspection. A drawback of this technique is low reliability of the stiffness change measurements: after re-mounting the specimen back in the grips of the testing machine, the alignment is not exactly the same. As an alternative, edge replicas on loaded specimens were taken and cracks were then counted on replicas under the microscope. The results from both techniques were very similar, a 1-2% higher crack density was obtained using the replicas. The reason for the difference is that the replica is taken on a loaded specimen, where the cracks are widely open, whereas the direct edge observations are

performed on unloaded specimens, where the cracks are only slightly open due to thermal stresses and therefore some of them can be missed during the observation.

The stress state in the plies at specimen edges is more complex than in the bulk of the laminate. Therefore optical edge observations do not necessary give a correct description of the damage state in the laminate. Larger differences between the damage on the edges and in the bulk are expected in thin layers and/or in fatigue loading, where cracks may grow in a stable manner from edge towards the centre of the specimen. Two methods were used to prove that crack density counted on the specimen edges is representative. In the first method the specimen edge was grinded down by approximately 1mm step, the new edge was polished as described above and inspected optically. The same procedure was repeated after the consecutive steps of grinding. In the second method CT was used on small 15*11*2mm specimens cut from the gauge length region of some of the tested specimens. These two methods led to a conclusion that intralaminar cracks in the 90-plies of the studied materials are indeed tunnelling cracks going from one specimen edge to another. This means that the crack density on the edge of the 90-ply is statistically the same as in the bulk of the material and hence the edge crack density is representative.

# 3. Theoretical considerations

## 3.1 Initiation strength distribution

Since currently a reliable micromechanics based evaluation of the necessary applied strain or stress level for crack initiation in a position with a certain fiber distribution is not possible, we define the initiation strength, $\sigma_{in}$ as a material dependent mesoscale stress level in the layer required to initiate a defect large enough to grow. As described in Section 1 the initiation strength is not a single number but a distribution of values due to the non-uniform fiber distribution in the layer. The discussion in this paper is limited to the intralaminar cracking cases, when in quasi-static loading the propagation stress is lower than the initiation strength and in cyclic loading the crack propagation requires significantly less cycles than the initiation.

In tension the crack surfaces are traction free: the in-plane stresses on the crack surface are zero. Very high out-of-plane shear stresses at the ply interface in the vicinity of the crack tip ensure effective stress transfer from the undamaged ply to the damaged one and with increasing

distance from the crack the in-plane stresses in the ply asymptotically approach the far-field (CLT) value. The described stress recovery mechanism allows creating multiple cracks in the same layer with increasing external load.

The intralaminar damage in a ply is characterized by the crack density $\rho_k$ (cracks/mm) in the k-th layer. During loading the crack density may approach the asymptotic value, often called the crack density at saturation or the "characteristic damage state" (CDS **[1]**. At CDS the spacing between cracks is approximately equal to the ply thickness $t_k$. Thus

$$\rho_{k,max} \approx {}^{1}/_{t_k} \quad (1)$$

The CSD value depends on the geometrical and elastic parameters of the adjacent layers and on possible local delaminations at the intralaminar crack tip. However, these details are irrelevant for the methodology used in this paper, where only the data at low crack density are analysed. When the crack density is high, the maximum value of the in-plane stress between two cracks is much lower than the CLT value and creation of a new crack may require significantly higher applied load to the laminate. In this region, the crack density growth rate model discussed in **[21,22]** is preferable. The following analysis is described for the case with transverse stresses only. However, it does not affect the generality of the approach and cracking under combined transverse and shear stress can be implemented, for example, using the equivalent stress instead of the transverse stress.

Each ply in its in-plane transverse direction is considered as consisting of many small elements. Each element has its individual intralaminar cracking initiation strength. We use a simple approach previously used in **[27,34]**, assuming a rather large length of the element. The only conditions for selecting the element length are that a) to calculate the failure probability each element cannot have more than one crack; b) the stress state in the element is as in the CLT: it is not affected by failure of the adjacent element. Both conditions imply that the crack densities used in data reduction should be significantly lower than the $\rho_{k,max}$. Therefore, the element length selection analysing the low crack density data is rather arbitrary but the distribution parameters correspond to the selected length. Consequently the $\rho_{k,max}$ is not necessary the experimental value at the CDS. Using the standard procedure the distribution parameters can be recalculated for any other element length, if necessary for simulations. We assume that the element length is equal to $t_k$ and, hence, the number of elements in a ply over length $L$ is

$$M = \frac{L}{t_k} = L \cdot \rho_{k,max} \quad (2)$$

The Weibull transverse strength distribution is assumed to describe the variation but the geometrical position of an element with a given $\sigma_{in}$ is random. The distribution is in the form

$$P_{in} = 1 - exp\left[-\frac{V}{V_0}\left(\frac{\sigma_{T0}}{\sigma_{in0}}\right)^m\right] \quad (3)$$

In (2) $P_{in}$ is the probability that crack is initiated when the transverse tensile stress in the element is $\sigma_{T0}$; $m$ and $\sigma_{in0}$ are the shape and the scale parameters respectively obtained from tests of reference specimens with element volume $V_0$ ; $V$ is the volume of the considered element when (3) is applied to plies of different thickness.

The analysis presented in this paper is not a Monte Carlo type of simulation, where the failure of each individual small element is considered explicitly based on the local stress distribution between the existing cracks and the individual failure properties of the element. Monte Carlo simulation is applicable even at high crack density. Instead, here we express the probability of cracking through crack density without specifying which particular element has failed and ignoring the effect of a crack on stress distribution in other elements. Due to low crack density the stress, $\sigma_T$ in an unbroken element is equal to the CLT value, $\sigma_T = \sigma_{T0}$ . The number of broken elements at stress $\sigma_{T0}$ can be expressed through the crack density

$$M_{cr} = L \cdot \rho_k(\sigma_{T0}) \quad (4)$$

The probability $P_{in}(\sigma_{T0})$ of element cracking at stress $\sigma_{T0}$, can be defined as the number of elements with cracks $M_{cr}$ versus the total number of elements $M$ in the ply

$$P_{in} = \frac{M_{cr}}{M} = \frac{\rho_k(\sigma_{T0})}{\rho_{k,max}} \quad (5)$$

The transverse stress is calculated using CLT from the applied load (or strain) and from the temperature difference $\Delta T$ between manufacturing and testing conditions

$$\sigma_{T0} = \sigma_{T0}^{mech} + \sigma_{T0}^{thermal} \quad (6)$$

Standard procedure has to be applied to determine parameters in the distribution (3) and to check its validity. The experimental probability of failure data is presented as $\ln(-\ln(1 - P_{in}))$ against $\ln(\sigma_{T0})$. Data following Weibull distribution will then have a linear dependence. Using linear fit to these data we obtain parameters $m$ and $\sigma_{in0}$ in (3).

More accurate values of Weibull parameters can be found performing Monte-Carlo simulations and comparing with experiment or using the probabilistic approach developed in [**25**]. Both

approaches require reliable analytical models for stress distribution between two cracks, which are applicable for high crack density.

The Weibull distribution (3) for crack initiation strength with parameters $m$ and $\sigma_{in0}$ identified can be used together with (5) to predict the density of the initiated cracks, $\rho_k$ in an arbitrary k-th layer of a multidirectional laminate subjected to known general quasi-static thermo-mechanical loading.

## 3.2 Cyclic loading (fatigue) effect on intralaminar crack initiation strength

The resistance to transverse failure in a given position is changing as a result of cyclic loading (fatigue). To adapt the Weibull distribution to cyclic loading, we have to make several assumptions.

The non-uniform fiber distribution is the same in the quasi-static and in the cyclic test (the same composite). Therefore we assume that the weakest position in the layer regarding crack initiation in the quasi-static loading is also the weakest position in cyclic loading. We assume the same about the next weakest position, etc. In this approach the Weibull shape parameter $m$ is a measure on the layer scale of the fiber distribution non-uniformity and, hence, it has the same value in both tests.

An alternative discussion with a very different conclusion would start with assuming existing defect state as usual in Weibull statistics. It is reasonable to expect that the initial defects of different size would have different evolution during the cyclic loading. The larger defects would grow faster than the small ones (for example, following Paris law, if applicable). That would result in larger defect size variation, which means that the Weibull shape parameter $m$ would be reduced. Both described alternatives regarding the shape parameter will be inspected in Section 4.4 comparing results from quasi-static and cyclic loading tests.

We assume that the cyclic loading leads to an overall reduction of the resistance of the layer to transverse failure initiation. In terms of (3) it can be interpreted as a monotonous decrease of the scale parameter$\sigma_{in0}$ with the number of cycles and the stress level during the cyclic loading. For example, the stress characterizing parameter could be the maximum stress in the cycle $\sigma_T^{fat}$. We will inspect the applicability of the following simple function:

$$\sigma_{in0} = \sigma_0 N^{-\alpha} \left(\frac{\sigma_T^{fat}}{\sigma_{F0}}\right)^{-\gamma}, \qquad \gamma \geq 0 \qquad \alpha \geq 0 \qquad N \gg 1 \qquad (7)$$

Parameters $\sigma_0$ , $\alpha, \gamma$ and $\sigma_{F0}$ are unknown material constants. Substituting (7) in (3) we obtain the following expression for probability of intralaminar cracking in the layer under cyclic loading

$$P_{in} = 1 - exp\left[-\frac{V}{V_0} N^n \left[\left(\frac{\sigma_{T0}^{fat}}{\sigma_{F0}}\right)^{\gamma} \frac{\sigma_{T0}}{\sigma_0}\right]^m\right] \quad (8)$$

In (8) a new unknown constant $n = \alpha \cdot m$ was introduced. This expression describes the distribution of the residual initiation strength after N cycles at $\sigma_T^{fat}$ and the intralaminar cracking dependence on the transverse stress $\sigma_{T0}$ in successive quasi-static loading. Without losing generality we can assume that both unknown parameters are equal

$$\sigma_{F0} = \sigma_0 \quad (9)$$

For cracking analysis in a purely cyclic test $\sigma_{T0} = \sigma_T^{fat}$ and expression (8) becomes

$$\frac{\rho_k\left(\sigma_{T0}^{fat},N\right)}{\rho_{k,max}} = 1 - exp\left[-\frac{V}{V_0} N^n \left(\frac{\left(\sigma_{T0}^{fat}\right)^{1+\gamma}}{\sigma_0^{\gamma+1}}\right)^m\right] \quad (10)$$

or

$$\frac{\rho_k\left(\sigma_{T0}^{fat},N\right)}{\rho_{k,max}} = 1 - exp\left[-\frac{V}{V_0} N^n \left(\frac{\sigma_{T0}^{fat}}{\sigma_0}\right)^{m(1+\gamma)}\right] \quad (11)$$

According to equation (11) the shape parameter for the stress dependence in (11)

$$m^* = m(1+\gamma) \quad (12)$$

is larger in cyclic loading than in quasi-static loading. The value of $\gamma$ will be estimated by analysing the cyclic loading tests. With regard to the fiber clustering, it is expected that $\gamma \ll 1$ and its effect can not be distinguished from the measurement errors. This conclusion is confirmed by the experimental results presented in **Section 4.4**. The expression used in following is

$$\frac{\rho_k\left(\sigma_{T0}^{fat},N\right)}{\rho_{k,max}} = 1 - exp\left[-\frac{V}{V_0} N^n \left(\frac{\sigma_{T0}^{fat}}{\sigma_0}\right)^{m}\right] \quad (13)$$

An similar expression based on different arguments was suggested in **[32].**

The following methodology is suggested for parameter determination in expression (13):

- Use the measured crack density with respect to the strain in quasi-static test to find the parameter $m$
- Use one "representative" stress level for cyclic test and determine $n$ and $\sigma_0$

In this paper several stress levels in the cyclic loading will be used to justify the assumption $\gamma \ll 1$ and to validate the assumed power law dependence of the scale parameter on $N$ as in (13).

# 4. Results and analysis

An edge view of two [-45/90/+45/0]s NCF specimens with intralaminar cracks in all off-axis layers introduced in quasi-static loading are shown in **Figure 1c** and **1d**. In all off-axis plies these cracks cover the whole thickness of the layer. Edge grinding followed by inspection with optical microscopy and CT confirmed that cracks in the 90-plies not only cover the whole ply thickness but they also go through the whole width of the specimen from one edge to another forming well defined tunnels. In **Figure 3a** the average value of the crack density for four specimens is presented as a function of the strain level in the quasi-static tests. The crack density growth during cyclic loading is shown in **Figure 3b**.

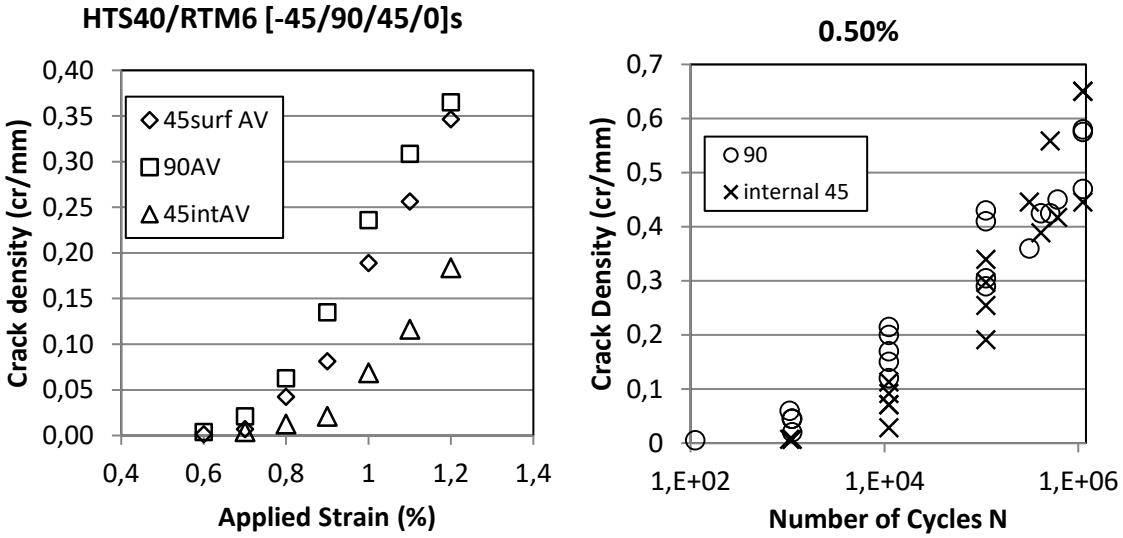



***Figure 3: Intralaminar crack density in layers of [-45/90/+45/0]s laminate: a) as a function of the applied strain in quasi-static tensile loading; b) as a function of number of cycles under 0.5% strain cyclic loading.***

## 4.1 Cracks in 45-plies

It is noticeable that the cracking in the -45, +45 and 90-plies in the quasi-static loading starts at the same strain level and in the cyclic loading at the same number of cycles. This feature

becomes even more peculiar when the crack density is presented versus the CLT stress in the ply, as in **Figure 4**: cracking in the 45-plies starts at much lower transverse stress than in the 90-ply. This result contradicts with any stress or energy based failure criterion.

The first explanation coming in mind is the presence of the shear stress $\sigma_{LT}$ in the 45-plies, which would contribute to the crack initiation (similar to the shear stress and transverse stress interaction in the quasi-static Tsai-Hill criterion). However, at 1% applied strain the transverse thermo-mechanical stress in the 45-ply is 81.4 MPa whereas $\sigma_{LT} = 52\ MPa$. In fatigue test at 0.5% $\sigma_{LT} = 26\ MPa$ and $\sigma_T = 60.7\ MPa$ . The shear stress contribution (for example, when using the equivalent stress) would slightly shift the curves in **Figure 4** but not by almost 50 MPa as can be seen in **Figure 4**. Therefore we omit the mixed mode effects as a possible explanation for cracking behavior of the 45-plies.

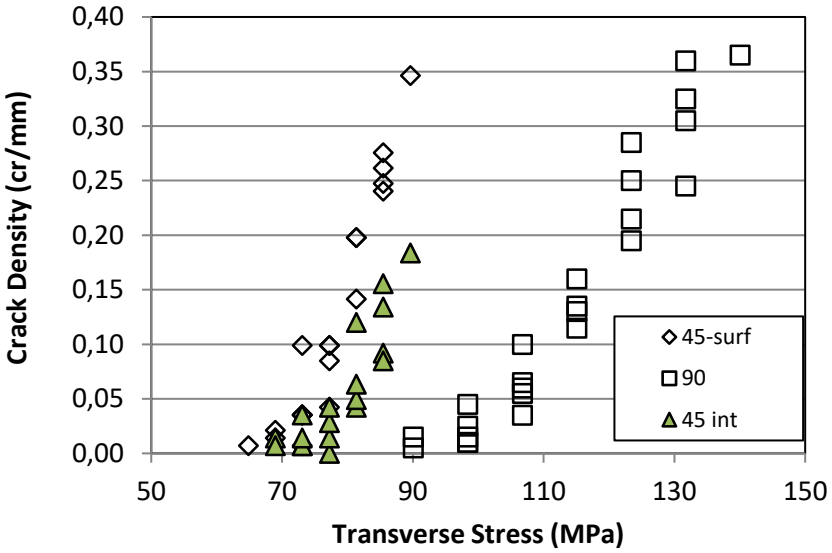



***Figure 4: Crack density in off- axis plies versus the transverse stress in the layer for $[-45/90/45/0]_s$ laminate subjected to quasi-static loading.***

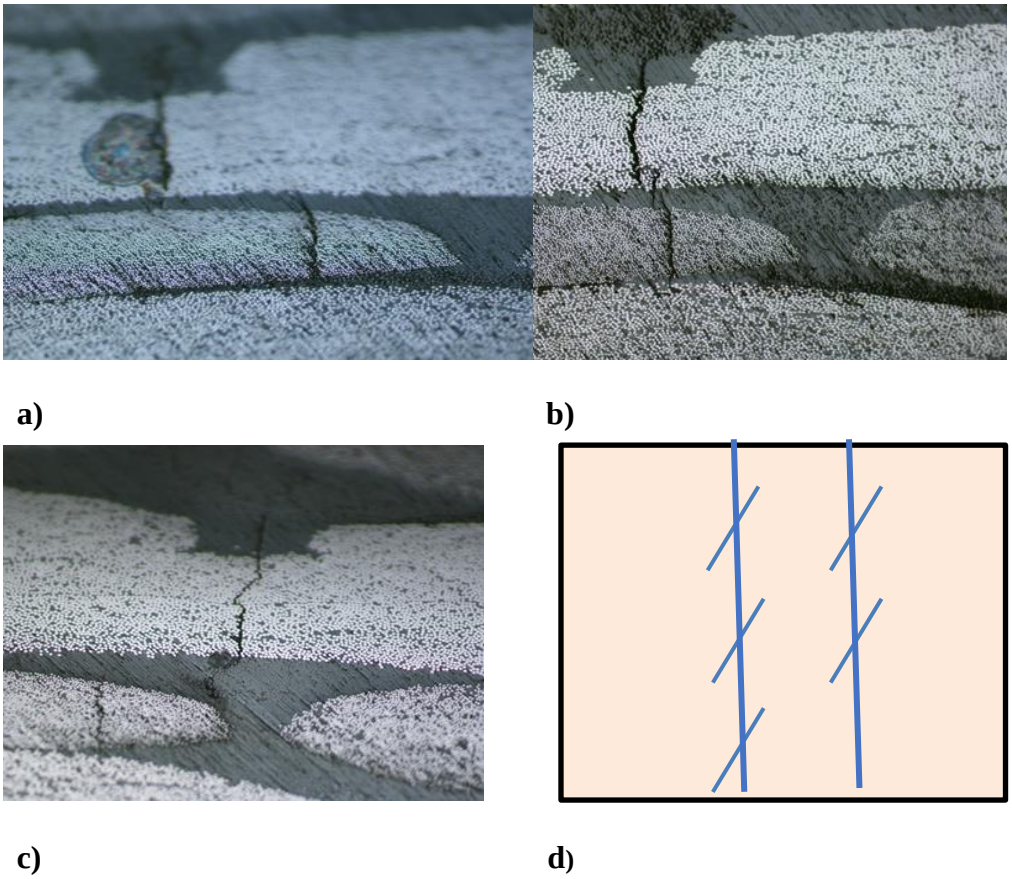



***Figure 5: Intralaminar cracks in 45-plies: (a)-( c) Optical micrographs of cross-sections perpendicular to the fiber orientation in the +45-ply at several positions along the fiber direction; (d) schematic surface view showing intralaminar cracks of limited length in the local stress concentration region caused by cracks in the 90-ply.***

The performed CT and also the specimen edge grinding and optical observation showed that the 45-ply cracks form in regions, where the 90-ply crack meets the interface with the 45-ply. Thus the reason for the premature cracking in the 45-plies is the local stress-concentrations appearing as soon as cracks appear in the neighboring 90-ply. **Figure 5 a-c** shows optical micrographs taken in cross-sections perpendicular to the fiber orientation in the +45-ply. A well-defined intralaminar crack in the +45-ply can be seen close to the matrix region between the bundles . An intralaminar crack in the 90-ply on the top of the +45-ply and the stitching yarn parallel to the fibers in the 90-ply are seen to “move” from the left to the right when several micrographs are taken in different positions along the fiber direction in the +45-ply. The +45-ply crack is a very well-defined tunnel from one ply interface to another. Simple geometrical estimate shows that the distance between micrographs in **Figure 5a** and **c** in the

+45-ply direction is at least 4-5 times the ply thickness, which means that the length of this particular tunneling +45-ply crack is at least 1.2 mm.

Measurements using CT show that the 45-ply cracks are of limited length, which increases with the applied load or with number of cycles. Usually they do not build perfect tunnels extending from one edge of the specimen to another one. Rather it is a system of short (0.5-2.0 mm) but well defined intralaminar cracks along the fiber direction and their propagation can be shielded by another system of cracks originating from the next 90-ply crack region, see **Figure 5d**. In spite of the finite length, the average number of the 45-ply cracks in any cross-section perpendicular to the fiber direction in the ply is almost the same. This observation motivates the use of crack density to characterize this type of cracking. Dependent on the stress level in the local stress concentration zone, the distance between the 45-ply cracks caused by the same 90-ply crack should be larger than at CDS. Therefore, due to finite length only the closest crack to the observed cross-section reached this section.

The CT image in **Figure 6** confirms that all 45-ply cracks cover the whole thickness of the ply. It shows that the crack distribution in the considered area is very non-uniform: there is one crack in the bottom surface ply and no cracks in the top ply. There are in total five cracks in both internal 45-plies.

To authors' knowledge, this type of cracks was first characterized using X-ray images in **[37],** where they were called micro-cracks originated from matrix cracks. Unfortunately, only the specimen surface view is provided in **[32]** and it is not possible to analyze the crack size in the ply thickness direction. In **[38],** performing thermal fatigue tests at cryogenic temperatures on quasi-isotropic laminates these cracks, due to their appearance, were called "stitch cracks" and they were observed close to the cracks in thick 90-plies. Similar phenomenon was found in quasi-static tests performed in **[34]**: in quasi-isotropic laminates the internal 45-plies adjacent to the 90-ply had many more cracks than the internal plies of the same orientation not in a contact with the 90-ply.

It appears that the 45-ply cracks caused by cracks in the adjacent 90-ply propagate fast through the high stress region and their propagation slows down or stops when they exit the high stress region. An accurate stress concentration analysis has to be performed before the initiation and growth of these cracks can be analyzed quantitatively.

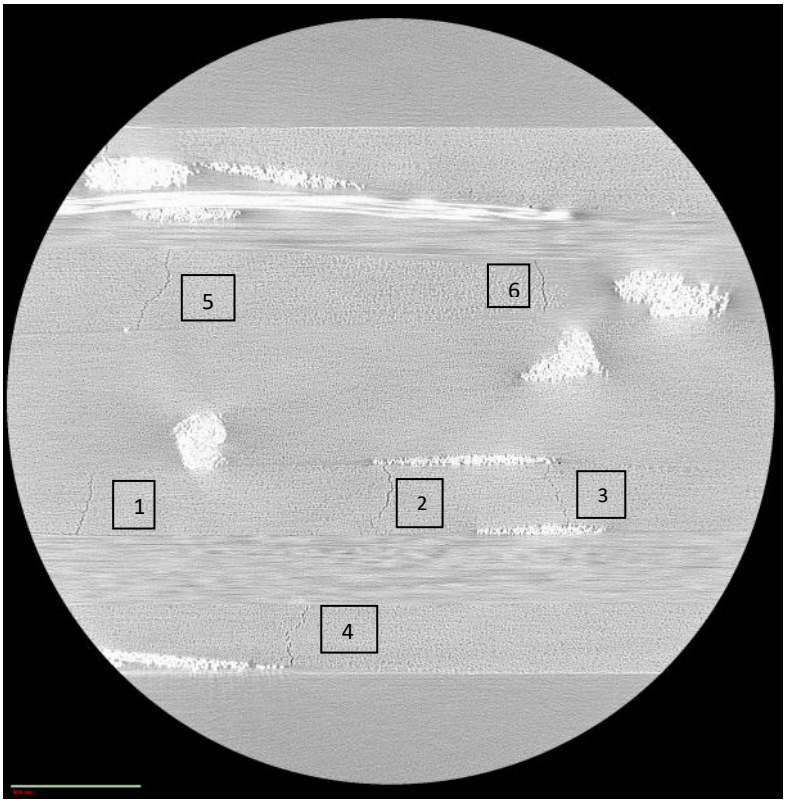



***Figure 6: Micro CT image of five cracks in the internal 45-plies and one crack in the surface -45-ply after 500 000 cycles at 0.5% strain. Cross-section of the laminate perpendicular to the fiber direction in the central 0-ply.***

The crack density in the surface -45-ply and in the 90-ply is very similar. In the internal +45-ply the crack density is systematically lower. The observed higher crack density in the surface -45-ply comparing with the internal 45-ply is easy to explain: propagation of a crack linked with the free surface requires much less energy.

## 4.2 Quasi-static loading: data reduction

In order to perform statistical analysis for the cracks in the 90-layer by finding Weibull parameters $m$ and $\sigma_{in0}$ as described in Section 3.1, the thermo-mechanical transverse stress in the 90-layer was first calculated using CLT. The highest crack density in the 90-layer is much lower than the saturation value, which is close to 4 cracks/mm for the layer thickness of 0.25 mm and therefore the simple analysis proposed in Section 3.1 is applicable. The crack density was recalculated to probability of failure $P_{in}$ using (5). According to (3) with $V = V_0$

$$\ln(-\ln(1 - P_{in})) = m \ln \sigma_T - m \ln \sigma_{in0} \quad (14)$$

The data from all four specimens are presented in **Figure 7a** and **b** as $\ln(-\ln(1-P_{in}))$ versus $\ln\sigma_T$. The data in both figures are the same, but the fitting procedure is different. Whereas, in **Figure 7a** all data points were used to find the linear trendline using the method of least squares , in **Figure 7b** the first 8 data points (two for each specimen) are ignored when calculating the trendline. The reason is that the first data points (stress when the first crack appears) are very unreliable: one specimen could have zero cracks at selected stress (in this case the ln(-ln()) value would be $-\infty$ ), whereas another specimen may have one crack or two cracks with very different value of ln(-ln()). The calculated $m$ values in both fittings are rather different. Fitting in **Figure 7a** using all points ( $m = 10.74$ $\sigma_{in0} = 163.1\ MPa$ ) seems to be slightly better, with only the last points deviating from the main linear trend. However, these last points are of most significance and reliability. At this crack density the interaction between the cracks is still low. In contrary, the first experimental data points are less reliable and therefore we consider the trendline in **Figure 7b** as more representative and the values $m = 7.11$ and $\sigma_{in0} = 187.5\ MPa$ are used in following as representative values from the quasi-static test.

The sensitivity of the predicted crack density with respect to the $m$ value is shown in **Figure 7c** and **d**. Both approximations are used to self-predict the increase of crack density. Predictions are very similar and the difference is noticeable only at stresses higher than 100 MPa. It is rather obvious that fitting using $m = 7.11$ leads to better agreement. Nevertheless, it has to be noted that the sensitivity of predictions with respect to $m$ is rather low and, therefore, there is no practical meaning in its very accurate determination.

## 4.3 90-ply cracks in cyclic loading

First, we inspect the applicability of the statistical model (13) by analyzing the experimental data in **[36]** where tension-tension fatigue tests were conducted on $[0/90_m/0]$ T800H/3631cross-ply specimens, determining the number of cycles for the first intralaminar crack to appear. Cyclic tests were performed at several levels of maximum strain, finding that independent on the 90-layer thickness the relationship between the strain and the number of cycles for the first crack to appear is linear, when presented in logarithmic axes. The following experimental relationship was established:

$$\Delta\varepsilon N^{\alpha} = const \qquad (15)$$

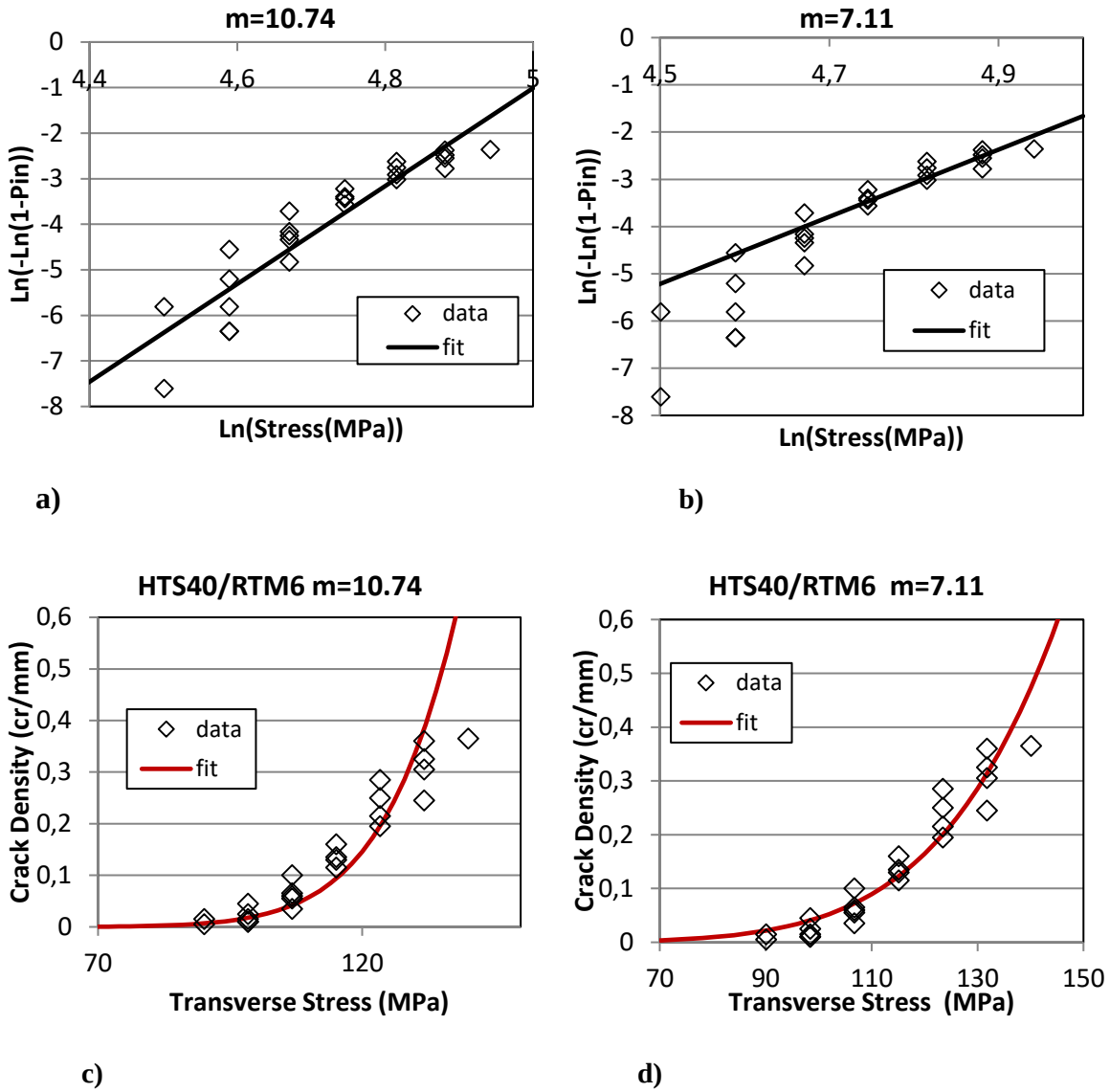



***Figure 7: Weibull analysis of the crack density in the 90-layers of [-45/90/+45/0]s specimens: a) and b): fit of data in logarithmic axes using all points (a) and neglecting the first two for each specimen (b); c) and d): experimental data and fitting using the obtained Weibull parameters.***

The same type of relationship follows also from (13) considering combinations of conditions to reach any predetermined crack density. It can be reached in many combinations of the applied stress and the number of cycles (the first crack is one particular case of this analysis). From (13) follows that the condition for reaching the same crack density is to have

$$N^n \left(\frac{\sigma_{T0}^{fat}}{\sigma_0}\right)^m = const \qquad (16)$$

in all the performed tests. Of course, there is a difference in formulation: in **[36]** $\Delta\varepsilon = \varepsilon_{max} - \varepsilon_{min}$ was used whereas in (13) we used the maximum stress values. The discussion of this difference is not the topic here: the important thing is that in both formulations there is a power function relationship between the number of cycles to introduce the first crack and the load level, and, hence, (13) is not contradicting these earlier experimental observations.

In the present paper the cyclic testing was conducted at five maximum strain levels ( $\varepsilon_{x,max} = 0.4; 0.45; 0.50; 0.55; 0.60$ %) interrupting the test after certain number of cycles and determining the crack density as described in Section 2. Four specimens for each level were used. The thermo-mechanical transverse stresses in the 90-layer corresponding to these strains are 73.4; 77.6; 81.8; 85.9 and 90.1 MPa. It has to be noted that the macroscopic stress ratio was $R = 0.1$ but the transverse stress ratio in the 90-layer when the thermal stress is included was different. For example, in the test with $\varepsilon_{x,max} = 0.4\%$ the maximum stress was $\sigma_{T0}^{fat} = 73.4\ MPa$ and the minimum value 43.4 MPa leading to $R_{90} = 0.59$ in the 90-layer. The ratio decreases with increasing mechanical stress component reaching 0.50 in the test with $\varepsilon_{x,max} = 0.6\%$. The R-effect was studied in **[29]** showing that at higher R the fatigue resistance is higher but the sensitivity is not high enough to make conclusions for the region used in our tests.

The crack density versus the number of cycles for the four strain levels is shown in **Figures 8** and **9**. From (13)

$$\ln(-\ln(1 - P_{in})) = n \ln N + m \ln \frac{\sigma_{T0}^{fat}}{\sigma_0} + \ln \frac{V}{V_0} \qquad (17)$$

According to (17) the $\ln(-\ln(1 - P_{in}))$ dependence on $\ln N$ has to be linear with the slope coefficient being equal to $n$. The cyclic test data are presented in this form, see **Figure 10,** for two strain levels. Similarly as in quasi-static loading, the data points corresponding to first cracks (extremely low crack density) are not reliable. For this reason the first 3 points in **Figure 10 a** were not used when the linear regression curve was obtained. In **Figure 10 b** the first point to the left was not included. Similar data reduction was performed for all groups of specimens tested at different strain levels obtaining parameter $n$ from the slope of the fitting curve. The free term $b$ in the fitting equation according to (17) is linked to the rest of constants

$$b = m \ln \frac{\sigma_{T0}^{fat}}{\sigma_0} \qquad (18)$$

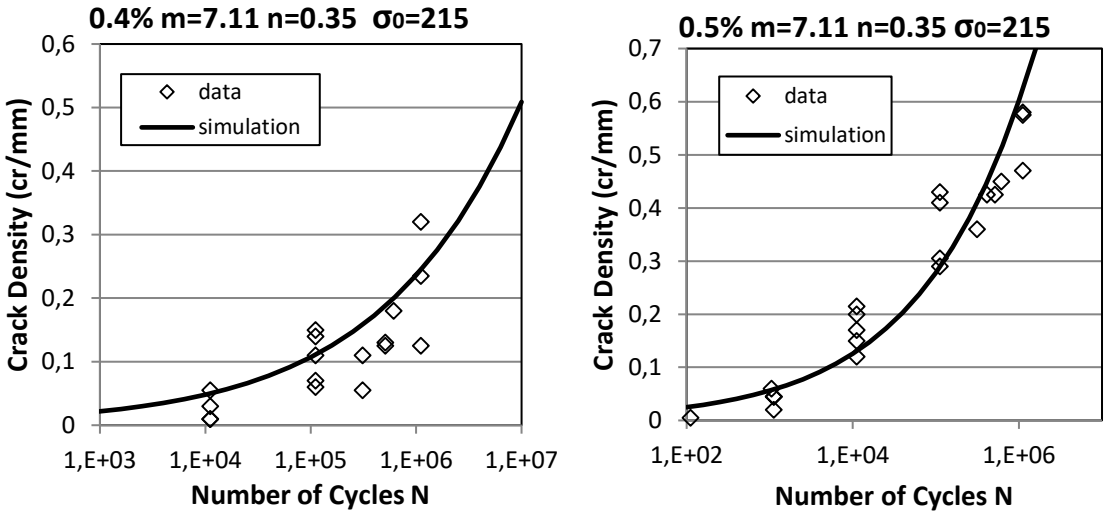
Assuming that parameter $m$ has the same value as in the quasi-static test, i.e., $m = 7.11$, we calculated all other parameters as summarized in **Table 1.** These parameters obtained from

tests at different loads are slightly different (note that $\sigma_0$ is systematically larger than $\sigma_{in0}$ ). However, we could not see any obvious trend in the variation and, since all discussions in Section 3 are based on assumption that $m$ and $\sigma_0$ do not depend on the stress level, in following we use $n = 0.35$ and $\sigma_0 = 215\ MPa$. This selection is quite arbitrary and does not coincide with any of the data presented in **Table 1** and neither is it a calculated average. The selection is motivated by ambition to demonstrate that the simulation results are not sensitive with respect to this choice.

| $\varepsilon_{x,max}(\%)$ | 0.4 | 0.45 | 0.5 | 0.55 | 0.6 |
|---|---|---|---|---|---|
| $\sigma_{T0}^{fat}(MPa)$ | 73.4 | 77.6 | 81.8 | 85.9 | 90.1 |
| $n$ | 0.29 | 0.44 | 0.35 | 0.32 | 0.34 |
| $\sigma_0(MPa)$ | 246 | 256 | 210 | 222 | 208 |

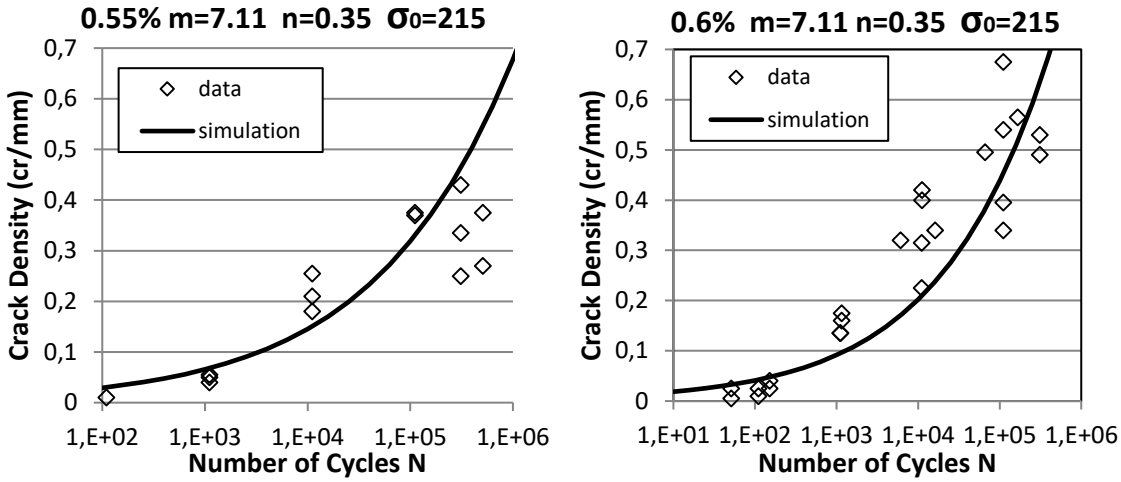
***Table 1: Values of parameters in distribution (13) assuming $m = 7.11$***

The adequacy of this approximation is demonstrated in **Figures 8** and **9,** where the fatigue test data for several used load levels are presented together with predictions based on these values of $m, n$ and $\sigma_0$.




**a)** b)

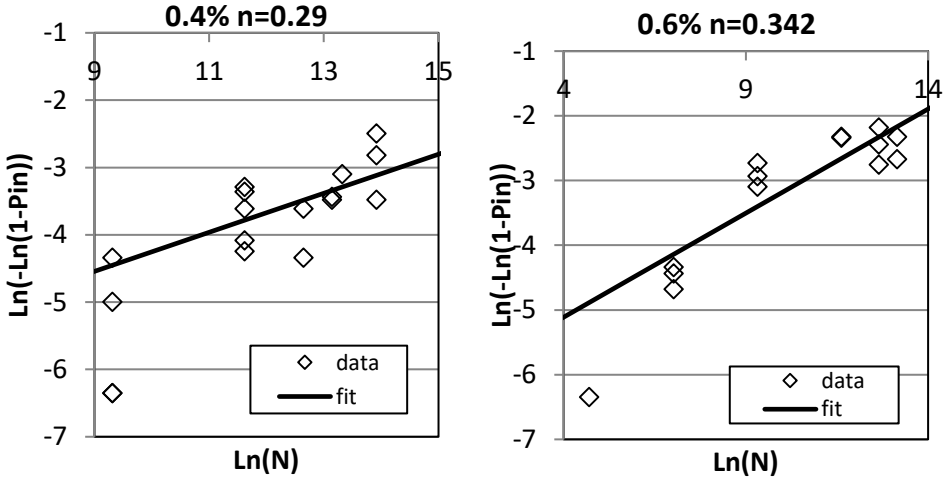
***Figure 8 Crack density growth with the number of cycles: a) 0.4%; b) 0.5% strain cyclic tests.***




a) b)

***Figure 9: Crack density growth with the number of cycles: a) 0.55%; b) 0.6% strain cyclic tests.***

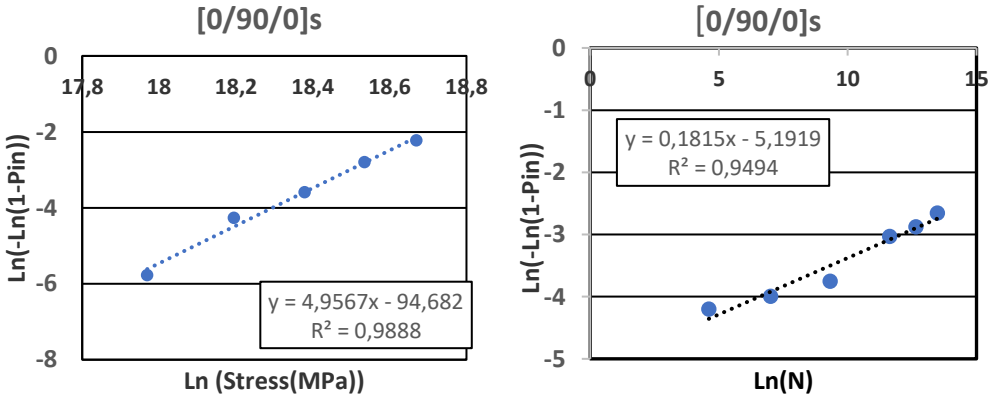
Considering the data scatter, the simulation accuracy is good but not perfect. Any systematic differences were not noticed. Rather large local delaminations developed from intralaminar crack tips during testing at 0.6%. However, the crack density in these tests is rather low and the rate of cracking was not noticeably affected by the additional stress state weakening between cracks caused by delaminations.




**a)** **b)**

***Figure 10: Probability of intralaminar cracking in the 90-ply of [-45/90/+45/0]s specimens versus the number of cycles in logarithmic axes and linear fit to data using (13): a) 0.4% strain; b) 0.6% strain.***

The assumptions in the proposed crack density growth model regarding the power function dependence on the stress and on the number of cycles were checked in quasi-static and cyclic tests on thin ply TR50S/EP cross-ply laminates with 90-ply thickness of 0.15 mm. The crack density in this very thin ply was very low. One specimen was tested in quasi-static test and another one in cyclic test corresponding to 0.5% strain.



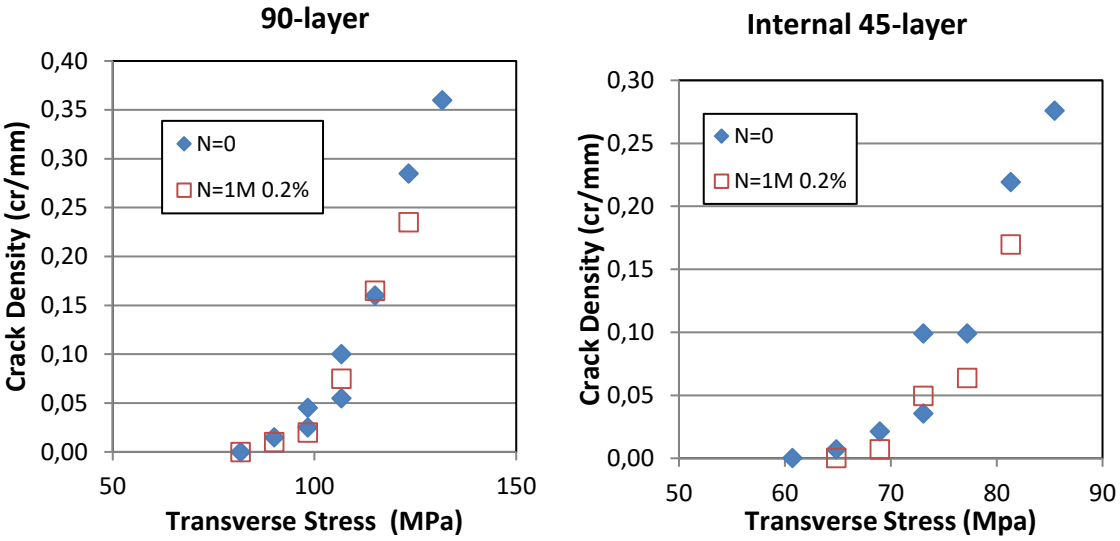

**a)** **b)**

***Figure 11: Intralaminar cracking TR50S/EP cross-ply laminate: a) dependence on stress in quasi-static loading; b) dependence on number of cycles in cyclic loading corresponding to 0.5% strain***

Even for this composite the stress dependence of the probability of failure in quasi-static test and the dependence on number of cycles in cyclic test follows the power law, see **Figure 11**. As typical for pre-preg tape laminates, the data scatter for cracking is much lower than for the NCF laminates.

Finally, we will check the validity of the model with parameters given above for a case with $\varepsilon_{x,max} = 0.2\%$ where after 1 million load cycles two cracks in the 90-ply over 100 mm distance were observed. Calculations using (13) give 4 cracks per 100 mm, which, due to high variability in the onset of first cracks, is a good agreement. The crack density after 1 million load cycles is so low that we can define this strain level as a "threshold" for fatigue. According to our model there is no threshold, cracks would appear even at lower stress, only the number of cycles for that would be much higher. After the cyclic test (N=$10^6$, $\varepsilon_{x,max} = 0.2\%$) the same specimen was subjected to quasi-static loading obtaining crack density with respect to transverse stress. The purpose of this exercise was to see whether there is any noticeable overall reduction of the cracking resistance as the result of the performed cyclic loading. The crack

density in the 90-ply and also in the internal 45-layers of this specimen is presented in **Figure 12,** where the crack density for two non-cycled specimens is also shown for reference.



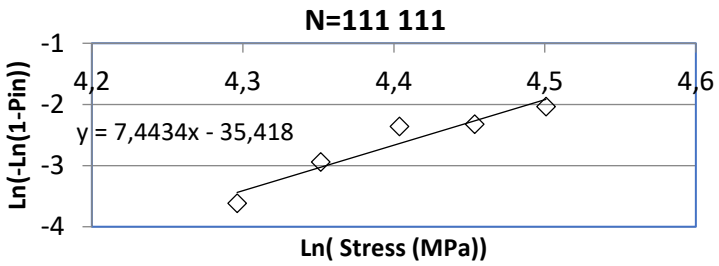

**a)** **b)**

***Figure 12: Intralaminar cracking in a) 90-layer; b) internal 45-layer of [-45/90/45/0]s specimens in quasi-static test. Cycled (N=1M (1 million cycles) at 0.2% maximum strain) and non-cycled (N=0) specimens.***

As shown in **Figure 11**, there is no effect of the cycling on cracking in the subsequent quasi-static loading. The crack density in the cycled specimens is even slightly lower than in the non-cycled specimens, which is most probably only due to the scatter.

## 4.4 The Weibull shape parameter

In Section 4.3 we used the shape parameter $m = 7.11$ from quasi-static tests, assuming that it represents the non-uniform distribution of the fibers and is therefore also valid in cyclic loading. However, with the data obtained in cyclic tests at different stresses, we can obtain the $m$ value independently. According to (17) at fixed $N$ the relationship between $\ln(-\ln(1-P_{in}))$ and the maximum stress in the cycleln $\sigma_{T0}^{fat}$ is linear.



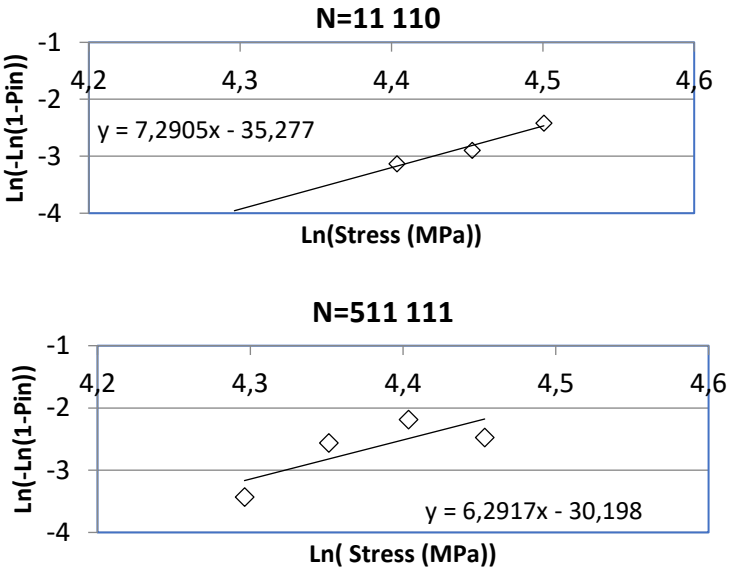



***Figure 13: The probability of cracking presented as $ln(-ln(1-P_{in}))$ versus $ln\,\sigma_{fat}$ after certain number of cycles N. Linear fit to data and the fitting equation to find the shape parameter $m$ are also shown.***

This relationship after $N = 11\,110;\ 111\,111;$ and $511\,111$ cycles is presented in **Figure 13,** where also linear fit and the fitting equations are shown. Each data point in the figure with certain number of cycles corresponds to different specimen, which explains the high scatter. The obtained $m$ values are: 7.29; 7.44 and 6.29 correspondingly. The average value $m = 7.01$ is sufficiently close to the before used value 7.11 obtained in quasi-static tests.

Hence, the performed cyclic tests do not present any evidence that the stress related shape parameter in Weibull distribution should be different (smaller) in cyclic loading than in quasi-static loading, thus, confirming the hypothesis in Section 3.2 that this parameter is related to the non-uniformity of the fiber distribution in composite.

# 5. Conclusions

Simple probabilistic model is presented for simulation of intralaminar crack density increase in cyclic loading. The model is limited to low stress levels and to low crack densities. This model complements the existing phenomenological model for cyclic loading valid in high crack density region, in which the crack density growth rate change is governed by the crack interaction.

Different positions in a ply require different level of the nominal stress for a crack to appear and this variation is described by Weibull distribution. We assume that the variability described by the Weibull shape parameter is related to the inherent fiber distribution non-uniformity in the composite. Further assuming that the weakest position in tensile quasi-static loading is also the weakest position in tension-tension cyclic loading, the Weibull's shape parameter with respect to stress is the same in both cases, which is proven experimentally in this work. It is further assumed that the Weibull scale parameter, which is related to the residual strength reduces in cyclic loading. The reduction with the number of cycles is described by a power function. The performed cyclic tests confirm applicability of these shape functions and allow to determine the involved parameters.

The required amount of testing to find the parameters for the proposed model is significantly reduced, since part of the parameters are determined from quasi-static tests and part from cyclic loading tests.

It was found that intralaminar cracks in the 45-plies are initiated in local stress concentration zones, where the adjacent 90-ply has cracks. The 45-ply cracks cover the ply thickness, they propagate fast along fibers in the stress concentration zone but the growth slows down and eventually stops after existing the high stress zone.

## Acknowledgments.

This work was performed within the Swedish Aeronautical Research Program (NFFP6), Project 2014-00882, jointly funded by the Swedish Armed Forces, Swedish Defense Material Administration, the Swedish Governmental Agency for Innovation Systems and GKN Aerospace Sweden. The research was also funded through the Joint European Doctoral Program in Material Science and Engineering (DocMase). Authors would like to thank prof. R. Joffe for performed CT studies.

# References


1. Reifsnider KL and R Jamison, Fracture of fatigue-loaded composite laminates, Int J of Fatigue, 1982, 187-197.
2. Sisodia S, EK Gamstedt, F Edgren and J Varna, Effects of voids on quasi-static and tension fatigue behaviour of carbon-fibre composite laminates, J of Composite Materials; 49 (17), 2015, 2137-2148.
3. Parvizi, A, and Bailey, J, On multiple transverse cracking in glass fibre epoxy cross-ply laminates, J of Materials Science, 13(10), 1978, 2131-2136.
4. Quaresimin M, Carraro PA, LP Mikkelsen, N Lucato, L Vivian, P Brøndsted, BF Sørensen, J Varna, R Talreja, Damage evolution under cyclic multiaxial stress state: A comparative analysis between glass/epoxy laminates and tubes, Composites Part B: Engineering, 61, 2014, 282-290.
5. Varna J, Modeling Mechanical Performance of Damaged Laminates, J of Composite Materials, 47(20-21), 2013, 2443-2474.
6. Singh CV and R Talreja, A Synergistic Damage Mechanics Approach to Mechanical Response of Composite Laminates with Ply Cracks, J of Composite Materials, Volume: 47( 20-21), 2013, 2475-2501.
7. Kashtalyan M, C Soutis, Stiffness and fracture analysis of laminated composites with off-axis ply matrix cracking, Composites: Part A 38, 2007, 1262-1269.
8. Kashtalyan M, Soutis C. Analysis of composite laminates with intra- and interlaminar damage. Progress in Aerospace Sciences, 41, 2005:152-173.
9. París F, Cano J, and Varna J, The fiber-matrix interface crack—a numerical analysis using boundary elements, Int. J. Fract., 82(1), 1990, 11-29.
10. Zhuang L, R Talreja and J Varna, Transverse crack formation in unidirectional composites by linking of fibre/matrix debond cracks, Composites Part A, 2018, 107, 294-303.
11. Sandino C, Correa E, and París F, Numerical analysis of the influence of a nearby fibre on the interface crack growth in composites under transverse tensile load, Engineering Fracture Mechanics, 168, Part B, 2016, 58-75.
12. Zhuang L, Pupurs A, Varna J, Talreja R, Ayadi Z, Effects of inter-Fiber spacing on fiber-matrix debond crack growth in unidirectional composites under transverse loading, Composites Part A, 2018, 109, 463-471.

13. Varna J, Zhuang L, Pupurs A, Ayadi Z, Growth and interaction of debonds in local clusters of fibers in unidirectional composites during transverse loading, Key Engineering Materials, v.754, 2017, 63-66.
14. Herráez M, D Mora, F Naya, CS Lopes, C González, J LLorca, Transverse cracking of cross-ply laminates: A computational micromechanics perspective, Composites Science and Technology, 110, 2015, 196-204.
15. Paris F, A Blazquez, LN McCartney, V Mantic, Characterization and evolution of matrix and interface related damage in [0/90]S laminates under tension. Part I: Numerical predictions,Composites Science and Technology 70, 2010, 1168–1175.
16. Dvorak GJ, N Laws, Analysis of progressive matrix cracking in composite laminates II. First ply failure, J. of Composite Materials, 21, 1987, 309-329.
17. Nairn J, The strain energy release rate of composite microcracking: a variational approach, J of Composite Materials, 23(11), 1989, 1106-1129.
18. Nairn JA, S Hu and JS Bark., A critical evaluation of theories for predicting microcracking in composite laminates, J Mat. Sci., 28, 1993, 50-99.
19. Johnson P, Chang F., Characterization of matrix crack-induced laminate failure – Part II: Analysis and verification, J of Compos. Materials, vol. 35 (22), 2001, 2037-2074.
20. Varna J., Crack separation based models for microcracking, Elsevier, Comprehensive Composite Materials II, V. 2, 2018, 192-220.
21. Liu S and J. A. Nairn, "A Fracture Mechanics Analysis of Composite Microcracking: Fatigue Experiments," Proc. of the 5th Meeting of the American Society of Composites, 1990, 287-295.
22. Nairn JA, Microcracking, Microcrack-Induced Delamination, and Longitudinal Splitting of Advanced Composite Structures,NASA Contractor Report 4472, November 1992.
23. Hashin Z., Analysis of cracked laminates: a variational approach. Mech of Mater, North-Holland 4, 1985, 121-136.
24. Mohammadi B, Pakdel H, Fatigue driven matrix crack propagation in laminated composites, Materials and Design, 146, 2018, 108–115.
25. Hajikazemi M, Sadr MH, Hosseini-Toudeshky H, Thermo-elastic constants of cracked symmetric laminates: A refined variational approach. Int J Mech Sci; 89: 2014, 47–57.
26. McCartney LN and Schoeppner GA and Becker W, Comparison of models for transverse ply cracks in composite laminates, Comp. Sci. Technol., 60, 2000, 2347-2359.

27. Peters PWM, The strength distribution of 90-plies in 0/90/0 Graphite-Epoxy laminates, J of Composite Materials, 18, 1984, 545-556.
28. Manders P.W., Chou T-.W., Jones R.J., ROCK J.W., Statistical analysis of multiple fracture in 0°/90°/0° glass fibre/epoxy resin laminates, J of Materials Science, vol. 18, (10), 1983, 2876-2889.
29. Tong J, F Guild, SL Ogin & PA Smith, On matrix crack growth in quasi-isotropic laminates- I. Experimental investigation, Composites Science and Technology 57, 1997, 1527-1535
30. Varna J, Quantification of damage and evolution modeling in multidirectional laminates, Proc. of the 27th RISÖ International symposium on material science, Roskilde, Denmark, 2006, 349-356.
31. Huang, Y, J Varna, R Talreja, Statistical Methodology for Assessing Manufacturing Quality Related to Transverse Cracking in Cross Ply Laminates, Composites Science and Technology, 95, 2014,100-106.
32. Carraro PA, L Maragoni, M Quaresimin, Prediction of the crack density evolution in multidirectional laminates under fatigue loading, Composites Science and Technology, 145, 2017, 24-39.
33. Quaresimin M, PA Carrao, L Maragoni, Influence of load ratio on the biaxial behavior and damage evolution in glass/epoxy tubes under tension-torsion loading, Composites: Part A, 78, 2015, 294-302.
34. Varna J and H Zrida, Analysis of microdamage in thermally aged CF/Polyimide laminates, Mechanics of Composite Materials, vol. 53(1), 2017, 45-58.
35. Joffe R, J Varna and LA Berglund, Acoustic Emission Signals from Composite Laminates with Well Known Fatigue Damage Characteristics, AECM -5 , 10-14 July 1995, Sundsvall, Sweden,179-186.
36. Takeda N, Sh Ogihara and A Kobayashi, Microscopic damage progress in CFRP cross-ply laminates, Composites, 26, 1995, 859-867.
37. Johnson P, Chang F. Characterization of matrix crack-induced laminate failure – Part I: Experiments, J of Compos Materials, vol. 35 (22), 2001, 2009-2035
38. Bechel VT, M Negilski, J. James, Limiting the permeability of composites for cryogenic applications, Composites Science and Technology, 66, 2006, 2284–2295.

# Paper B

# Intralaminar cracking and specimen edge interaction induced local delaminations in quasi-isotropic CF/EP NCF composites in fatigue

H. Ben Kahla[1,2] , Z. Ayadi[1] and J. Varna[1*]

(1) Department of Engineering Sciences and Mathematics, Luleå University of Technology, SE-97187,Luleå,Sweden

(2) Institut Jean Lamour, SI2M, Université de Lorraine, EEIGM 6 Rue Bastien Lepage, F-54010 Nancy, France

## Abstract:

Experimental results are presented on local delamination onset and propagation caused by interaction between specimen edges and intralaminar cracks in fiber bundles of 90-layers in quasi-isotropic [-45/90/45/0]s CF/EP non-crimp fabric laminates subjected to tension-tension fatigue loading. It is confirmed that the first damage mode is intralaminar cracking in 90-layers that consists of intra-bundle cracks and cracks in the matrix between bundles (often initiated from stitches). This damage mode triggers cracking in off-axis layers and local delaminations in positions where the 90-layer crack meets the adjacent layer. The process of local delamination is significantly enhanced at specimen edges where the out-of-plane edge stresses contribute to local delamination. During cyclic loading, delaminations grow and coalesce along the edge and propagate towards the specimen center. These processes are quantified experimentally at different cyclic load levels. In a low stress fatigue, very high number of cycles is required to detect small edge delaminations and they stay at the edge. In high stress cyclic tests, delaminations grow faster inside the composite: about 20% of the interface in the central zone can be delaminated. It is found that the axial modulus reduction is proportional to the relative delaminated area, proving that delamination is the major stiffness reduction factor in these laminates.

**Keywords:** Delamination; Intralaminar cracks; Fatigue; Stiffness, NCF composite

# 1. Introduction

The large variation of parameters in composites (fibers, matrices, constituent volume fractions, reinforcement architecture on different scales, stacking sequences, manufacturing methods…), the time consuming and limited characterization tools and methods together with current lack of reliable multi-scale models prevent of using one general approach to predict the behavior for all composites. Non-crimp fabric (NCF) composites, considered as a compromise between straight fiber prepreg tape and "crimped" woven composites are known for their good mechanical properties and their relatively easy and cost-effective production. The research carried out on NCF laminates demonstrates complex and sometimes unexplained behavior **[1-3]** that emphasizes the necessity for better understanding of the damage mechanisms in these materials, their growth under different loading conditions, to develop reliable methods describing the damage effect on the integrity of the composite structure.

The damage development in NCF composites under different quasi-static load cases and the influence of the damage on the residual properties have been investigated in many papers. For example, Mattsson et al**.[2]** studied the damage behavior of cross ply NCF composites under tensile loading and investigated the dependence of the mechanical properties on the stacking sequence. Edgren et al.**[4]** quantified different modes of cracking in NCF laminates, performed stress state analysis with FEM, showing that due to the bundle meso-structure the out-of-plane stress at layer interfaces are large.

Mikhaluk et al.**[5]** investigated damage initiation and evolution in quasi–isotropic NCF composites under tensile load, and developed a finite element model to predict damage growth. They observed correlation between damage zones and the resin-rich zones created by stitching pattern. Hence, parameters related to the stitch pattern have to be added for comprehensive analysis of damage in NCF composites, making the analysis even more complicated. Extensive studies of biaxial and quadri-axial NCF composites in different types of quasi-static loading are published by Lomov et al. **[3,6-8]**.

The NCF composites behavior in fatigue is much less studied. Vallons et al**.[3]** studied behavior of bi-axial NCF composites in tension-tension fatigue and the post-fatigue behavior. Testing specimens of $[0/90]_s$, $[90/0]_s$ and $[45/-45]_s$ orientations with respect to the axial loading direction, they used X-ray radiography, for detailed studies of intralaminar cracking in 90-bundles. Peculiar was the observation that surface 90-bundles do not have intra-bundle cracks.

Another unusual phenomenon was found in CF/EP NCF $[+45/-45/0/90]_s$ composites: early delamination in the middle of the 90-layer **[9]**. It grew rapidly, dividing the sample into two halves, kept together by the clamped ending tabs. Intralaminar cracking in high temperature CF/polyimide 8-harness quasi-isotropic laminates in thermal cycling was studied in **[10],** determining the intra-bundle crack density in different layers versus the number of thermal cycles. In **[11],** the tensile fatigue behavior of a biaxial NCF composite was investigated for stresses similar to the damage initiation stress in 90-bundles, detected by acoustic emission in a quasi-static test. It was found that numerous intralaminar cracks developed during the cycling showing strong fatigue effect while the decrease in tensile modulus was very small.

Whether it is quasi-static or cyclic tensile loading, the damage mechanisms are similar and the most common damage modes in continuous fiber composites are intralaminar cracking, delamination and fiber breakage **[12].** These modes can act separately or can interfere, either bolstering or delaying or even arresting each other.

Interlayer delaminations usually start at specimen edges and the presence of intralaminar cracks meeting the interface significantly accelerates the process. Many papers have been written discussing the delamination resistance of CFRP laminates **[13-16].** The effect of delaminations, locally originating from intralaminar cracks, on stiffness reduction in prepreg tape $[0_m/90_n]_s$ laminates was analyzed, for example, in **[17].** Takeda and coworkers **[18,19]** used shear-lag analysis to calculate Energy Release Rate (ERR) for delamination growth in CFRP prepreg tape cross-ply laminates. In the above studies the effect of specimen edge, where the delamination usually starts, was not included. For quasi-static loading of prepreg tape laminates, the initiation and growth of edge delamination considering the effects of intralaminar cracks was performed in **[20,21].** In **[10],** the initiation and growth of edge delamination under cyclic loading of over 100 M cycles considering the edge-crack interaction was studied using quasi-isotropic $[45/0/-45/90]_s$ CFRP specimens. Analyzing ERR they concluded that certain critical crack density has to be reached before the delamination growth takes over and the cracking decays. It was also found that the edge delamination growth rate with the number of cycles follows Paris law.

In **[13]** the delamination growth from transverse cracks in GLARE was studied finding that delaminations of approximately the same size developed from both tips of the intralaminar crack in cases when the delamination was in almost pure Mode II. In case of non-symmetric meso-geometry (including staggered cracks) the fracture mode mixity changed and the delaminations on different sides of the same intralaminar crack grew differently. They also

showed that the delamination growth rate follows Paris law. The same law for interface crack propagation was experimentally confirmed and modelled in **[22,23]** on a much lower fiber debond scale.

In **[12]**, applying optical microscopy, SEM and X-ray computed tomography (CT) to more complex architectures than NCF laminates (3D woven), authors found that delamination between the stitch yarns and the surrounding material is very significant. In surface layers the first intralaminar cracks were found in the matrix between bundles. Many cracks in the matrix channels between bundles were found also in other studies **[24-27]** of 3D woven composites, observing that in the resin rich channel between the tows inside the material. It seems that even in 3D woven composites, the most probable origin of delamination is intralaminar crack, however, large delaminations may start also from local delaminations between yarns and from longitudinal cracks in the stitch yarn. Similar features were observed in fatigue of plain weave composites **[27],** where cracks in the transverse fiber bundles appeared first, then being deflected to cause delaminations.

The presented brief review shows differences and similarities in damage patterns during tension-tension cyclic loading in NCF reinforced composites and in much more complex woven fabric composites. The most typical sequences of damage development leading to large delaminations seem to be related to specimen edge interactions with intralaminar (intrabundle or between bundles) cracks in layers. Nevertheless, due to large variation and different combinations of geometrical and mechanical properties, currently we are still far from complete understanding of different effects and even more distant from reliable simulations and predictions regarding delaminations in damaged NCF laminates.

We hope that the current paper, which presents data and analysis on damage development in carbon fiber/epoxy $[-45/90/45/0]_s$ NCF laminates in tension-tension cyclic loading, will contribute to better understanding of matrix related fatigue phenomena. The intralaminar cracking development in layers of the laminate and its effect on local delaminations (starting from cracks) in interaction with specimen edge are analyzed and the effect of different damage modes on the laminate stiffness are estimated.

# 2. Experimental procedures

## 2.1 Material description

Quasi-isotropic $[-45/90/45/0]_s$ NCF carbon fiber/ epoxy HTS40/RTM6 laminates, manufactured at 180 ℃, consisting of unidirectional (UD) weave layers with 12K fiber bundles, see **Figure 1**, were studied. The areal density of the layer is 242 g/m$^2$, the bundle width and thickness in the composite are 3.5 mm and 0.25 mm respectively. The bundles in the UD weave are kept together with two sets of stitches, see X-ray CT and optical pictures in **Figure 1.** Table 1 shows elastic properties of the corresponding UD composite. The average longitudinal modulus of the $[-45/90/45/0]_s$ specimens was 43.7 GPa, which correlates well with the value of 46 GPa obtained by analytical estimate, using the Classical Laminate Theory (CLT) and the UD elastic properties in Table 1.

| Property | $E_L$ (GPa) | $E_T$ (GPa) | $G_{LT}$ (GPa) | $\gamma_{LT}$ | $\alpha_L$ ($10^{-6}1/℃$) | $\alpha_T$ ($10^{-6}1/℃$) |
|---|---|---|---|---|---|---|
| UD | 120 | 9.18 | 9.94 | 0.311 | 0.32 | 31.6 |

***Table 1. Thermo-elastic constants of the unidirectional Non-Crimp Fabric CF/EP composite***

Specimens of length 180 mm were cut from produced plates, both edges were polished using sequence of sand papers (P240, P600, P1200, P2500, P4000) followed by liquid diamond slurry (from 9 micron to 0.25 micron). The specimen was about three bundle-width wide: the specimen width $w$ was approximately 10 to 12 mm after grinding and polishing. The 10 kN load capacity was the main limiting factor for width selection. Wider specimens would have less scatter in stiffness and in damage development.

Since GFRP end tabs were glued to each specimen by Araldite 2011 2-component epoxy adhesive, the gauge length was 100 mm.

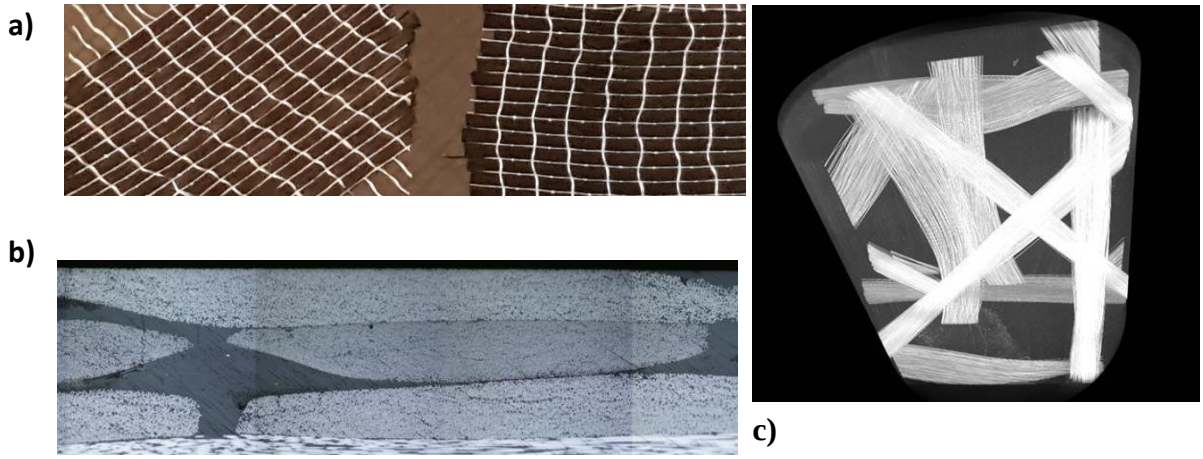



***Figure 1: Quasi-isotropic $[-45/90/45/0]_s$ laminate: a) photograph of the fabric surface; b) optical micrograph of the laminate edge; c) X-ray CT picture of the stich pattern in the laminate.***

## 2.2 Experiments

### 2.2.1 Cyclic loading parameters

In cyclic loading the test frequency of 5 Hz was used, which is typical to avoid internal heating of the composite **[28]**. Tests were performed keeping the maximum stress constant in cycles with sinusoidal waveform and with ratio of the minimum to the maximum stress in the cycle R= 0.1. Using an ElectroPulsTM E10000 Linear-Torsion machine with 10 KN load capacity the cyclic testing was carried out at several maximum stress levels, determined before cycling in a quasi-static tensile pre-test with displacement rate 2mm /min, individually for each used specimen, to correspond to strain levels 0.4; 0.45; 0.5; 0.55 and 0.6%. These strain levels are used in the text to refer to particular cyclic loading conditions. The axial modulus was determined from the slope of the stress-strain curve within the strain interval 0.05%-0.25%. After each block of cycles, it was re-measured in the same strain interval. The longitudinal strain in the pre-test was measured using a 50 mm gauge length extensometer.

The test was stopped after each block of cycles ( $\Delta N$= 1, 10, $10^2$, $10^3$, $10^4$,…) and edge replicas were taken. The final block was shorter or equal to 1 M cycles, which is a typical limit for laboratory cyclic testing. After each block of cycles, the damage state (the crack density in layers and the delamination length along different interfaces) at both edges of the specimen was determined through microscopy analysis of the edge replicas reproducing the surface topography of the specimen. Since using replicas, the specimen is not removed from the

machine, its alignment with the loading direction does not change and this technique is suitable for small laminate axial modulus change measurements in a quasi-elastic manner described above. At least three specimens were used for each level of strain in the cyclic loading.

### 2.2.2 Micro-damage characterization

The respective number of cracks $n_i$ over distance $L = 50\,mm$ in a layer with index $i$ was counted and the crack density was calculated as:

$$\rho_i = n_i/(L \cdot sin\,\theta_i) \quad (1)$$

where $\theta_i$ is the fiber orientation angle in the considered layer.

The delamination length, $l_d$ was defined as the total length of all local delaminations observed on one interface on the specimen edge, measured over a distance *L*, in the same region where the strain for stiffness reduction and the crack density is measured. The largest delaminations were observed at the interfaces between the 90-layer and ±45-layers. Since, delaminations at the 45/0 interface were very small and initiated only at very high loading, they were not quantified. After each loading step, the delaminations at the -45/90 and 90/45 interfaces, denoted in following $l_{-45/90}$ and $l_{90/45}$ were determined in measurements at both edges of each specimen. Since due to symmetry in a $[-45/90/45/0]_s$ laminate for each edge we have two interfaces of a certain type (-45/90 or 90/45), actually, for each type of the interface the delaminations were measured over 4X50=200 mm distance, which, as will be shown in Section 3, is rather representative.

The relative delamination length is presented as a delamination length and interface length ratio

$$l_{drel} = \frac{l_d}{4L} \quad (2)$$

where $d = -45/90$ or $90/45$

Usually the delamination length $l_d$ at the specimen edge is not representative for the extent of delamination apart from the edge (inside the specimen). To evaluate it in the bulk of the material, one edge of the specimen was step-wise grinded, then polished and examined under Nikon Eclipse MA200 microscope equipped with DS-U3 camera control unit and the NIS-Elements software. Since this method is destructive, it was applied to specimens only after the final cyclic loading block. This type of destructive sectioning has been used to quantify damage as a function of fatigue cycles also in **[29].**

# 3. Results and discussion

In the following discussion we will refer to *x*,*y* axes, where *x* is in the loading direction and *y* is in the specimen width direction. Although the damage modes are the same for both NCF and prepreg tape laminates, the damage prediction in NCF composites due to their heterogeneous meso-structure is much more complex. In contrast to prepreg tape composites, the damage state in NCF composites is affected by the stitching pattern and the layer meso-structure containing bundles, see **Figure 1.** Both of them lead to local stress concentrations and, therefore, the first damage to appear is intralaminar cracks in the 90-layer, in positions coinciding with the stitch positions. It is similar to findings in **[12]** for 3D woven composite that the debonding between the stitch yarns and the surrounding material is the main damage initiation mechanism.

With increasing number of cycles, cracks initiate at more random, not stitch related, positions inside the bundle (actually, these positions are Weibull strength distribution governed). At higher crack densities and at larger local delamination length the intralaminar cracking slows down due to weakened stress field between existing cracks. The 90-layer intralaminar cracks generate interlaminar stresses at the crack tips promoting initiation of local delamination at the interface with ±45-layers. Stress magnification in layers adjacent to the cracked 90-layer, in local regions were the 90-cracks are located, is the reason for early short intralaminar crack formation in the adjacent off-axis layers. Due to their geometrical appearance, in damaged tape laminates they are often referred to as “stitch cracks” (not to be mixed with stitches in the current paper) **[30].** In our material, these cracks are not “tunnels” that would cover the whole width of the specimen. With increasing number of cycles, they slowly grow outside the local stress concentration region **[31].** The 45-layer cracks may start also from stress concentration or material imperfections created by transverse stitches (at the interface) or longitudinal stitches (in-between bundles) in the layer, see **Figure 2**. In our material, cracks in the 90-layer after initiation usually propagated very rapidly from one specimen edge to another building well-defined tunnels.

The 90-crack induced delamination and cracking in adjacent off-axis layers start almost simultaneously. Since the crack plane in the 45-layer is oriented at 45 degrees with respect to the 90-crack plane, observing the specimen edge, the 45-layer crack is seen shifted with respect to the 90-crack. The shifting distance depends on how far from the edge the initiation point for this particular 45-layer crack has been. The couple of cracks (one in the 90-layer and another

one in the 45-layer) when crossing close to the edge accelerates delamination between these cracks which in the *x,y* –plane has the form of a triangle connected with the free edge.

Hosoi and al. **[32]** observed a similar damage sequence in CFRP $[45/0/-45/90]_s$ using optical edge observations and soft X-ray photography: edge delaminations started only in local regions with intralaminar cracks in the 90-layer. Interestingly enough, delamination did not start in **[10]** from a single pre-crack introduced in a quasi-static manner before the fatigue test, according to authors, indicating some difference in the geometry of the quasi-static crack or a necessity to have certain crack density. However, a difference with our observations have to be noted: we did not observe coalescence of all local delaminations and such extremely large delaminated areas as in **[10].**

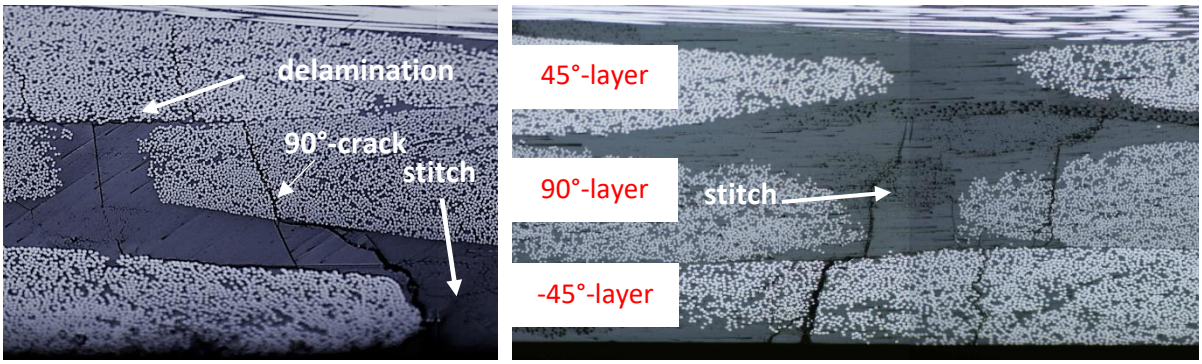



***Figure2: Examples of damage state in the lower part of the $[-45/90/45/0]_s$ laminate after 1 M cycles in 0.5 % strain loading***

## 3.1 Local delaminations at specimen edge

Local edge delamination in presence of intralaminar cracks are caused by high out-of-plane stresses (some of them may be singular in a linear elastic analysis) at the interface in the edge region: a)$\sigma_{zz}$, $\sigma_{xz}$ and the large corresponding Mode I and Mode II ERR for growth along the edge and b)$\sigma_{xz}, \sigma_{zz}$ for propagation inside the specimen.For the different specimens tested, delaminations without any link to intralaminar cracks were rarely observed. **Figure 3** shows the growth of the relative delamination length measured on the edge at the -45/90 and at the 90/45 interface with the number of fatigue cycles. The $l_{drel}$ is shown separately for two edges (A and B) of one specimen for each loading case. The similarity of the values found for both edges confirms the representativeness of the measurement. Therefore, the average of delamination length on both edges is presented in following.

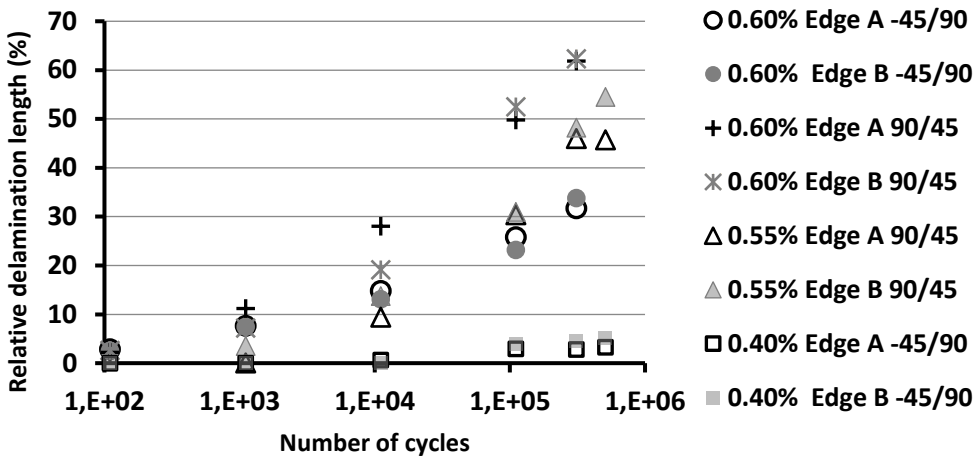



***Figure 3: Comparison of the relative delamination length, $l_{drel}$ growth between edge A and edge B of the specimen. The strain and the particular interface are indicated in the legend.***

In low stress fatigue tests (at strain <0.45 %, see **Figure 4**), delamination starts after more than 50 000 cycles, growing slowly with increasing number of cycles. For example, less than 10 % of the specimen edge is delaminated after 1M cycles in the 0.4 % test. The final $l_{drel}$ valuesare in the same range as in a quasi-static loading test at 1% strain, performed on specimens of the same lay-up (unpublished results).

At higher cyclic stresses, large delaminations are developing. Measurable delamination starts already after 1000 cycles. The delamination growth rate increases with the cyclic stress applied. For example, the delamination length reached after 1M cycles at 0.4% strain, requires only 1000 cycles at 0.6% strain.

There is a clear difference between the development of delamination at the -45/90 and at the 90/45 interface, see **Figure 4**: the delamination length is significantly larger at the 90/+45interface. This difference can not be explained by different crack densities in the +45 and -45 layers. At high crack density in the 90-layer we have more cracks in the -45 layer than in the +45 layer. Nevertheless, the delaminations at the 90/45 interface are larger. It seems unlikely that cracks in the 45-layer being close to 90-cracks would delay delamination. Nevertheless, it indicates that the interaction between 90-cracks and 45-cracks does not accelerate local delamination and is not the reason for larger delaminations. 3-D FEM analysis of edge stresses in an undamaged laminate with homogeneous layers did not show any significant difference in stresses at both interfaces. The stitch pattern on both types of interfaces is also identical. Hence, the reason for larger delaminations at the 90/45 interface remains

unclear. Apparently, a 3-D FEM analysis with cracks in several layers with bundle meso-structure, meeting the edge, is required to explain these observations. Based on fracture mechanics, O'Brien [33], argued that the edge delamination growth can be at different ratios of fracture modes (I, II and III) depending on the laminate lay-up and the loading conditions. Therefore, the stitched structure combined with the intralaminar cracking state at the edge and the interaction between the different damage modes could be the reason for the observed differences.

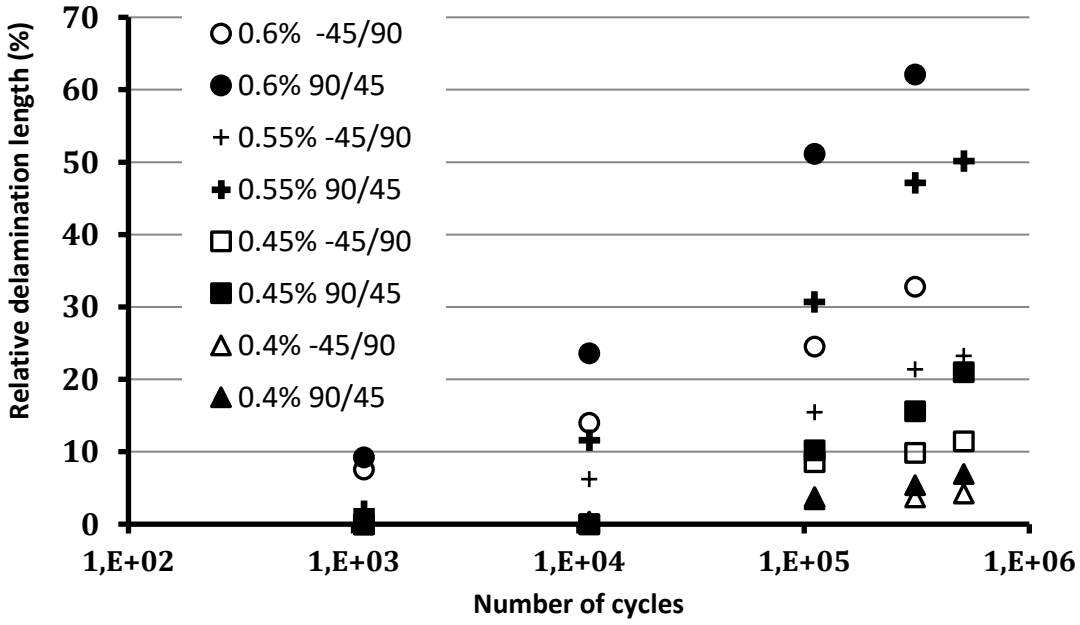



***Figure 4: Evolution of the relative delamination length $l_{drel}$ with the number of cycles. Load levels and the particular interface are indicated in the legend. (All specimens were loaded up to not more than 1 M cycles except for 0.6% that was loaded up to 0.3M cycles)***

Some additional features can be seen in **Figure 5**. For a low strain fatigue loading, local delamination starting from the intralaminar crack tip at one interface (for example, between 90°/45° layers) prevents initiation and propagation of a symmetric (with respect to the crack) delamination of the same interface. Also, a delamination on the same side from the crack, but on the other interface (-45/90 in the considered example) is prevented (**Figure 5a**). Usually, the delamination migrates from one interface to another through intralaminar crack in the 90-layer, **Figure 5c**. At higher strain levels in fatigue (0.55% and above) the pattern changes, delaminations were observed at both interfaces, (**Figure 5d**), but they do not grow in the same way as in **Figure 5b**. It could be related to higher number of cracks and longer local delaminations. The interaction between multiple delaminations alters the value of the strain

energy release rate at the tip of the original delamination crack **[34]**. The imperfect mesostructured of the layer (bundles do not have a rectangular cross-section and are not perfectly aligned) enhance the irregularity comparing with very symmetric delaminations shown in **[13].** Alderliesten et al.**[35]** reported symmetry loss when the intralaminar cracks in different layers are staggered and the delamination progresses in a mixed mode instead of Mode II. They noticed that in this case the delamination propagation on the opposite side of the separating layer was prevented until the first delamination had reached about 2 to 3 mm of length.

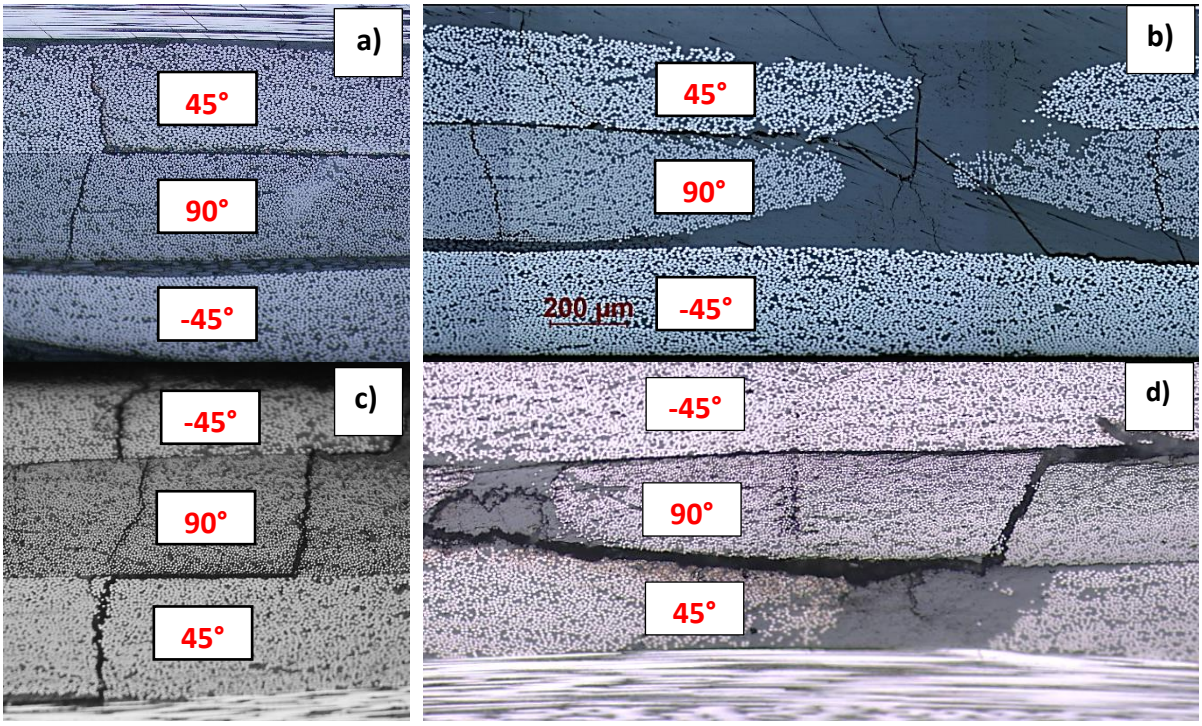



***Figure 5: Features of local delaminations: a), b) and c) delaminations in low load cyclic loading; d) delaminations in high stress cyclic loading***

**Figure 4** represents the evolution of the total edge delamination with the number of cycles (in logarithmic axis). Apparently, it does not follow the Paris law which predicts linear dependence on the number of cycles in a steady state region at certain ERR value. In order to understand the significance of the crack density on this process, we calculated the delamination length corresponding to one hypothetical intralaminar crack using in this calculation $l_{drel}$ and crack density $\rho_{90}$. Comparing different stress levels, there was no systematic dependence that reminds Paris law. It seems, that the simple procedure introducing the delamination per one hypothetical crack is not good, because different cracks appear after very different number of cycles and the time for individual debond growth is very different. Other factors making the situation very

complex, is the meso-structure which makes pure Mode II propagation in a steady state questionable and the close presence of other cracks with their own local delaminations.

## 3.2 Delamination depth (dependence on the distance from the edge)

Interior delaminations (far from the specimen edges) could be initiated from manufacturing defects e.g. incomplete curing or voids between layers and, most definitely, from local stress concentrations in the vicinity of intralaminar cracks, created during the cyclic loading. Since the out-of-plane stress state in the edge region is severe and the above-mentioned imperfections and damage are as typical in the edge region as in the interior, we can expect the interlayer delaminations growing along the interface from the edge region inside the specimen. In other words, the relative delamination length depends on "depth" which is the distance from the edge in y-direction, the relative delamination length being the largest at the specimen edge.

To inspect this assumption, one edge of the specimen was gradually grinded, then polished as described in Section 2 and analyzed later using optical microscope.

As shown in **Figure 6**, at low fatigue stress levels (under 0.45% of strain), local delaminations develop close to the edge and rapidly vanish within the first millimeter from it. The delamination does not grow deeper inside even with high number of cycles. Similar behavior was found in quasi-static loading at high strain (unpublished results). For higher fatigue stresses, the delamination is not at the edge only but $l_{drel}$ is consistently larger at the edge. The higher the fatigue stress, the deeper delaminations grow inside of the material. The dependence on the depth coordinate is roughly linear. As **Figure 6** shows, the specimen subjected to 0.3 M cycles at 0.6 % of applied strain has at the edge about 60 % of its 90/45 interface delaminated, whereas it has 20 % relative delamination in the middle of the specimen. A specimen subjected to 1M cycles at 0.55 % of strain, has at the same interface a lower value of relative delamination length at the edge (43%) and the relative delamination length drops to about 4 % in the middle of the specimen. The above discussed feature that the relative delamination length on the edge is systematically larger at the 90/+45 interface than at the -45/90 interface holds also inside the specimen.

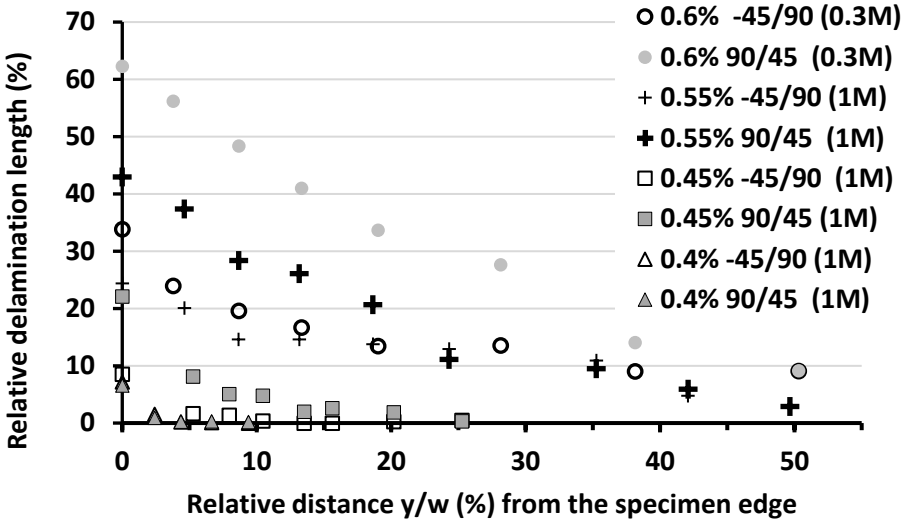



***Figure 6: Relative delamination length at the -45/90 and 90/45 interfaces as a function of the distance from the edge***

The effect of both types of delamination on the laminate stiffness, despite of the difference of the delamination length between -45/90 and 90/45 interfaces, is expected to have a similar character: they reduce the participation of involved layers in load sharing. Therefore, in Section 3.3 in order to simplify the analysis, the stiffness reduction will be correlated to the average of the delamination length at these two interfaces. The average delamination on the edge versus the number of cycles at different levels of loading is shown in **Figure 7** whereas the distribution along the width is shown in **Figure 8**.

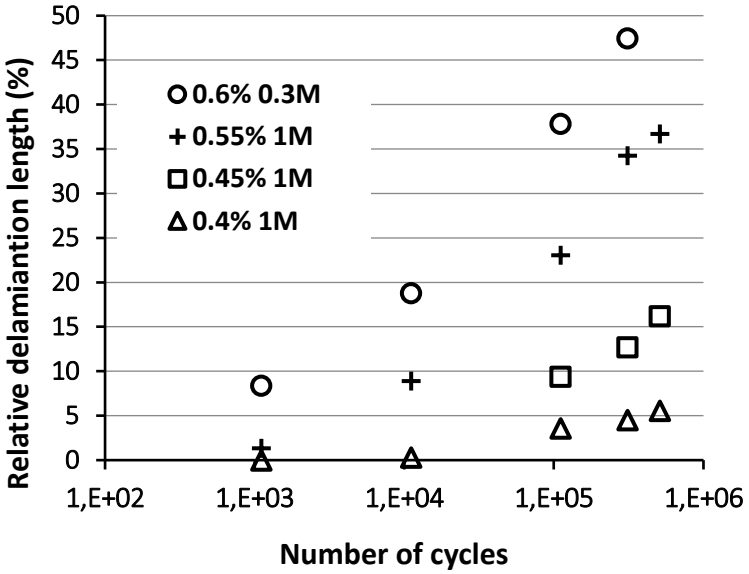



***Figure 7: Growth of the relative delamination length on the edge: average over both interfaces***

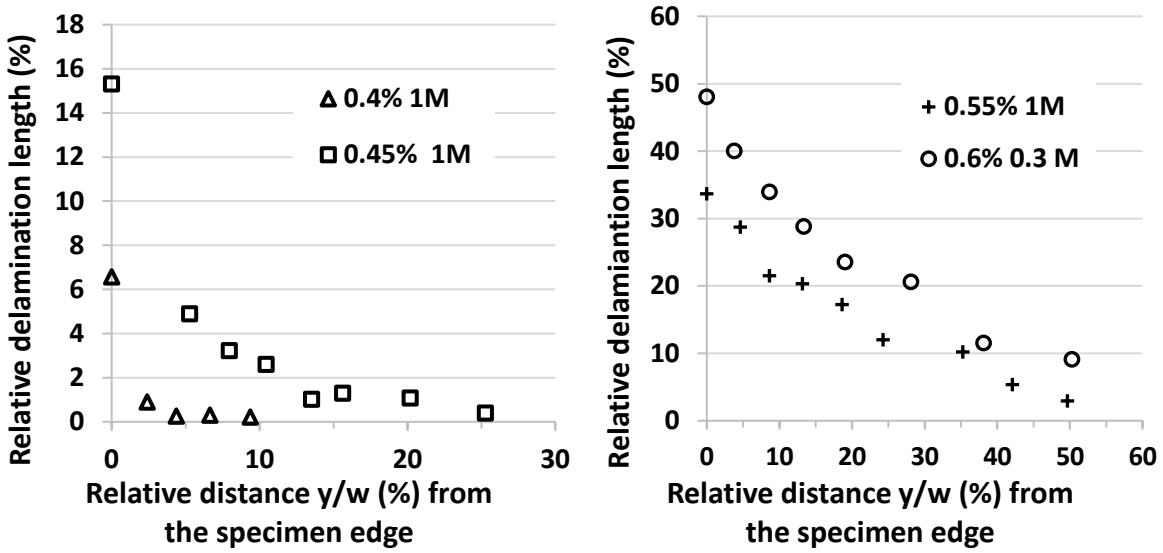



***Figure 8: Delamination length averaged over both interfaces as a function of the distance from the edge: a) low stress loading; b) high stress loading.***

## 3.3 Axial modulus reduction

The axial modulus degradation was measured before and after each block of cycling as described in Section 2, and results for some selected specimens are presented in **Figure 9**. The simultaneous growth of several damage modes and their interaction make it difficult to assess the contribution of each damage mode to the stiffness reduction. For example, local delaminations increase the opening and sliding displacements of intralaminar cracks, thus these cracks cause much larger stiffness reduction than cracks without delaminations; when the delaminations at both interfaces are large, the cracked layer is separated from the rest of the laminate and the crack density in the layer loses its importance.

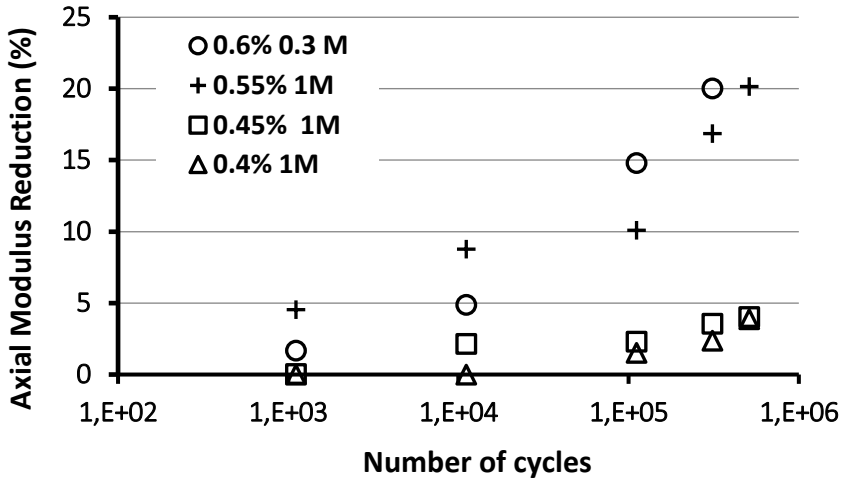



***Figure 9: Axial modulus reduction evolution with number of cycles***

The importance of intralaminar cracks on stiffness reduction can be estimated using CLT together with the modified ply-discount model which assumes zero values of the transverse and shear modulus in damaged layers (this corresponds to infinite intralaminar crack density). Assuming infinite crack density in the 90-layer and using CLT the axial modulus of the quasi-isotropic laminate drops by 4 % only, which is much less than the experimentally observed reduction at high loads but comparable with modulus reduction in low stress fatigue also shown in **Figure 9**. It has to be noted that the so-called normalized crack density defined as the ratio between the layer thickness and the distance between cracks was very far from infinite: it reaches 0.1 after 1 M cycles at 0.5% strain. Assuming in addition that the 45-layers of both orientations also have an infinite number of intralaminar cracks and using CLT leads to 13% of laminate axial modulus reduction. Even if this value is closer to the measured stiffness reduction in the performed high cycle tests, the real crack density was not high and the predicted axial modulus reduction is still much lower than in the high stress cyclic loading, see **Figure 9** where the reduction reaches 20%. Obviously, the large delaminations in a high stress loading have the strongest influence on stiffness degradation. Therefore, in **Figure 10,** the axial modulus change is plotted with respect to the relative delamination length on the edge. To qualitatively explain the rather linear relationship, we approximate the delamination length dependence on the depth in **Figure 8** by linear function (assuming a triangle form of the delaminated area) to conclude that the delaminated area is roughly proportional to the delamination length on the edge. Thus, we can interpret the results in **Figure 10** as the axial modulus reduction being almost proportional to the delaminated area. This indicates a rule of mixture (RoM) type of behavior:

in a part of the laminate, where the delamination has led to almost full separation between layers, some layers are not participating in the load sharing even in the fiber direction.

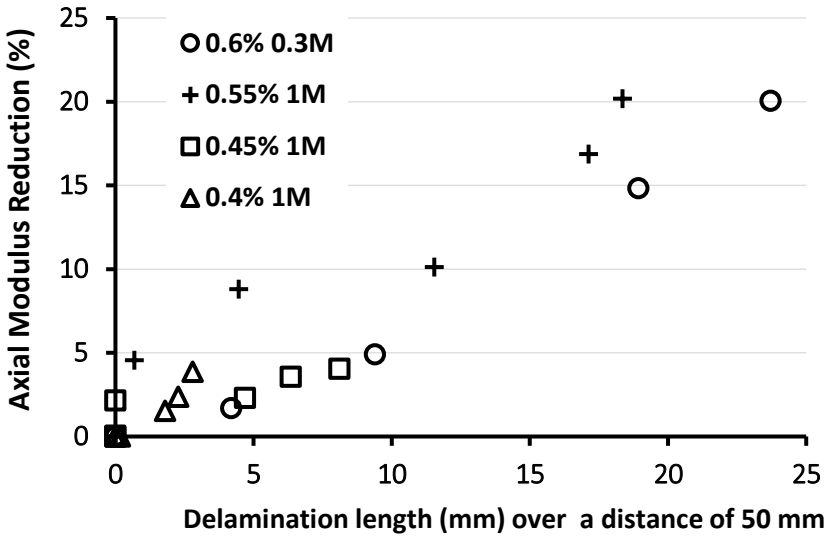



***Figure 10: Axial modulus reduction versus the relative delamination lengths averaged over both interfaces***

Therefore, we assume that in region of width $w_d$ close to the edge, the -45/90/+45 sublaminate is separated from the 0-layer and is not participating in the load sharing (even the longitudinal stress in these layers is zero and therefore $E_L = E_T = G_{LT} = 0$).In the middle region of the laminate we assume that all layers are acting in the longitudinal direction while the ply-discount model is applied for the transverse and the shear modulus of the damaged layers only ($E_T = G_{LT} = 0$). We use CLT for each region separately obtaining $E_x = 0.65\ E_{x0}$ and $E_x = 0.87\ E_{x0}$. Then we use RoM to find the axial modulus reduction for the whole laminate. Estimating from **Figure 8** that approximately 25% of the interface is delaminated at the end of 0.60% strain cyclic loading, the RoM gives that according to this oversimplified model the laminate axial modulus is 0.81 of its initial value. The 19% estimate of reduction is rather close to the measured maximum value of the modulus reduction for this loading case shown in **Figure 10.**

Very similar reduction rate of the axial modulus with delamination length can be observed in **Figure 10** for different test conditions (the maximum stress and the number of cycles).

# 3. Concluding remarks

This paper presents experimental investigation results on delamination growth initiated from intralaminar cracks in CF/EP quasi-isotropic $[-45/90/+45/0]_s$ NCF laminates. Damage development analysis in tension-tension cyclic tests has led to this realization:

- The first mode of microdamage is always intralaminar (intra-bundle and between bundles) cracking in 90-layers. Almost immediately it triggers two other mechanisms: a) small crack formation in adjacent off-axis layers in local stress concentration regions in the vicinity of a crack in the 90-layer; b) local delaminations in the same region.
- The delaminated area and the length of the 45-layer cracks grow during cyclic loading. So, does also the crack density in the 90-layer. For a currently unknown reason, the delaminated area between the 90/+45 layers is consistently larger than at the -45/90 interface.
- Local delamination is more enhanced in the specimen edge region, at high stress and large number of cycles reaching there almost 60%.
- It is possible to distinguish two patterns of behavior in fatigue, dependent on the fatigue stress level: in high stress fatigue the zone with delaminations goes through the whole width of the specimen; whereas in low stress fatigue, delaminations are at the edge only.
- The large axial modulus reduction is proportional to the delaminated area showing that delamination is the major factor. The effect can be estimated using the ply-discount model in different modifications: in some layers only the transverse and shear modulus are reduced due to cracking, whereas in regions where layers are fully separated from the laminate, even the longitudinal modulus of the layer has to be null.

## Acknowledgments

Authors would like to acknowledge support from the Swedish Aeronautical Research Program (NFFP6), Project 2014-00882, jointly funded by the Swedish Armed Forces, Swedish Defense Material Administration, the Swedish Governmental Agency for Innovation Systems and GKN Aerospace and the Joint European Doctoral Program in Material Science and Engineering (DocMase).

# References:


1. Mattsson, D., Joffe, R., & Varna, J. (2007). Methodology for characterization of internal structure parameters governing performance in NCF composites. *Composites Part B: Engineering*, *38*(1), 44-57.
2. Mattsson, D., Joffe, R., & Varna, J. (2008). Damage in NCF composites under tension: effect of layer stacking sequence. *Engineering Fracture Mechanics*, *75*(9), 2666-2682.
3. Vallons, K., Lomov, S. V., &Verpoest, I. (2009). Fatigue and post-fatigue behaviour of carbon/epoxy non-crimp fabric composites. *Composites Part A: Applied Science and Manufacturing*, *40*(3), 251-259.
4. Edgren, F., Mattsson, D., Asp, L. E., & Varna, J. (2004). Formation of damage and its effects on non-crimp fabric reinforced composites loaded in tension. *Composites Science and Technology*, *64*(5), 675-692.
5. Mikhaluk, D. S., Truong, T. C., Borovkov, A. I., Lomov, S. V., & Verpoest, I. (2008). Experimental observations and finite element modelling of damage initiation and evolution in carbon/epoxy non-crimp fabric composites. *Engineering Fracture Mechanics*, *75*(9), 2751-2766.
6. Lomov, S. V., Belov, E. B., Bischoff, T., Ghosh, S. B., Chi, T. T., &Verpoest, I. (2002). Carbon composites based on multiaxial multiply stitched preforms. Part 1. Geometry of the preform. *Composites Part A:Applied science and manufacturing*, *33*(9), 1171-1183.
7. Lomov, S. V., Verpoest, I., Barburski, M., & Laperre, J. (2003). Carbon composites based on multiaxial multiply stitched preforms. Part 2. KES-F characterisation of the deformability of the preforms at low loads. *Composites Part A:Applied Science and Manufacturing*, *34*(4), 359-370.
8. Lomov, S. V., Barburski, M., Stoilova, T., Verpoest, I., Akkerman, R., Loendersloot, R., & Ten Thije, R. H. W. (2005). Carbon composites based on multiaxial multiply stitched preforms. Part 3: Biaxial tension, picture frame and compression tests of the preforms. *Composites Part A: Applied Science and Manufacturing*, *36*(9), 1188-1206.
9. Pagano, N.J., & Schoeppner, G.A. (2000) Delamination of Polymer Matrix Composites: Problems and Assessment. Comprehensive Composite Materials, Elsevier Science, 433–528.
10. Varna, J., &Zrida, H. (2017). Analysis of Microdamage in Thermally Aged CF/Polyimide Laminates. *Mechanics of composite materials*, *53*(1), 45-58.
11. Vallons, K., Zong, M., Lomov, S. V., &Verpoest, I. (2007). Carbon composites based on multi-axial multi-ply stitched preforms–Part 6. Fatigue behaviour at low loads: Stiffness degradation and damage development. *Composites Part A:Applied Science and Manufacturing*, *38*(7), 1633-1645.
12. Hojo, M., Matsuda, S., Fiedler, B., Kawada, T., Moriya, K., Ochiai, S., & Aoyama, H. (2002). Mode I and II delamination fatigue crack growth behavior of alumina fiber/epoxy laminates in liquid nitrogen. *International Journal of Fatigue*, *24*(2-4), 109-118.
13. Brunner, A. J., Stelzer, S., Pinter, G., &Terrasi, G. P. (2016). Cyclic fatigue delamination of carbonfiber-reinforcedpolymer-matrix composites: Data analysis and design considerations. *International Journal of Fatigue*, *83*, 293-299.

14. Brunner, A. J. (2015). Fracture mechanics characterization of polymer composites for aerospace applications. In *Polymer composites in the aerospace industry* (pp. 191-230). Woodhead Publishing.
15. Brunner, A. J., Blackman, B. R. K., & Davies, P. (2008). A status report on delamination resistance testing of polymer–matrix composites. *Engineering Fracture Mechanics*, *75*(9), 2779-2794.
16. American Society for Testing and Materials (2015) ASTM D 6671-13. Standard Test Method for Mixed Mode I-Mode II Interlaminar Fracture Toughness of Unidirectional Fiber Reinforced Polymer Matrix Composites. ASTM Int.
17. Kashtalyan, M., &Soutis, C. (2000). The effect of delaminations induced by transverse cracks and splits on stiffness properties of composite laminates. *Composites Part A:Applied Science and Manufacturing*, *31*(2), 107-119.
18. Takeda, N., &Ogihara, S. (1994). Initiation and growth of delamination from the tips of transverse cracks in CFRP cross-ply laminates. *Composites science and technology*, *52*(3), 309-318.
19. Takeda, N., Ogihara, S., & Kobayashi, A. (1995). Microscopic fatigue damage progress in CFRP cross-ply laminates. *Composites*, *26*(12), 859-867.
20. Zhang, J., Soutis, C., & Fan, J. (1994). Effects of matrix cracking and hygrothermal stresses on the strain energy release rate for edge delamination in composite laminates. *Composites*, *25*(1), 27-35.
21. Xu, L. Y. (1994). Interaction between matrix cracking and edge delamination in composite laminates. *Composites science and technology*, *50*(4), 469-478.
22. Pupurs, A., & Varna, J. (2011). Fracture mechanics analysis of debond growth in a single-fiber composite under cyclic loading. *Mechanics of composite materials*, *47*(1), 109.
23. Pupurs, A., Goutianos, S., Brondsted, P., & Varna, J. (2013). Interface debond crack growth in tension–tension cyclic loading of single fiber polymer composites. *Composites Part A: Applied Science and Manufacturing*, *44*, 86-94.
24. Mouritz, A. P., & Cox, B. N. (2010). A mechanistic interpretation of the comparative in-plane mechanical properties of 3D woven, stitched and pinned composites. *Composites Part A:Applied Science and Manufacturing*, *41*(6), 709-728.
25. Rudov-Clark, S. A., &Mouritz, A. P. (2008). Tensile fatigue properties of a 3D orthogonal woven composite. *Composites Part A: Applied Science and Manufacturing*, *39*(6), 1018-1024.
26. Mouritz, A. P. (2008). Tensile fatigue properties of 3D composites with through-thickness reinforcement. *Composites science and technology*, *68*(12), 2503-2510.
27. Pandita, S. D., Huysmans, G., Wevers, M., &Verpoest, I. (1999). Tensile fatigue damage development in plain weave and knitted fabric composites (GFRP). In *Proceedings of the 12th international conference on composite materials* (pp. 5-9).
28. Carvelli, V., &Lomov, S. V. (Eds.). (2015). *Fatigue of textile composites*. Elsevier.
29. Tsai, K. H., Chiu, C. H., & Wu, T. H. (2000). Fatigue behavior of 3D multi-layer angle interlock woven composite plates. *Composites Science and Technology*, *60*(2), 241-248.

30. Bechel, V. T., Negilski, M., & James, J. (2006). Limiting the permeability of composites for cryogenic applications. *Composites Science and Technology*, *66*(13), 2284-2295.
31. Kahla, H. B., Ayadi, Z., Edgren, F., Pupurs, A., & Varna, J. (2018). Statistical model for initiation governed intralaminar cracking in composite laminates during tensile quasi-static and cyclic tests. *International Journal of Fatigue*, *116*, 1-12.
32. Hosoi, A., Sato, N., Kusumoto, Y., Fujiwara, K., &Kawada, H. (2010). High-cycle fatigue characteristics of quasi-isotropic CFRP laminates over 108 cycles (initiation and propagation of delamination considering interaction with transverse cracks). *International Journal of Fatigue*, *32*(1), 29-36.
33. O'Brien, T. K. (1982). Characterization of delamination onset and growth in a composite laminate. In *Damage in Composite Materials: Basic Mechanisms, Accumulation, Tolerance, and Characterization*. ASTM International.
34. Yu, B., Bradley, R. S., Soutis, C., Hogg, P. J., & Withers, P. J. (2015). 2D and 3D imaging of fatigue failure mechanisms of 3D woven composites. *Composites Part A:Applied Science and Manufacturing*, *77*, 37-49.
35. Alderliesten, R. C., Schijve, J., & Van der Zwaag, S. (2006). Application of the energy release rate approach for delamination growth in Glare. Engineering Fracture Mechanics, 73(6), 697-709.

# Paper C

# Effect of intralaminar cracking induced local delaminations on laminate stiffness

H. Ben Kahla[1,2] , Z. Ayadi[2] and J. Varna[1*]

(1) Department of Engineering Sciences and Mathematics, Luleå University of Technology, SE-97187,Luleå,Sweden

(2) Institut Jean Lamour, SI2M, Université de Lorraine, EEIGM 6 Rue Bastien Lepage, F-54010 Nancy, France

## Abstract:

Thermo-elastic constants of damaged laminates with intralaminar cracks in plies and local delaminations starting from intralaminar crack tip are analyzed using the crack opening displacement (COD) and sliding displacement (CSD) based GLOB_LOC approach used in (**Varna,2013)**, showing that the displacement gap on the delamination crack surfaces does not enter the stiffness expressions explicitly. The delamination affects the stiffness via increasing COD and CSD of the intralaminar crack. This finding allows using the same stiffness expressions for cracked laminates with and without delaminations. FEM parametric analysis shows that the COD is significantly larger for cracks with delaminations and the COD dependence on ply parameters is rather complex. The numerical COD values were used to find the whole stiffness matrix of the damaged laminate, which in turn was used to back-calculate the "effective transverse modulus " (EFTM) of the damaged ply- a concept which allows to use Classical Laminate Theory for the damaged laminate. It is shown that the influence of surrounding plies on the EFTM is negligible and simple and accurate fitting expressions for EFTM, describing the dependence on crack density and delamination length, are suggested. Examples comparing with FEM and the GLOB-LOC model show that the effective stiffness approach has an excellent accuracy.

**Key words:** laminates, intralaminar cracks, local delaminations, thermo-elastic constants, crack face displacements

# 1. Introduction

Structural elements may contain laminates with ply (unidirectional (UD) composites) orientation selected to meet design specifications regarding service loads and environmental conditions. Microdamage, appearing in plies and between plies long before the macroscale failure of the laminate, changes the load sharing between plies affecting thermo-elastic constants of the laminate.

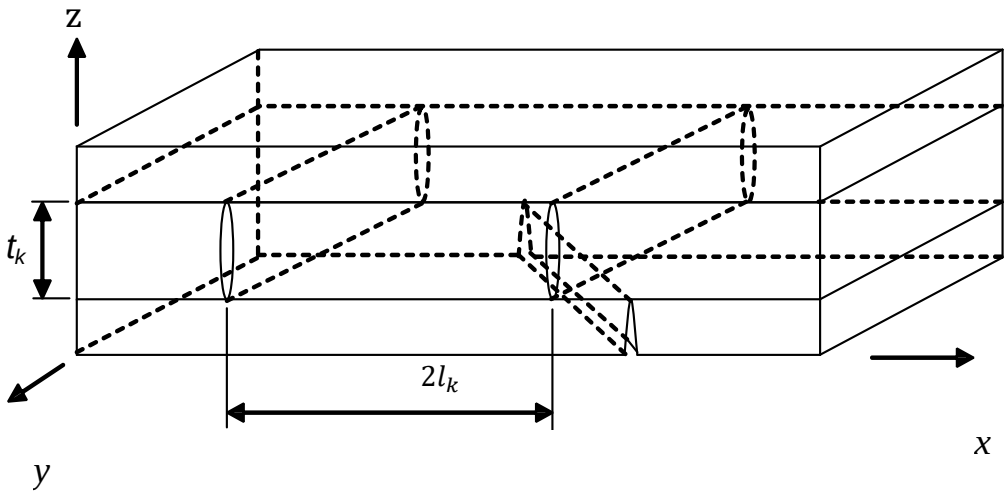
This first mode of microdamage **(Parvizi and Bailey, 1978; Jamison et al., 1984**) is called "intralaminar cracking". These cracks are often called matrix cracks, tunneling cracks or transverse cracks. Intralaminar cracks, see **Figure 1a**, run along fibers in the ply and usually the crack is well defined, the crack plane being perpendicular to the laminate middle-plane. The crack covers the whole thickness of the ply and, may be with except for extremely thin plies and fatigue loads, it propagates over the whole width of the tensile specimen.The crack propagation is in a mixed mode, with indications that Mode I is the most dominant in propagation criteria.

The effect of each individual intralaminar crack on laminate stiffness is very small. When the number of cracks increases, they may significantly change the thermo-elastic constants of the laminate **(Joffe et al., 1999),** also initiating other damage modes, such as local delaminations at the crack tips **(Kashtalyan and Soutis, 2005; Takeda et al., 1995**) and fiber breaks in adjacent layers, **Figures 1b** and **1c**.

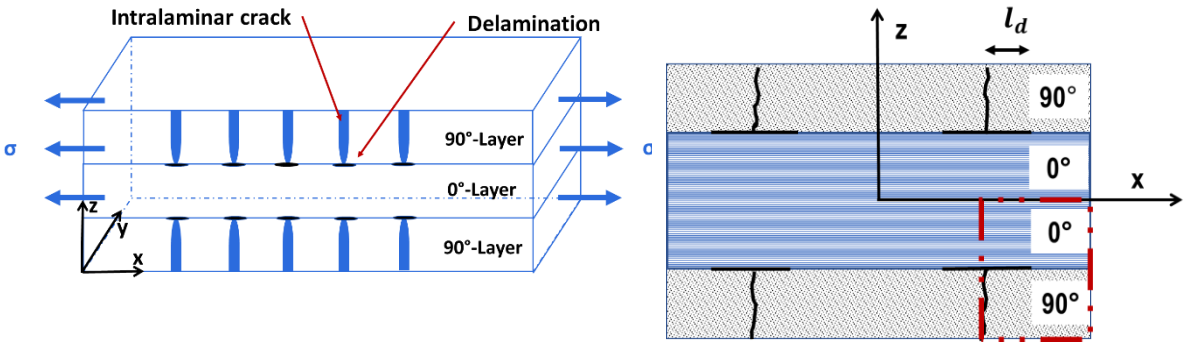
The intralaminar damage state in a ply is described with an averaged metric called crack density, which is defined as the number of cracks per unit distance measured in the direction perpendicular to the crack plane. The stress state is different in different plies and so is the crack density.

The crack density in k-th layer, denoted $\rho_k$, is inverse to the average distance between cracks, called crack spacing

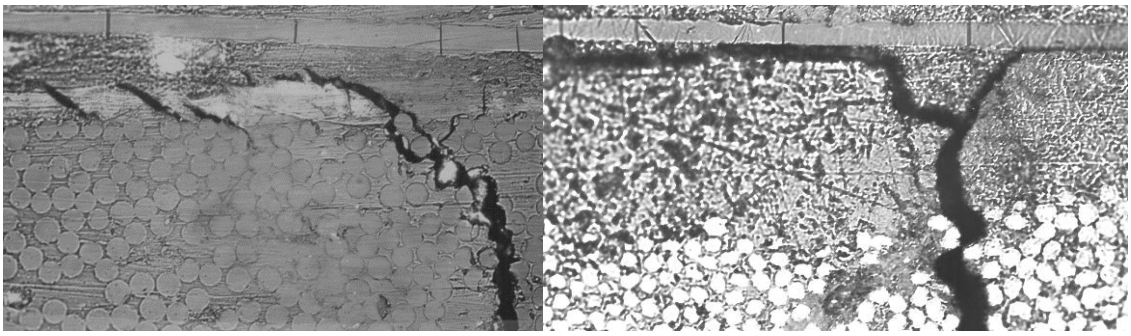
$$2l_k = 1/\rho_k. \qquad (1)$$




***a)*** *Upper part of a symmetric laminate with cracks in layers*




***b)*** *Surface layer of the laminate with open cracks and delaminations at the ply interface*



***c)*** *photos showing local delaminations and fiber breaks at the intralaminar crack tip*

***Figure 1: Intralaminar cracksand local delaminations in symmetric laminates***

Since stiffness depends only on the ratio of geometrical parameters (not on real dimensions) "normalized spacing" $2l_{kn}$ and "normalized crack density" $\rho_{kn}$ are introduced to describe the damage state and its effect on stiffness

$$2l_{kn} = 2l_k/t_k \,, \qquad \rho_{kn} = {}^{t_k}/_{2l_k} = \rho_k t_k \qquad (2)$$

Laminates with the same ply thickness ratio and normalized crack density have identical stiffness. The meaning of the normalized average spacing is similar to fibre aspect ratio in short fibre composites.

The two surfaces of an intralaminar crack are traction free if the crack is open: the in-plane transverse and shear stresses on the crack surface are zero. With increasing distance from the crack these stresses recover. The rest of plies in this region are overloaded which is the cause of laminate stiffness change. The stress transfer from the undamaged layer to the damaged is through out-of-plane shear stresses; shear-lag models approximately describe it, for example. The distance needed to recover most of the CLT stress state depends on the stiffness and thickness ratios of the damaged and the adjacent layers and on the local delamination length.
Analytical and/or numerical methods have been used to calculate the stress state in the cracked layer in order to predict laminate stiffness degradation. In this so called "micromechanics modelling", the focus is on the local stress state determination between two cracks. The simplest approximate solutions are based on shear lag assumptions or on variational principles **(Nairn et al., 1994; Smith et al., 1990; Hashin, 1985; Varna et al., 1991; Varna et al., 1994; Zhang et al., 1992; McCartney et al., 2000 A)**. Unfortunately, most of the analytical solutions are applicable to cross-ply type of laminates only. Higher accuracy requires more complex models and the calculation codes become very complex **(McCartney et al., 2000 B; Hajikazemi and McCartney, 2016).**

Alternative descriptors reflecting the average in-plane stress change are opening and sliding displacements of the crack faces (COD and CSD). It has been shown (**Varna, 2015)** that COD and CSD are proportional to the average of in-plane stress perturbations in the ply that controls the amount of stiffness change. Delaminations starting from crack tip would increase the COD and CSD. The most extreme case is fully delaminated unit between two cracks resulting in zero in-plane stresses in the cracked layer. This case corresponds to the maximum possible values of COD and CSD.

The use of COD and CSD for laminate stiffness predictions is suggested in **(Gudmundson et al., 1992; Gudmundson et al., 1993)** using homogenization to derive expressions for thermo-elastic constants of 3-D laminate. These expressions are exact but they have two unknown parameters to be obtained from a local problem: the average COD and crack face sliding CSD.

The local boundary value problem has to be solved, which can be done only numerically. **(Gudmundson et al., 1992)** suggested taking these parameters from a known analytical solution for a periodic system of cracks in an infinite medium. **(Nuismer et al, 1988)** showed that it results in significant overestimation of the laminate compliance change.

**(Lunmark and Varna, 2003; Lundmark and Varna, 2005; Varna, 2013)** presented a similar approach in the framework of the Classical Laminate Theory (CLT). The formulation (GLOB-LOC approach) follows the same procedure as developing the CLT. Exact expressions for stiffness matrix, compliance matrix and thermal expansion coefficients of an arbitrary symmetric laminate with cracks in plies are presented. These relationships contain thermo-elastic constants of the UD composite, geometrical characteristics of the lay-up, crack density for all plies and two very robust parameters of the crack: the average crack face opening (COD) and the average sliding displacement (CSD) normalized with respect to the CLT stress in the ply**.** In **(Lundmark and Varna, 2005; Joffe et al., 2001; Lundmark and Varna, 2006; Lundmark and Varna, 2011; Loukil et al., 2013),** the normalized COD and CSD were analyzed using FEM and approximated by power law functions.

The same two alternatives (a) average stress; b) COD and CSD) we have when developing stiffness prediction tools for laminates with intralaminar cracks and local delaminations starting from the crack tip. Tools for Energy Release Rate (ERR) based delamination growth have been developed in **(O'Brien, 1982; McCartney et al., 2012; Takeda et al., 1995).** The objectives of the present paper are:

a) to generalize the COD and CSD based GLOB-LOC model for the case with delaminations;

b) to perform FEM analysis of the opening and sliding displacements of involved cracks to identify important parameters.

c) to use the COD and CSD data to investigate the reduction of the "effective transverse modulus" of the damaged ply with increasing the crack density and the delamination length, back-calculating the effective transverse modulus of the ply from the damaged cross-ply laminate stiffness, determined using the GLOB-LOC model with input from a very accurate FEM solution.

d) to use the "effective ply stiffness" in CLT to predict all thermo-elastic constants of general laminates with cracks in 90-plies.

# 2. General theory

## 2.1 Damaged laminate stress-strain response

In this section, we will present a methodology for calculation of in-plane thermo-elastic constants of symmetric laminates. The upper half of the considered symmetric *N*- layer laminate is shown in **Figure 1a.** The *k*-th ply of the laminate has thickness $t_k$ and the fiber orientation angle is $\theta_k$. Direction "1" is the local fiber direction in the ply and direction "2" is transverse to fibers (called also L and T directions). The thickness of the laminate, $h = \sum_{k=1}^{N} t_k$ . Each layer may contain certain number of intralaminar cracks which is quantified by crack density in the layer $\rho_k$ or by the dimensionless crack density $\rho_{kn}$, see (1) and (2). Delamination length, $l_d$, see **Figure 1 b**, and its value normalized with respect to ply thickness or the crack spacing are parameters characterizing the damage. We assume that the number of cracks is the same in two layers symmetrically located with respect to the midplane. "Vector" (column) and matrix objects are in following denoted by { } and [ ] respectively. A bar above the matrix and vector entities indicates ply thermo-elastic constants in the global coordinate system x,y.

For an **undamaged** laminate the macroscopic elastic stress-strain relationship, expressed through stiffness matrix $[Q]_0^{LAM}$ and thermal expansion coefficient vector$\{\alpha\}_0^{LAM}$ is

$$\{\sigma\}_0^{LAM} = [Q]_0^{LAM}(\{\varepsilon\}_0^{LAM} - \{\alpha\}_0^{LAM}\Delta T) \tag{3}$$

The undamaged laminate stiffness in CLT is calculated as

$$[Q]_0^{LAM} = \frac{1}{h}\sum_{k=1}^{N}[\bar{Q}]_k t_k \tag{4}$$

Thermal expansion coefficients $\{\alpha\}_0^{LAM}$ are obtained solving the thermal CLT problem

$$\frac{1}{h}\{N\}^{th} = [Q]_0^{LAM}\{\alpha\}_0^{LAM}\Delta T, \{N\}^{th} = \Delta T\sum_{k=1}^{N}[\bar{Q}]_k\{\bar{\alpha}\}_k t_k \tag{5}$$

$$\{\bar{\alpha}\}_k = [T]_k^T\begin{Bmatrix}\alpha_1\\ \alpha_2\\ 0\end{Bmatrix}$$

In **(5)** $[T]_k^T$ is transposed stress transformation matrix between local and global coordinates for ply with fiber orientation angle $\theta_k$. The undamaged laminate compliance matrix is $[S]_0^{LAM} = ([Q]_0^{LAM})^{-1}$.

The stress-strain relationship for the **damaged** laminate can be written as

$$\{\sigma\}_0^{LAM} = [Q]^{LAM}\left(\{\varepsilon\}^{LAM} - \{\alpha\}^{LAM}\Delta T\right) \quad (6)$$

In the damaged laminate, the same applied stress as for the undamaged laminate will cause a different strain response. The damaged laminate has an unknown stiffness matrix $[Q]^{LAM}$ and an unknown vector of thermal expansion coefficients $\{\alpha\}^{LAM}$. The objective is to derive expressions for them that will depend on UD thermo-elastic constants, the laminate lay-up and on the crack densities in plies.

Derivation of constitutive equations for the damaged laminate follows the path as in the case without delaminations **(Lundmark and Varna, 2005)**. The stresses averaged over the whole laminate volume $V = hS$ and the strains averaged in each ply with volume $V_k = St_k$ ($S$ is the in-plane surface area of the RVE) are defined as

$$\{\sigma\}^{(av)} = \frac{1}{V}\iiint_V \{\bar{\sigma}\}\, dv \qquad \{\bar{\varepsilon}\}_k^{(av)} = \frac{1}{St_k}\iiint_{V_k}\{\bar{\varepsilon}\}_k\, dv \quad (7)$$

From the divergence theorem follows, see **(Allen and Yoon, 1998)**, that the average (macroscopic) stress applied to the laminate RVE boundary is equal to the volume averaged stress

$$\{\sigma\}_0^{LAM} = \{\sigma\}^{(av)}\ , \quad (8)$$

An integral over the laminate volume can be expressed via integrals over volumes of all plies, leading to

$$\{\sigma\}_0^{LAM} = \sum_{k=1}^{N}\frac{t_k}{h}\{\bar{\sigma}\}_k^{(av)} \quad (9)$$

Hook's law for the volume averaged stresses in a ply has the same expression as in each point

$$\{\bar{\sigma}\}_k^{(av)} = [\bar{Q}]_k\left(\{\bar{\varepsilon}\}_k^{(av)} - \{\bar{\alpha}\}_k\Delta T\right) \quad (10)$$

The average strain in the ply, $\{\bar{\varepsilon}\}_k^{(av)}$ entering (10) can be expressed through the external boundary averaged strains (it is the same as the macroscopic laminate strain $\{\varepsilon\}^{LAM}$ ) and through displacements on crack surfaces,( see **(Allen and Yoon, 1998)** for details)

$$\{\bar{\varepsilon}\}_k^{(av)} = \{\varepsilon\}^{LAM} + \left\{\bar{\beta}\right\}_k \quad (11)$$

In (11) $\left\{\bar{\beta}\right\}_k$ is the Voigt vector representation of the Vakulenko-Kachanov tensor

$$\bar{\beta}_{ij}^k = \frac{1}{V_k}\int_{S_c}\frac{1}{2}\left(u_i^k n_j + u_j^k n_i\right)dS, \quad i,j = x,y \quad (12)$$

$$\left\{\bar{\beta}\right\}_k = \begin{Bmatrix}\bar{\beta}_{xx}\\ \bar{\beta}_{yy}\\ \overline{2\beta}_{xy}\end{Bmatrix}_k \quad (13)$$

Integration in (12) is over $S_C$ which is the total surface of all cracks in the layer, $u_i$ are displacements of the points on the crack surface, $n_i$ is the outer normal to the crack face.

Substituting (11) in (10) and using the result in (9) we obtain

$$\{\sigma\}_0^{LAM} = [Q]_0^{LAM}\{\varepsilon\}^{LAM} - \sum_{k=1}^{N}\frac{t_k}{h}[\bar{Q}]_k\{\bar{\alpha}\}_k\Delta T + \sum_{k=1}^{N}\frac{t_k}{h}[\bar{Q}]_k\{\bar{\beta}\}_k \quad (14)$$

Obtaining (14) we used CLT expression (4). The second term in (14) is "thermal force" (see definition (5)) per unit laminate thickness which according to (5) can be expressed through thermal expansion coefficients of the undamaged plies. This procedure results in

$$\{\sigma\}_0^{LAM} = [Q]_0^{LAM}(\{\varepsilon\}^{LAM} - \{\alpha\}_0^{LAM}\Delta T) + \sum_{k=1}^{N}\frac{t_k}{h}[\bar{Q}]_k\{\bar{\beta}\}_k \quad (15)$$

The last term in (15) represents the effect of the crack face displacements (opening and sliding) on the laminate stiffness analyzed in next section.

## 2.2 Displacements of delamination crack and intralaminar crack faces

Transformation between local and global coordinates for Vakulenko-Kachanov tensor $\beta_{ij}$ is given by

$$\{\bar{\beta}\}_k = [T]_k^T\{\beta\}_k \quad (16)$$

To find the meaning of $\{\beta\}_k$ , we consider the laminate in local coordinates of the damaged k-the ply where indexes 1, 2 and 3 correspond to the longitudinal (L), transverse (T) and thickness (z) directions.

We will use the definition (12) separately analyzing displacements on the surfaces of the delamination crack and the intralaminar crack.

A. The delamination crack has an orientation with surface normal vector $n_1 = n_2 = 0$ , $n_3 = \mp 1$. From (12), it follows that the delamination crack displacements are not contributing to $\{\beta\}_k$.It has to be noted that they would contribute to out-of-plane elastic constants of the laminate.
B. The intralaminar crack has the following outer normal vector to the two faces

$$n_1 = n_3 = 0\ ,\ n_2^+ = -1\ ,\quad n_2^- = +1 \quad (17)$$

"+" and "-"denote the "right" and "left" crack face in **Figure 1b**.

Using (12) for $\beta_{ij}^k$ in the k-th ply of volume $V_k = Lwt_k$, with one crack face surface area equal to $wt_k$ and with $M$ cracks inside it ($w$ is the width of the specimen), we see that the tensor contains only two non-zero in-plane elements: $\beta_{12}^k$ and $\beta_{22}^k$

$$\beta_{12}^k = \frac{w}{Lwt_k}\sum_{m=1}^{M}\int_{-\frac{t_k}{2}}^{+\frac{t_k}{2}}\frac{1}{2}[-u_1^{k+}(z) + u_1^{k-}(z)]dz \quad (18)$$

$$\beta_{22}^k = \frac{w}{Lwt_k}\sum_{m=1}^{M}\int_{-\frac{t_k}{2}}^{+\frac{t_k}{2}}[-u_2^{k+}(z) + u_2^{k-}(z)]dz \quad (19)$$

Since all cracks are equal and the crack distribution is uniform, $u_1^{k-} = -u_1^{k+}$ , $u_2^{k-} = -u_2^{k+}$

$$\beta_{12}^k = \frac{-M}{Lt_k}\int_{-\frac{t_k}{2}}^{+\frac{t_k}{2}}[u_1^{k+}(z)]dz \;\; \beta_{22}^k = \frac{-2M}{Lt_k}\int_{-\frac{t_k}{2}}^{+\frac{t_k}{2}}[u_1^{k+}(z)]dz \quad (20)$$

Using the definition of crack density (1) and (22)

$$\beta_{12}^k = -\rho_k u_{1a}^k \qquad \beta_{22}^k = -2\rho_k u_{2a}^k \quad (21)$$

In (21) $u_{1a}^k$ and $u_{2a}^k$ are averaged (index a) crack face opening (in T-direction) and crack face sliding (in L- direction) displacements defined as

$$u_{2a}^k = \frac{1}{t_k}\int_{-\frac{t_k}{2}}^{+\frac{t_k}{2}} u_2^k(z)dz \;, \qquad u_{1a}^k = \frac{1}{t_k}\int_{-\frac{t_k}{2}}^{+\frac{t_k}{2}} u_1^k(z)dz \quad (22)$$

In (22) $u_2^k$, $u_1^k$ is the distance in transverse and longitudinal direction respectively between corresponding points on the deformed crack surface and the crack plane (the surface connecting both crack tips). In (21) the crack density may be replaced with the normalized crack density $\rho_n$ using (2) and the average COD and CSD may be replaced with normalized values $u_{2an}^k$ and $u_{1an}^k$ defined as

$$u_{2an}^k = \frac{u_{2a}^k}{\sigma_{T0}^{(k)}t_k}E_T \qquad u_{1an}^k = \frac{u_{1a}^k}{\sigma_{LT0}^{(k)}t_k}G_{LT} \quad (23)$$

In (23) $\sigma_{T0}^{(k)}$ and $\sigma_{LT0}^{(k)}$ are CLT in-plane local stress components in the ply of an undamaged laminate at applied $\{\sigma\}_0^{LAM}$ .The obtained expressions can be written in matrix form

$$\{\beta\}_k = \begin{Bmatrix} 0 \\ \beta_{22} \\ 2\beta_{12} \end{Bmatrix}_k = -2\frac{\rho_{kn}}{E_2}[U]_k \begin{Bmatrix} \sigma_{L0} \\ \sigma_{T0} \\ \sigma_{LT0} \end{Bmatrix}_k \quad (24)$$

$$[U]_k = \begin{bmatrix} 0 & 0 & 0 \\ 0 & u_{2an}^k & 0 \\ 0 & 0 & \frac{E_T}{G_{LT}}u_{1an}^k \end{bmatrix} \quad (25)$$

The values of $u_{1an}^k$ and $u_{2an}^k$ depend on the crack density and the delamination length. These dependencies will be investigated in Section 3. However, formally the obtained expression for $\{\beta\}_k$ is exactly the same as in the case of zero delamination length. Hence, all expressions for damaged laminate thermo-elastic constants remain the same as in zero delamination case **(Varna, 2013)**

$$[Q]^{LAM} = \left([I] + \sum_{k=1}^{N} \rho_{kn} \frac{t_k}{h} [K]_k [S]_0^{LAM}\right)^{-1} [Q]_0^{LAM} \quad (26)$$

$$\{\alpha\}^{LAM} = \left([I] + \sum_{k=1}^{N} \rho_{kn} \frac{t_k}{h} [S]_0^{LAM} [K]_k\right) \{\alpha\}_0^{LAM} - \sum_{k=1}^{N} \rho_{kn} \frac{t_k}{h} [S]_0^{LAM} [K]_k \{\bar{\alpha}\}_k \quad (27)$$

In (26) a new matrix $[K]_k$ that shows the effect of a crack in a layer with index *k* is introduced

$$[K]_k = \frac{2}{E_T} [\bar{Q}]_k [T]_k^T [U]_k [T]_k [\bar{Q}]_k \quad (28)$$

Expressions (26) and (27) are exact formulas for thermo-elastic properties of damaged symmetric laminates with known damage state.

## 2.3 Stiffness of damaged laminates with 90-ply cracks

For symmetric balanced laminates with cracks only in 90-plies, the matrix operations in Section 2.3 can be performed analytically obtaining simple analytical expressions **(Loukil et al., 2013; Varna,2015; Varna and Loukil, 2016; Pupurs et al., 2016).**

$$\frac{E_x^{LAM}}{E_{x0}^{LAM}} = \frac{1}{1+2M\rho_{90n}\frac{t_{90}}{h}u_{2an}^{90}c_2} \qquad \frac{E_y^{LAM}}{E_{y0}^{LAM}} = \frac{1}{1+2M\rho_{90n}\frac{t_{90}}{h}u_{2an}^{90}c_4} \quad (29)$$

$$\frac{\nu_{xy}^{LAM}}{\nu_{xy0}^{LAM}} = \frac{1+2M\rho_{90n}\frac{t_{90}}{h}u_{2an}^{90}c_1\left(1-\frac{\nu_{LT}}{\nu_{yx0}^{LAM}}\right)}{1+2M\rho_{90n}\frac{t_{90}}{h}u_{2an}^{90}c_2} \qquad \frac{G_{xy}^{LAM}}{G_{xy0}^{LAM}} = \frac{1}{1+2M\rho_{90n}\frac{t_{90}}{h}u_{1an}^{90}\frac{G_{LT}}{G_{xy0}^{LAM}}} \quad (30)$$

$$c_1 = \frac{E_T}{E_{x0}^{LAM}} \frac{1-\nu_{LT}\nu_{xy0}^{LAM}}{(1-\nu_{LT}\nu_{TL})^2} \qquad c_2 = c_1\left(1-\nu_{LT}\nu_{xy0}^{LAM}\right) \quad (31)$$

$$c_3 = \frac{E_T}{E_{y0}^{LAM}} \frac{\nu_{LT}-\nu_{yx0}^{LAM}}{(1-\nu_{LT}\nu_{TL})^2} \qquad c_4 = \frac{E_T}{E_{yo}^{LAM}} \frac{\left(\nu_{LT}-\nu_{yx0}^{LAM}\right)^2}{(1-\nu_{LT}\nu_{TL})^2} \quad (32)$$

The thermal expansion coefficients of the damaged laminate are

$$\frac{\alpha_x^{LAM}}{\alpha_{x0}^{LAM}} = 1 - 2M\rho_{90n}\frac{t_{90}}{h}u_{2an}^{90}\frac{c_1}{\alpha_{x0}^{LAM}}\left(\alpha_2 - \alpha_{x0}^{LAM} - \nu_{12}\left(\alpha_{y0}^{LAM} - \alpha_1\right)\right) \quad (33)$$

$$\frac{\alpha_y^{LAM}}{\alpha_{y0}^{LAM}} = 1 - 2M\rho_{90n}\frac{t_{90}}{h}u_{2an}^{90}\frac{c_3}{\alpha_{y0}^{LAM}}\left(\alpha_2 - \alpha_{x0}^{LAM} - \nu_{12}\left(\alpha_{y0}^{LAM} - \alpha_1\right)\right) \quad (34)$$

Index 90 is used for the 90-ply thickness, crack density, COD and CSD. The quantities with upper index "LAM" are laminate constants, quantities with additional lower index 0 are undamaged laminate constants. For laminates with damaged central 90-ply M=1. For a couple of symmetrically located damaged 90-plies with the same crack density in both 90-plies the contribution to stiffness is the same and therefore terms with crack density in the ply, $\rho_{90n}$ have to be multiplied by M=2. If several couples of damaged 90-layers of different thickness are

present, a sum over contributions of all couples has to be used instead of M. These expressions will be used in Section 5 validating the developed approach.

It is noteworthy that the laminate shear modulus is not related to $u_{2an}^{90}$ and depends on sliding displacement only. On the other hand the sliding displacement $u_{1an}^{90}$ does not enter expressions for $E_x^{LAM}, E_y^{LAM}, \nu_{xy}^{LAM}$ and therefore predicting these constants the value of sliding is of no significance.

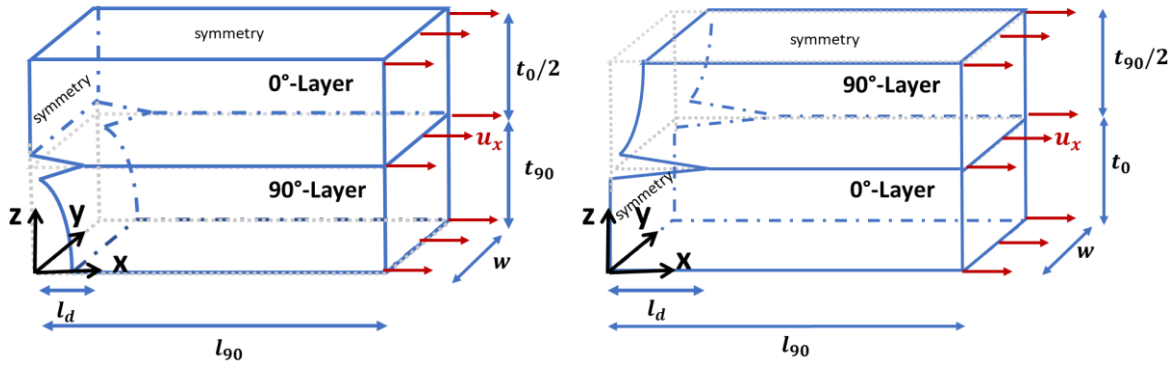
# 3. Crack opening displacement (COD) of 90-ply in cross-ply laminates

## 3.1 FEM modelling

### 3.1.1 Metodologi, materials and geometri

FE calculations on cross-ply laminates were performed to analyze the dependency of the normalized average crack opening displacement (COD) on the delamination length for different crack densities. The objective of this study is to obtain expressions for COD that could be used in expressions (26)-(28) of the GLOB-LOC approach to predict thermo-elastic properties of different laminates with damage in plies. To make it successful, the main material and geometrical parameters influencing COD have to be identified and the dependencies have to be described by sufficiently accurate fitting functions.

In all FE calculations the commercial code ANSYS 19 was used. In the model the intralaminar cracks are uniformly distributed and delaminations are symmetric with respect to the intralaminar crack plane. $t_{90}$ and $t_0$ are, respectively, the 90°-ply and the 0°-ply thicknesses. $l_{90}$ is the half distance between two intralaminar cracks and $l_d$ is the half length of the delamination (distance from the delamination crack tip to the intralaminar crack tip). A 3-D model was created to model the repeating unit shown in **Figure 2**. FE calculations were performed for Carbon fiber/epoxy and Glass fiber/ epoxy, $[90/0]_s$, $[90_2/0]_s$, $[90/0_2]_s$, $[0/90]_s$, $[0_2/90]_s$ and $[0/90_2]_s$ laminates. All plies are transversely isotropic and $E_2 = E_3$; $G_{12} = G_{13}$ and $\upsilon_{12} = \upsilon_{13}$.




a) b)

***Figure 2. Schematic representation of the representative volume element used for finite element analyses Model a) in the case of surface crack, b) inside crack***

The elastic properties of these materials are given in Table 1.

| Property | $E_L$ (GPa) | $E_T$ (GPa) | $G_{LT}$ (GPa) | $\gamma_{LT}$ | $\alpha_L$ ($10^{-6}1/°C$) | $\alpha_T$ ($10^{-6}1/°C$) |
|---|---|---|---|---|---|---|
| CF/EP | 120 | 6.14 | 5 | 0.4 | | |
| GF/EP | 45 | 15 | 5 | 0.3 | 10 | 30 |

***Table1. Elastic properties of the UD composites***

Series of calculations were performed for each material and for each geometrical configuration to study the effect of the length of the delamination on COD for different crack densities (different values of $l_{90}$). The displacement in x-direction for the nodes at the intralaminar crack surface was used to calculate the average value of the COD. The applied strain in the x direction was fixed. The obtained COD is averaged according to (22) and normalized (according to (23)) with respect to the thickness of the cracked ply and the far field stress in the ply transverse to the crack plane calculated using LAP (Laminate Analysis Program) based on Classical Laminate Theory.

Studying the normalized average crack opening displacement dependence on the length of the delamination, the delamination length $l_d$ was varied from 0 to 0.99*$l_{90}$ (from zero delamination to almost fully delaminated 90-layer).

### 3.1.2 Element type, boundary conditions and mesh

Default SOLID186 elements were used. For cross-ply laminates with surface cracked layer, bottom part is shown in **Figure 2 a**, constant displacement $u_x$ corresponding to 1% strain ($\varepsilon_x$) was applied to the surface $x = l_{90}$. Symmetry conditions were applied to the three surfaces defined by z= $t_{90}$+$t_0$/2 and at x=0 for $t_{90}$ < z < $t_{90}$+$t_0$/2). The bottom surface z= 0 and the crack surface defined by x=0 and 0 <z < $t_{90}$ are traction free. A displacement coupling in Y-direction is used for all points defining the surface y=0. The solution does not depend on y-coordinate and the edge effects are eliminated. It corresponds to solution for an infinite structure in the width direction. Obviously, these conditions correspond to generalized plane strain case and the size of the model in the y-direction could be reduced or 2D generalized plane strain elements could be used instead. 3D elements were used to use the same model and mesh for in-plane shear analysis. A constraint on all degrees of freedom is applied at the point (0, w, $t_{90}$+$t_0$/2).

In the case of $[0/90]_s, [0_2/90]_s$and $[0/90_2]_s$ laminates, similar boundary conditions were applied except that the symmetry as shown in **Figure 2 b**.

Only one element in the width direction of the FEM model was used, which as described above is sufficient for the used edge conditions. A refined mesh was used near to the damaged region. Depending on the crack density and on the delamination length, the number of elements was increased with $l_{90}$ and it was finer closer to the crack tip.

### 3.1.3 Use of contact elements

In the cases where the 90-ply is the central ply of the laminate and for long delaminations, part of the delaminated surfaces of the 90- and 0-ply may be interpenetrating as shown in **Figure 3**. To eliminate this problem, surface to surface contact elements (CONTA 174) in the 90-ply delaminated zone, were paired to target elements (TARGE 170) in the 0-layer delaminated region.The contact elements were set to comply with augmented Lagrange method which enforces minimum penetration with robust convergence when nodes are in contact. Checking the convergence of the solution and the penetration level in the contacts elements is an important part of modelling. Unacceptable level of penetration can be fixed using real constant FTOLN, known also as penetration tolerance parameter, in conjunction with the augmented Lagrange method. FTOLN is a factor based on the element thickness identifying an allowable maximum penetration. The default for FTOLN is 0.1. The smaller the value is the lower the speed of

convergence is, and the computational time is thus increased by the excessive number of iterations. Extremely small values or large ones prevent convergence of the model. **(Ansys 5.6, 1999; Bussetta et al., 2012)**

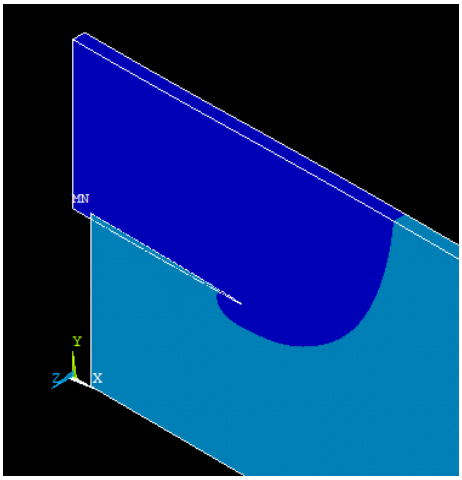



***Figure 3: Interpenetration in the delaminated zone in the GF/EP $[0/90]_s$ laminate,*** $l_d = 0.05t_{90}$; $\varepsilon_x = 1\%$

The use of contact elements shows no effect on the COD of the intralaminar crack (average x-displacement of the crack nodes). **Table 2** shows some examples.

| *Material* | GF/EP | | CF/EP | |
|---|---|---|---|---|
| Lay-up | $[0/90_2]_s$ | | $[0_2/90]_s$ | |
| $l_d/t_{90}$ | 0.03125 | 0.5625 | 0.0625 | 1.125 |
| $l_d/l_c$ | 0.05 | 0.9 | 0.05 | 0.9 |
| $u_{2a}CE\ (mm)$ | $1.13673e10^{-2}$ | $1.47540e10^{-2}$ | $6.67223e10^{-3}$ | $1.46138e10^{-2}$ |
| $u_{2a}NCE\ (mm)$ | $1.13673e10^{-2}$ | $1.47541e10^{-2}$ | $6.67223e10^{-3}$ | $1.46147e10^{-2}$ |

***Table 1. The difference in COD using contact elements (CE) or a model without contact elements (NCE) on the average x-displacement*** $(u_{2a})$***;*** $\varepsilon_x = 1\%$

## 3.2 COD of cracks in central ply

The normalized average COD, $u_{2an}^k$ referred in the following discussion as "COD", is presented in **Figure 4** for cracks in the central cracked ply of several GF/EP cross-ply laminates and in **Figure 5** for CF/EP laminates. Results, for four values of the normalized crack density $\rho_{90n}$ covering the realistic range of values, have certain common features:

- Three regions can be distinguished dependent on the delamination length $l_d/t_{90}$ : a) short delaminations where the COD is mainly affected by the shape of the original intralaminar crack without delamination; b) a steady state region where the COD increases proportionally to $l_d/t_{90}$: this region becomes shorter with increasing $\rho_{90n}$ c) interaction region where the delamination crack approaches to identical delamination crack coming from the adjacent intralaminar crack
- Relatively thicker 0-plies apply more constraint to the crack opening and the COD is smaller
- The 0-ply thickness effect is much smaller in CF/EP laminates.
- The COD at high normalized crack density is significantly lower
- In CF/EP composite the relatively very stiff 0-ply applies more constraint to COD than in GF/EP laminate and the COD is systematically lower.

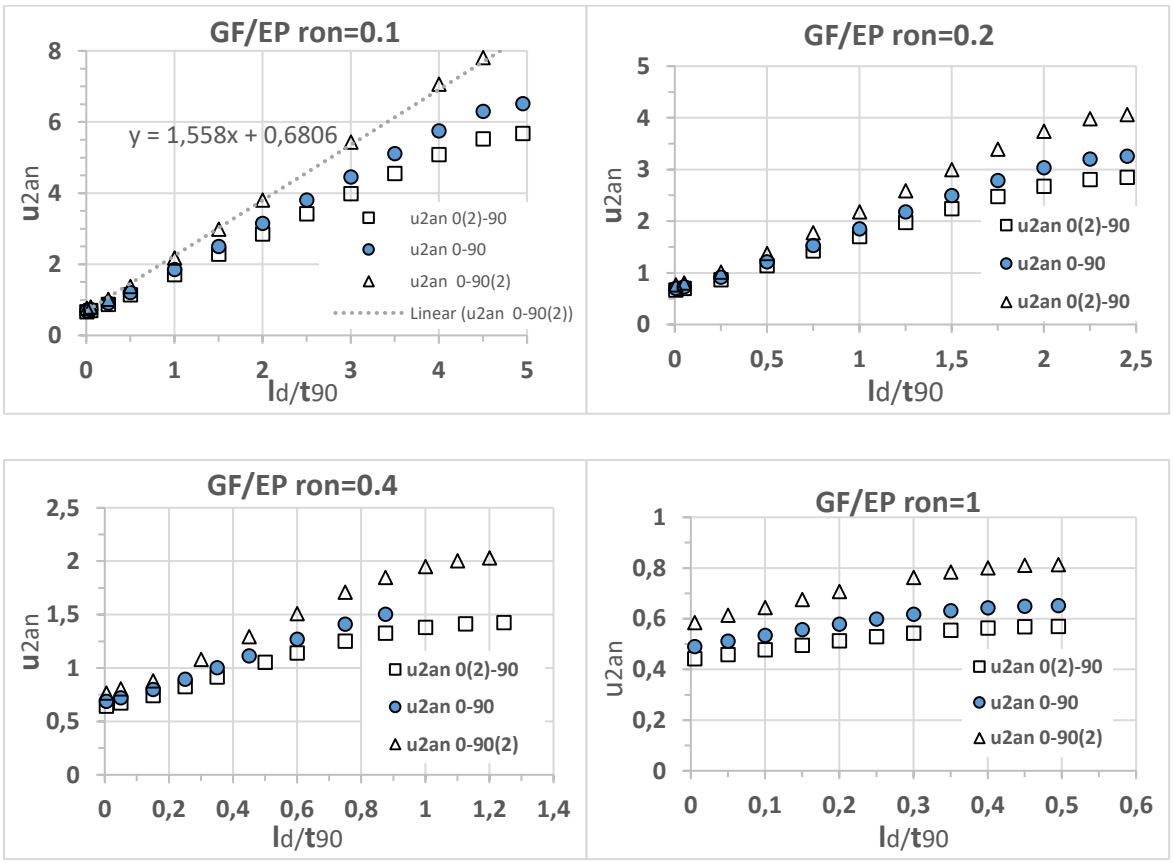



***Figure 4: Average normalized COD of a crack in a central 90-ply of GF/EP cross-ply laminates as a function of the delamination length for different values of $\rho_{90n}$ denoted "ron". Symbols 0(2)-90, 0-90 and 0-90(2) are representing $[0_2/90]_s$, $[0/90]_s$ and $[0/90_2]_s$ lay-ups.***

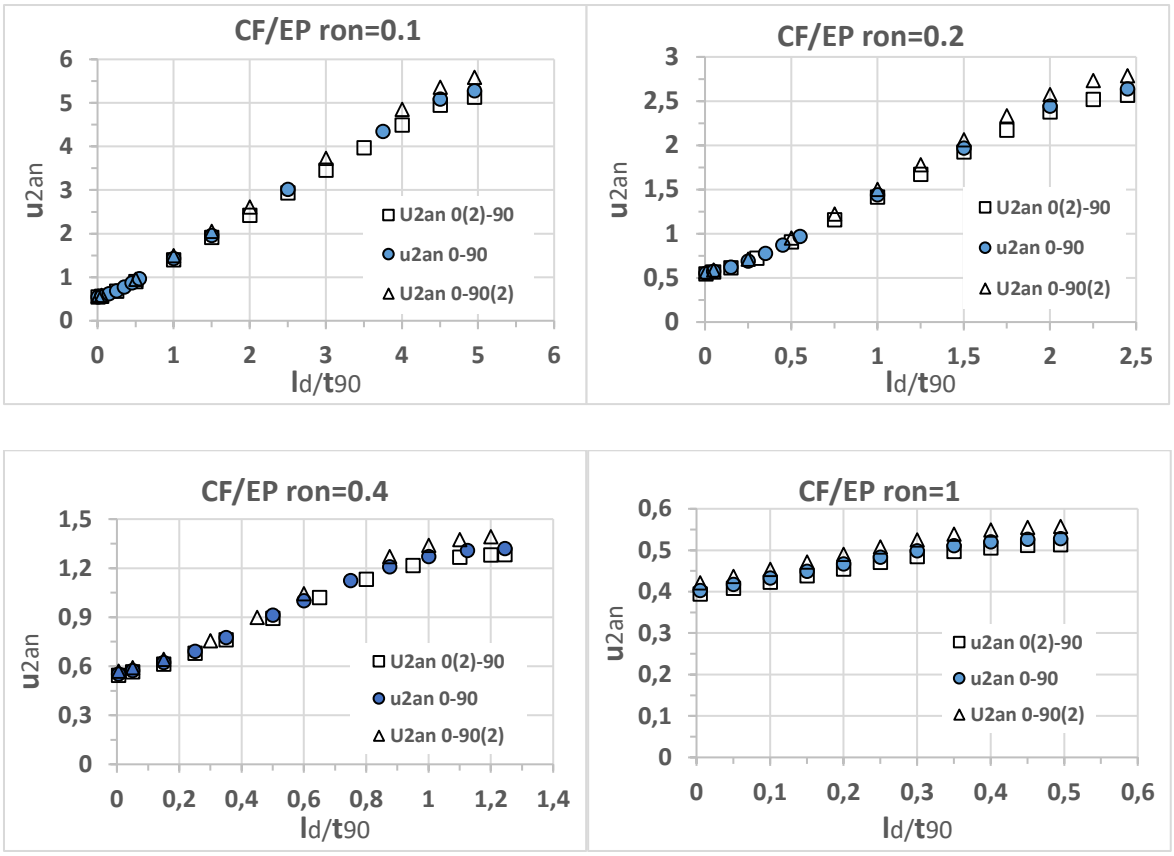



***Figure 5: Average normalized COD of a crack in a central 90-ply of CF/EP cross-ply laminates as a function of the delamination length for different values of $\rho_{90n}$. Symbols 0(2)-90, 0-90 and 0-90(2) are representing $[0_2/90]$, $[0/90]_s$ and $[0/90_2]_s$ lay-ups.***

## 3.3 COD of cracks in surface plies

Similar investigation using this time the model in **Figure 2 a** was performed with respect to cracks in surface layers of cross-ply laminates. Results presented in **Figure 6** and **Figure 7** confirm the observations of the role of different parameters listed in Section 3.2.

The COD for a given crack density $\rho_{90n}$ and large delamination length $l_d/t_{90}$ is very similar as in the case with cracks in centrally located 90-ply. For short delaminations the surface cracks open much more than internal cracks, which is a phenomenon related to the differences in the deformed crack shape.

Unfortunately, in spite of many more data present than shown in this paper we at present are not able to describe the role of different parameters by approximate functions that is a necessary condition for using the COD information in predictive tools. This may be done in future studies,

but right now we will use the COD data from FEM in a different way, see Section 4, using them to study the effective transverse modulus of the damaged ply and using it in thermo-elastic properties predictions for different laminates.

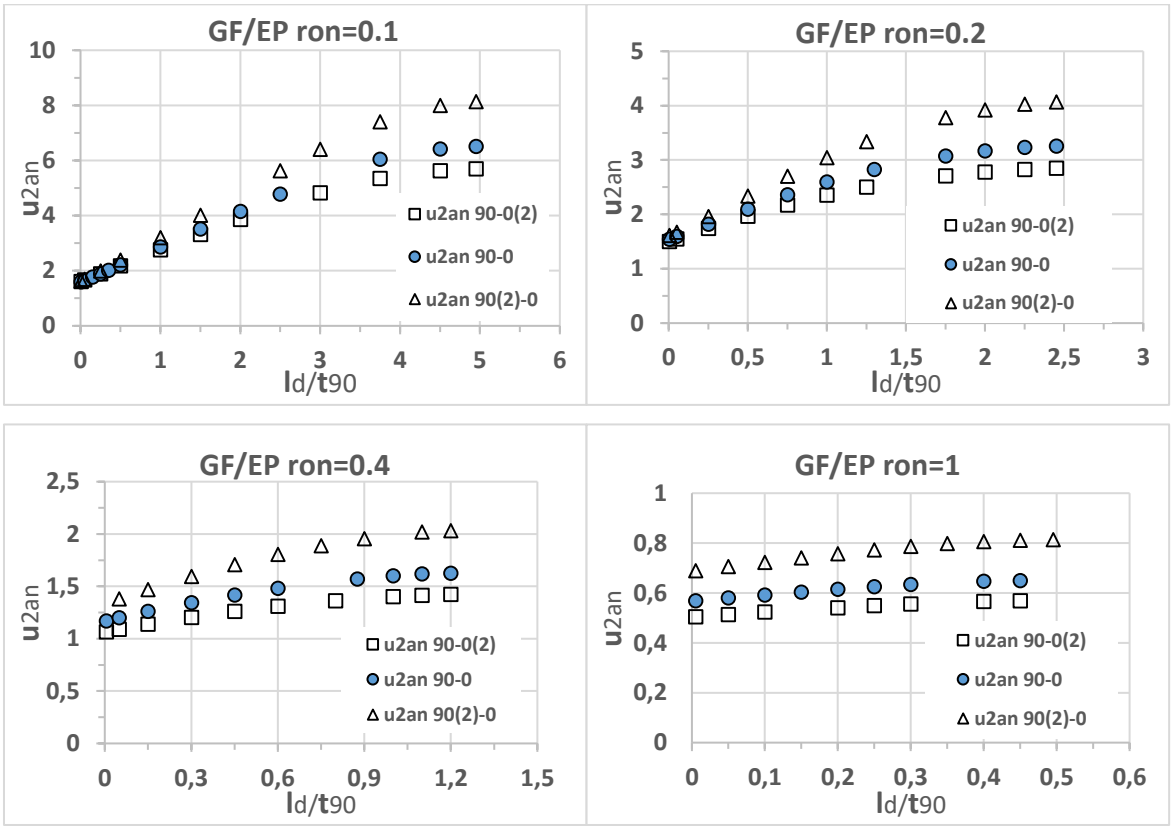



***Figure 6: Average normalized COD of a crack in a surface 90-ply of GF/EP cross-ply laminates as a function of the delamination length for different values of $\rho_{90n}$. Symbols 90(2)-0, 90-0 and 90(2)-0 represent $[90_2/0]_s$, $[90/0]_s$ and $[90_2/0]_s$ lay-ups.***

# 4. Effective transverse modulus of the damaged ply

## 4.1 Back-calculation expressions for balanced laminates with 90-cracks

In the effective stiffness approach we suggest using for the damaged laminate the constitutive law (6), calculating $[Q]^{LAM}$ as

$$[Q]^{LAM} = \frac{1}{h}\sum_{k=1}^{N} \bar{Q}_k^{eff} t_k \qquad (35)$$

and using (5) with effective ply stiffness for damaged laminate thermal expansion.

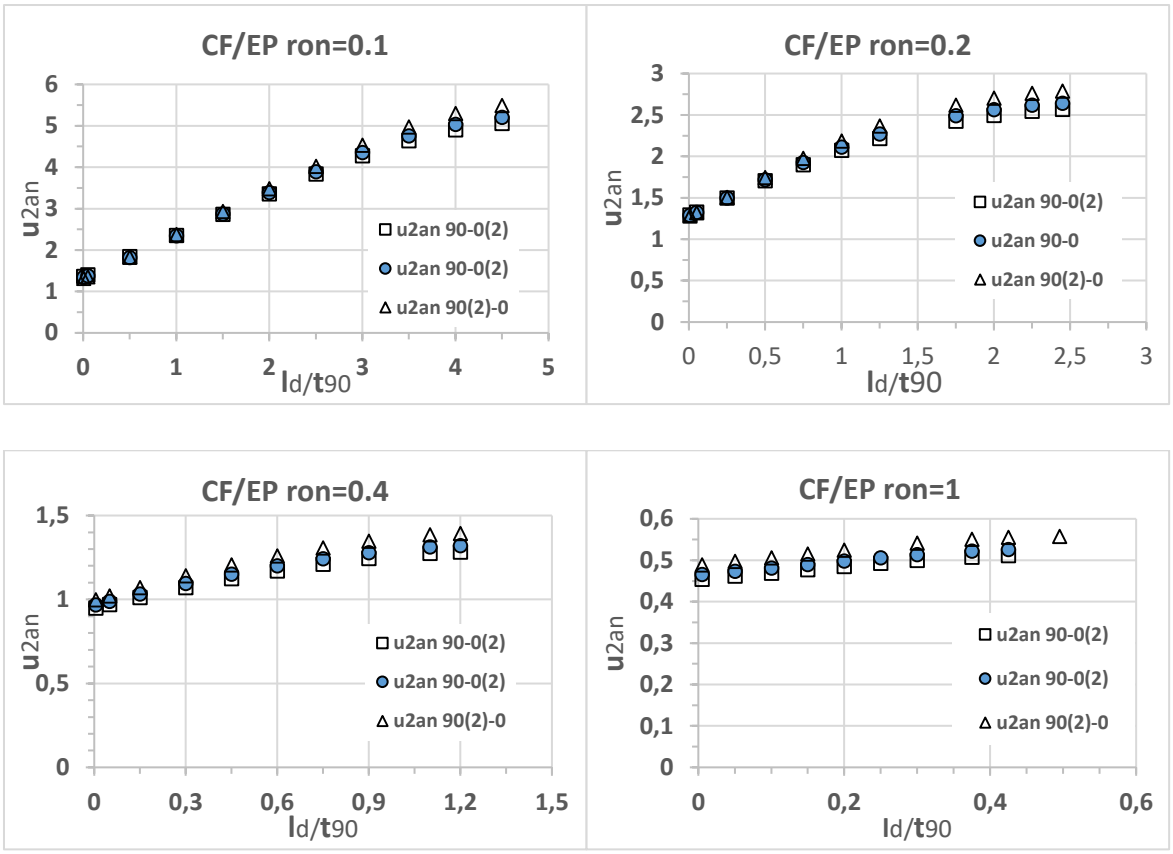



***Figure 7: Average normalized COD of a crack in a surface 90-ply of CF/EP cross-ply laminates as a function of the delamination length for different values of $\rho_{90n}$. Symbols 90(2)-0, 90-0 and 90(2)-0 represent $[90_2/0]_s$, $[90/0]_s$ and $[90_2/0]_s$ lay-ups.***

The effective stiffness of the damaged ply, strictly speaking, is not a ply property – it depends also on parameters of the surrounding material. We can find it by back-calculation from the laminate stiffness as explained below and analyze the effect of surrounding plies.

Assume that the two surface 90-plies of the cross-ply laminate with indexes 1 and $N$ are the ones that will be damaged, and their stiffness matrix in global coordinates is $[\bar{Q}]_{90}$ (index "90" is used to denote the ply which will have cracks). The undamaged symmetric laminate stiffness matrix can be written as

$$[Q]_0^{LAM} = 2\frac{t_{90}}{h}[\bar{Q}]_{90} + \sum_{k=2}^{N-1}\frac{t_k}{h}[\bar{Q}]_k \qquad (36)$$

In (36) $t_{90}$ is the thickness of the 90-ply. After cracking the effective stiffness of the 90-ply changes from $[\bar{Q}]_{90}$ to $\left[\overline{Q(\rho_c)}\right]_{90}^{eff}$ and according to CLT the extensional stiffness matrix of the laminate can be written as

$$[Q]^{LAM} = 2\frac{t_{90}}{h}[\bar{Q}]_{90}^{eff} + \sum_{k=2}^{N-1}\frac{t_k}{h}[\bar{Q}]_k \quad (37)$$

Subtracting (37) from (36) we obtain for laminate with a cracked surface 90-plies the effective stiffness matrix of the cracked surface ply in global coordinates

$$[\bar{Q}]_{90}^{eff} = [\bar{Q}]_{90} - \frac{h}{2t_{90}}\left\{[Q]_0^{LAM} - [Q]^{LAM}\right\} \quad (38)$$

If, instead, the central ply in the symmetric laminate is damaged, the expression is slightly different

$$[\bar{Q}]_{90}^{eff} = [\bar{Q}]_{90} - \frac{h}{t_{90}}\left\{[Q]_0^{LAM} - [Q]^{LAM}\right\} \quad (39)$$

From (39) the effective compliance matrix of the damaged ply in local axes can be obtained and used to find the effective engineering constants of the damaged layer

$$E_L^{eff} = 1/S_{11}^{eff}\ ,\ E_T^{eff} = 1/S_{22}^{eff}\ , \nu_{LT}^{eff} = -E_L^{eff}S_{12}^{eff},\ G_{LT}^{eff} = 1/S_{66}^{eff} = Q_{66}^{eff} \quad (40)$$

In this Section, we will use CLT to calculate the stiffness of the undamaged laminate. The damaged laminate stiffness at fixed crack density and delamination length will be found using GLOB-LOC expressions in Section 2.3 with COD calculated using FEM and presented in Section 3.

## 4.2 Parametric analysis and fitting expression

Calculations showed that the effective longitudinal modulus $E_L^{eff}$ and Poisson's ratio $\nu_{LT}^{eff}$ of the damaged ply do not change with crack density and delamination length change. It is not that the change would be small; the change is identically zero.

The effective transverse modulus $E_T^{eff}$ calculated as described in Section 4.1 from three different lay-ups with cracks in central 90-ply is presented in **Figure 8** for GF/EP and CF/EP 90-plies. The central 90-ply in these $[0_n/90_n]_s$ laminates has certain intralaminar crack density $\rho_{90n}$ and delamination length $l_d$ normalized with respect to the 90-ply thickness $t_{90}$. Results are illustrated only for two values of crack density: $\rho_{90n} = 0.1$ which in zero delamination case would represent non-interactive cracks and $\rho_{90n} = 1.0$ which is a very high crack density, close to so called "saturation state". The behavior is very similar also for other crack densities used in calculations but not shown.

An important observation is that the back-calculated effective transverse modulus dependence on the delamination length is practically independent on the ply thickness ratio in the laminate used for back-calculation. This conclusion holds for all investigated crack densities and delamination length. There are certain differences dependent on the material used: the CF/EP effective transverse modulus seems to have more linear dependence on the delamination length.

The next goal is to find a fitting function describing the dependence on delamination length for all data presented in **Figure 8**. Since the ply thickness ratio has a very small effect on the back-calculated $E_T^{eff}$, in the following analysis we use the $E_T^{eff}$ values of plies in $[0/90]_s$ laminates, considering them as representative.

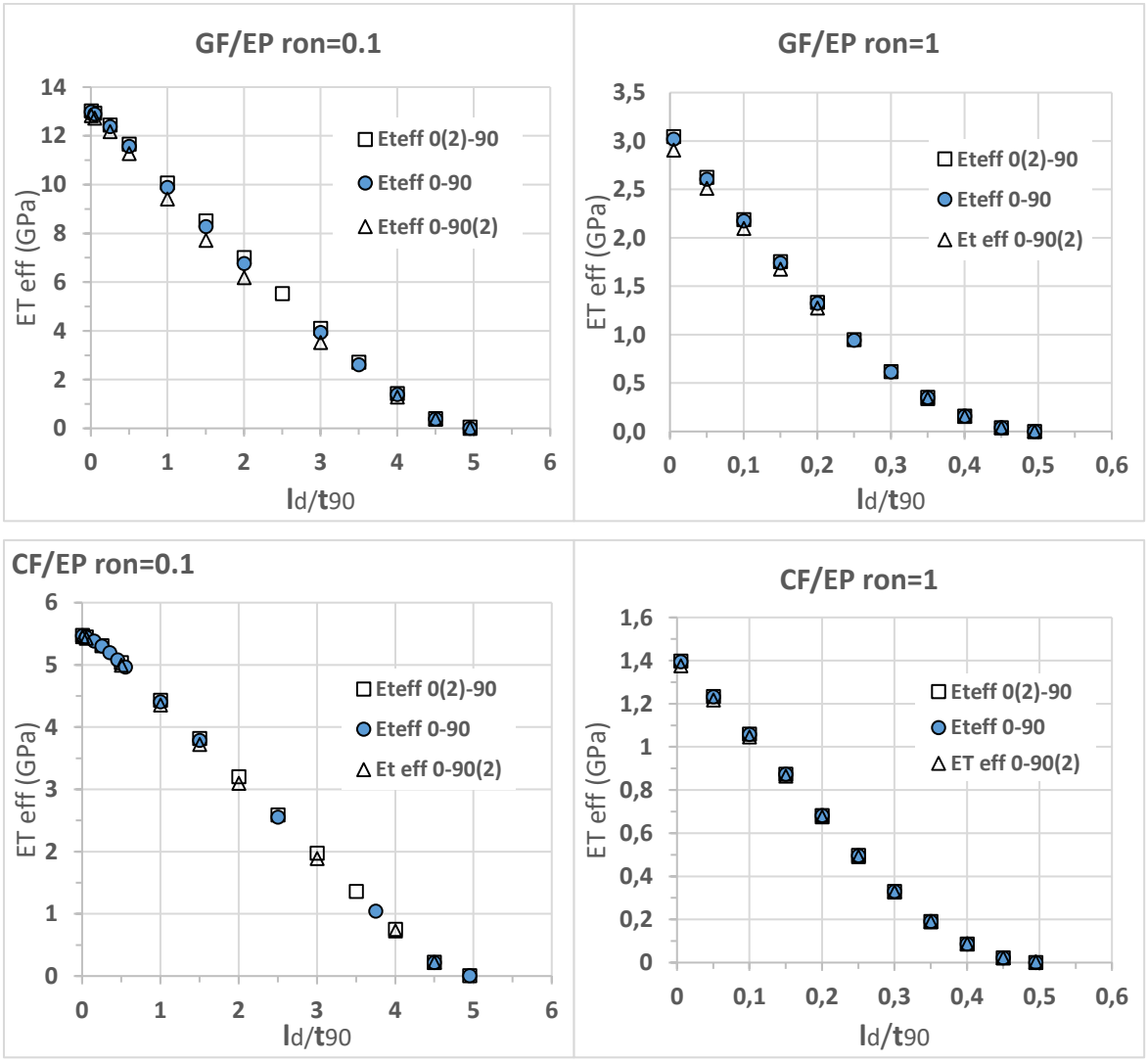



***Figure 8: Effective transverse modulus of a damaged central 90-ply in cross-ply laminates as a function of the delamination length for different values of $\rho_{90n}$. Symbols 0(2)-90, 0-90 and 0-90(2) represent $[0_2/90]_s$, $[0/90]_s$ and $[0/90_2]_s$ lay-ups.***

First, we introduce normalized delamination length which represents a half of the fraction of the interface which is delaminated

$$l_{dn} = \frac{l_d}{2l_{90}} \tag{41}$$

The effective transverse modulus at each crack density and delamination length is normalized with respect to $E_T^{eff}(\rho_{90n}, l_{dn} = 0)$ which corresponds to the effective modulus for this crack density but with zero delamination

$$E_{Tn}^{eff} = \frac{E_T^{eff}(\rho_{90n}, l_{dn})}{E_T^{eff}(\rho_{90n}, l_{dn}=0)} \tag{42}$$

In **Figure 9**, the effective transverse modulus data for four different crack densities are presented in the form with normalized values (41), (42). As a first approximation we assume that one single function can describe the data for all GF/EP and CF/EP laminates.

$$E_T^{eff} = E_T^{eff}(\rho_{90n}, l_{dn} = 0) \cdot \left(\frac{1-0.35l_{dn}}{1-l_{dn}} - 3.3l_{dn}\right) \tag{43}$$

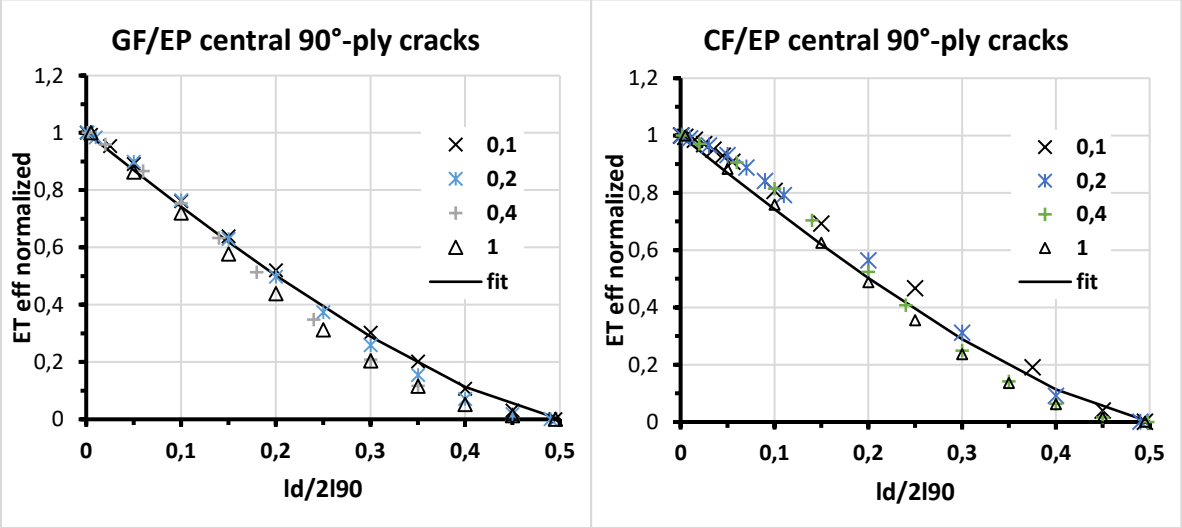



***Figure 9: Effective transverse modulus of a damaged central 90-ply in cross-ply laminates normalized with respect to its' value at the same crack density at zero delamination length. Dependence on relative delamination length (defined as $l_d/l_{90}$ ) for different values of $\rho_{90n}$. different symbols refer to different values of $\rho_{90n}$.Fitting using eq (43) is presented as solid line.***

The fitting accuracy shown in **Figure 9** is satisfactory and can always be replaced by a more accurate, for example, with different coefficients for CF/EP and GF/EP. However, that would

be require a very detailed analysis of the differences caused by different elastic properties. Another factor to consider is the required accuracy: at large intralaminar crack density the effective transverse modulus is low even without delaminations and the accuracy requirement for further reduction can be low.

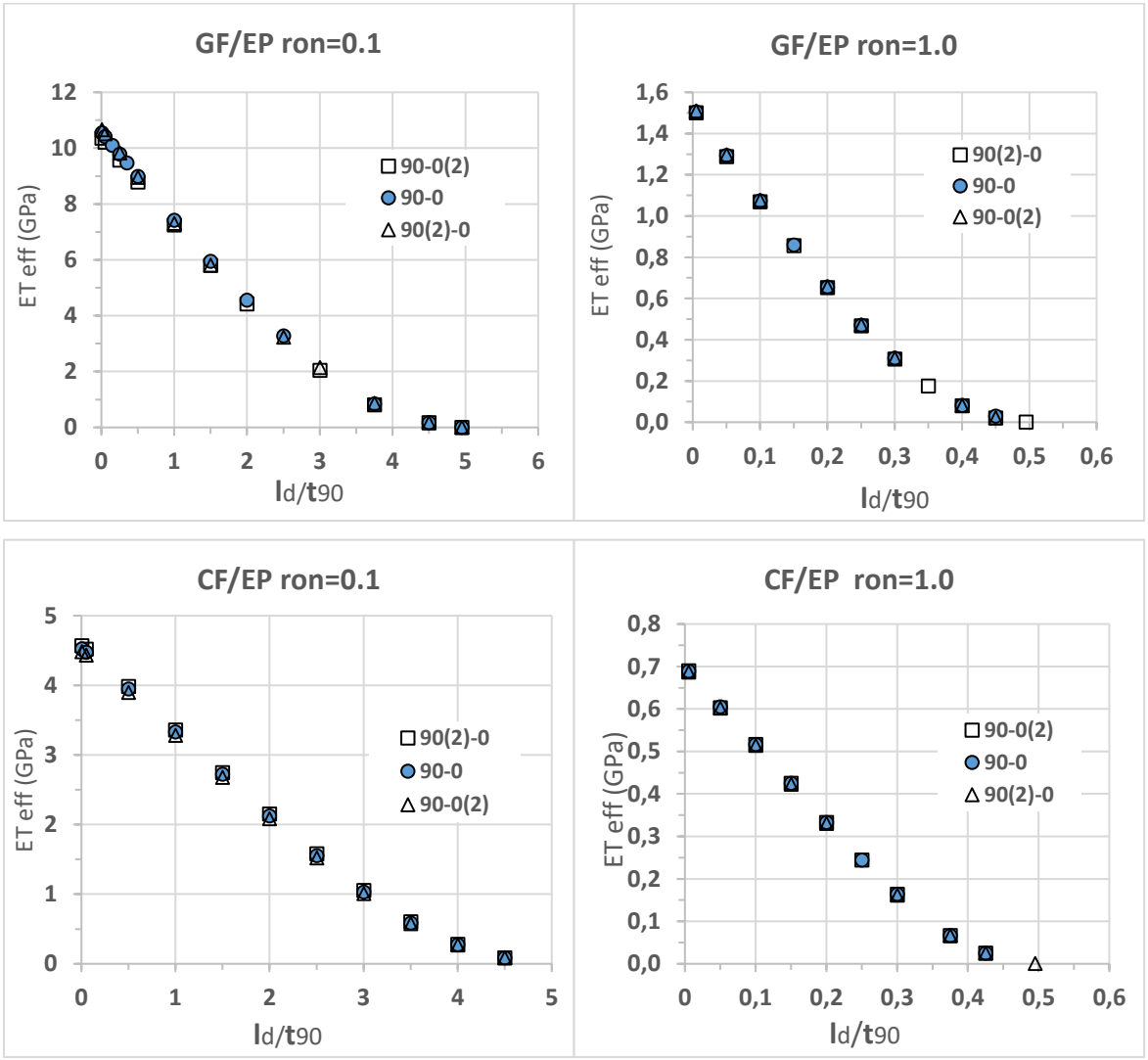



***Figure 10: Effective transverse modulus of a damaged surface 90-ply in cross-ply laminates as a function of the delamination length for different values of $\rho_{90n}$. Symbols 90(2)-0, 90-0 and 90-0(2) represent $[90_2/0]_s$, $[0/90]_s$ and $[90/0_2]_s$ lay-ups.***

The dependence on crack density of the effective transverse modulus of the ply $E_T^{eff}$ in absence of delaminations was thoroughly investigated in **(Varna J. and M. Loukil, 2016),** showing that for a wide range of material parameters, lay-ups and crack density the effective transverse modulus can be approximated by the expression:

$$E_T^{eff}(\rho_{90n}, l_{dn} = 0) = E_T\left(\frac{3}{5}\cdot e^{-2.5M\rho_n} + \frac{2}{5}\cdot e^{-0.9M\rho_n}\right) \quad (44)$$

Parameter $M = 1$ for central cracked ply and $M = 2$ for surface plies. The effect of adjacent ply properties on the effective transverse modulus is very small and it is neglected in (44).

**Figures 10** and **11** contain similar results for effective modulus of damaged surface plies of cross-ply laminates. The general trends are very similar but one coefficient in the fitting function (43), used also for these laminates, is slightly different:

$$E_T^{eff} = E_T^{eff}(\rho_{90n}, l_{dn} = 0)\cdot\left(\frac{1-0.35l_{dn}}{1-l_{dn}} - 3.6\, l_{dn}\right) \quad (45)$$

In **Figure 11** data for $E_{Tn}^{eff}$ are presented together with predictions based on the obtained fitting functions. Using expression (43) for laminates with damaged surface layers results in overestimated effective transverse modulus. A better fit is obtained using eq (45).

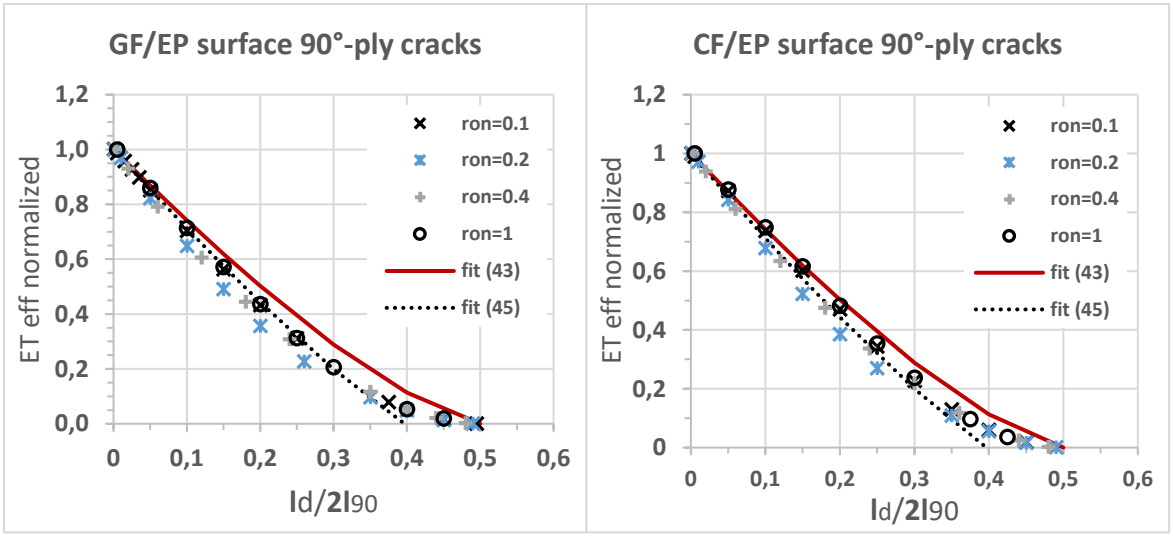



***Figure 11: Effective transverse modulus of a damaged central 90-ply in cross-ply laminates normalized with respect to its' value at the same crack density at zero delamination length. Dependence on relative delamination length (defined as $l_d/2l_{90}$ ) for different values of $\rho_{90n}$.***

## 5. Validation examples

In the following simulation examples equation (43) is used with the effective modulus $E_T^{eff}(\rho_{90n}, l_{dn} = 0)$ calculated using expression (44). Since currently we do not have similar expressions for effective shear modulus of the damaged ply, we will limit examples to cases

where the shear response of the damaged ply is of no relevance. These are loading cases and lay-ups where the in-plane shear stresses in the damaged play are zero. Comparison of thermo-elastic constants will be made between: a) FEM results; b) predictions based on effective stiffness together with CLT and c) the GLOB-LOC predictions using the FEM calculated values of the COD.

As the first example, see **Figure 12**, we consider two GF/EP cross-ply laminates and compare their axial modulus calculated in the three above-listed ways. Since the COD values for GLOB-LOC calculations come from the same FEM model as the presented axial modulus, it is not surprising that the GLOB-LOC and FEM values coincide: expressions in Section 2.3 are exact.

The predictions based on the CLT where the transverse modulus of the damaged ply is replaced by effective values from (43), (44) shown as CLT in **Figure 12** is very accurate in spite to rather rough approximation deriving (43) from **Figure 9.**

This is also the case in **Figure 13** where the Poisson's ratio and the axial thermal expansion coefficient for two cross ply laminates are presented. FEM solution coincides with the GLOB-LOC model. Using in predictions the CLT together with effective modulus described by (43), (44), the result is slightly different due to one simple fitting function used for all cases. Nevertheless, the predictions are in good agreement with FEM.

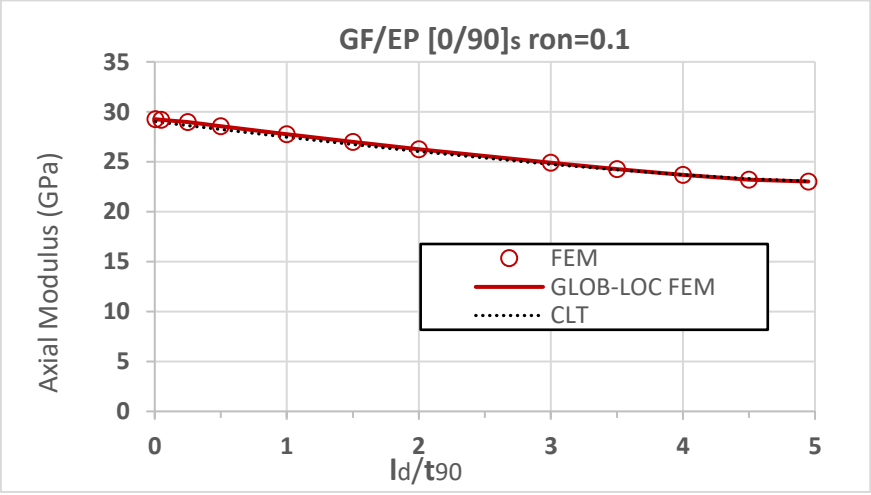



***Figure 12: Axial modulus of cross-ply laminate with damaged central 90-ply. Dependence on relative delamination length (defined as $l_d/t_{90}$ ) for $\rho_{90n} = 0.1$. Symbols represent FEM solution; GLOB-LOC has COD from FEM; the dotted line is by using eq (43), (44) in CLT.***

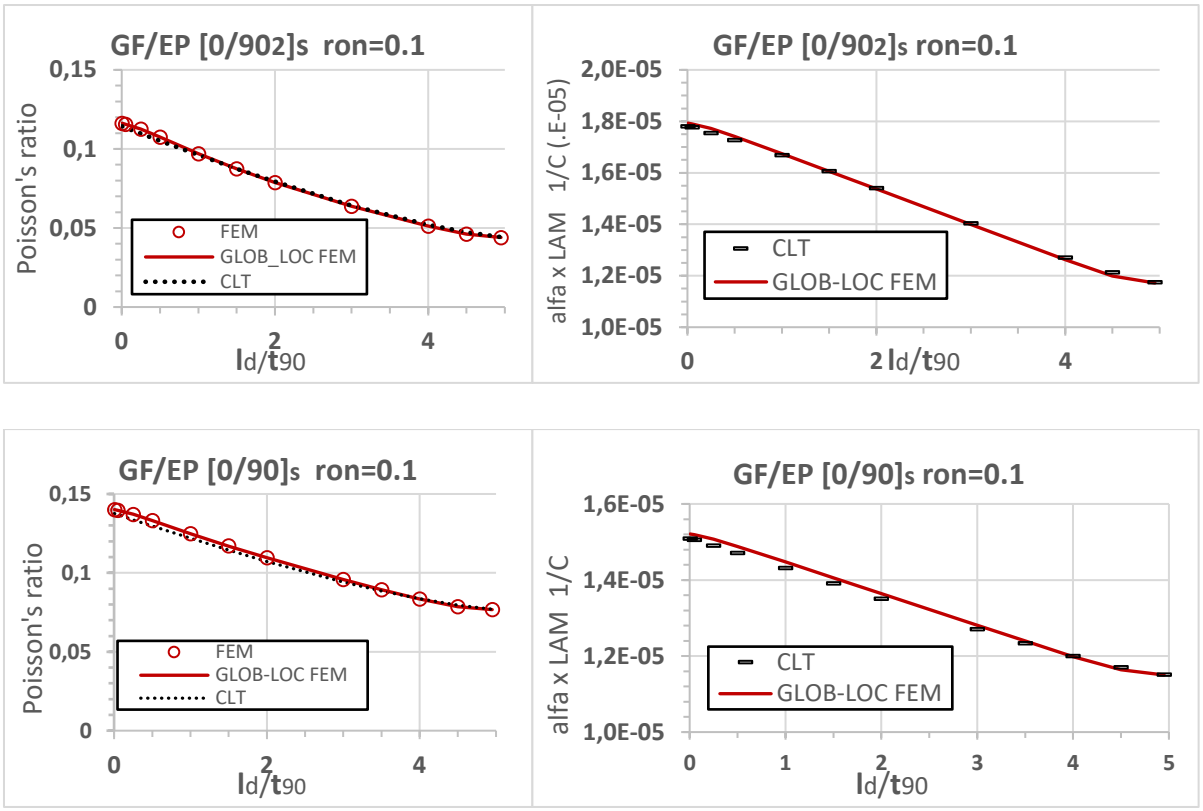



***Figure 13: Poisson's ratio of two cross-ply laminate with damaged central 90-ply. Dependence on relative delamination length (defined as $l_d/t_{90}$ ) for $\rho_{90n} = 0.1$. Symbols represent FEM solution; GLOB-LOC has COD from FEM; the dotted line is by using eq (43), (44) in CLT.***

# 6. Conclusions

Stiffness reduction in symmetric laminates with intralaminar cracks in plies and local delaminations originating at the intralaminar crack tip is analyzed using the crack opening (COD) and sliding displacement (CSD) based approach (GLOB-LOC) developed in (**Varna, 2013).** Analysis show that the displacement gap (sliding and opening) on the delamination crack surfaces does not enter the in-plane stiffness reduction expressions explicitly. Their influence on stiffness is via increasing opening of the intralaminar cracks. This finding allows using the same expressions for laminate thermo-elastic constants in cases with and without delaminations. However, the input values of COD and CSD in these expressions are different.

The performed FEM parametric analysis of the COD for cracks with delaminations in internal (central) and surface 90-plies of cross-ply laminates shows that the COD dependence on elastic constants and geometrical parameters is rather complex and simple and accurate fitting

functions were not found. Instead, the numerical COD data were used in the GLOB-LOC model to predict the whole set of thermo-elastic constants of the damaged laminate with selected lay-up and material properties. These values are as accurate as the FEM values would be if obtained using the same mesh and applying thermal and mechanical loads.

The obtained damaged laminate elastic constants were used to back-calculate the so called "effective stiffness" of the damaged ply, a parameter that when used in the Classical Laminate Theory would render exactly the same results as FEM. Theoretically the back-calculated values depend on the laminate analyzed that would limit their application. However, analysis showed that the surrounding plies (their elastic constants, orientation and thickness) have a negligible effect on the effective modulus. It allowed to introduce a simple and accurate fitting expression that describes the effective transverse modulus dependence on intralaminar crack density and on delamination length.

As expected, the axial modulus, Poisson's ratio for damaged laminates, calculated directly with FEM are coinciding with the GLOB_LOC model results when in this model the COD from FEM is used as input. Even predictions using the developed fitting functions for effective transverse modulus are in an excellent agreement with the numerical results for above elastic constants and for axial thermal expansion coefficients of laminates proving the efficiency and the validity of the effective ply stiffness concept used in CLT.

# References

Allen, D. H., & Yoon, C. (1998). Homogenization techniques for thermoviscoelastic solids containing cracks. *International Journal of Solids and Structures*, *35*(31-32), 4035-4053.

ANSYS 5.6 Structural Analysis Guide, 5th edition, ANSYS Inc, November 1999.

Bussetta, P., Marceau, D., &Ponthot, J. P. (2012). The adapted augmented Lagrangian method: a new method for the resolution of the mechanical frictional contact problem. *Computational Mechanics*, *49*(2), 259-275.

Gudmundson, P., & Zang, W. (1993). A universal model for thermoelastic properties of macro cracked composite laminates. *International Journal of Solids and Structures*, *30*(23), 3211-3231.

Hajikazemi, M., & McCartney, L. N. (2018). Comparison of Variational and Generalized Plane Strain approaches for matrix cracking in general symmetric laminates. *International Journal of Damage Mechanics*, *27*(4), 507-540.

Hashin, Z. (1985). Analysis of cracked laminates: a variational approach. *Mechanics of materials*, *4*(2), 121-136.

Jamison, R. D., Schulte, K., Reifsnider, K. L., &Stinchcomb, W. W. (1984). Characterization and analysis of damage mechanisms in tension-tension fatigue of graphite/epoxy laminates. In *Effects of defects in composite materials*. ASTM International.

Joffe, R., & Varna, J. (1999). Analytical modeling of stiffness reduction in symmetric and balanced laminates due to cracks in 90 layers. *Composites Science and Technology*, *59*(11), 1641-1652.

Joffe, R., Krasnikovs, A., & Varna, J. (2001). COD-based simulation of transverse cracking and stiffness reduction in [S/90n] s laminates. *Composites science and technology*, *61*(5), 637-656.

Kashtalyan, M., &Soutis, C. (2005). Analysis of composite laminates with intra-and interlaminar damage. *Progress in Aerospace Sciences*, *41*(2), 152-173.

Lundmark, P., & Varna, J. (2003). Modeling thermo-mechanical properties of damaged laminates. In *Key Engineering Materials*(Vol. 251, pp. 381-388). Trans Tech Publications.

Lundmark, P., & Varna, J. (2005). Constitutive relationships for laminates with ply cracks in in-plane loading. *International Journal of Damage Mechanics*, *14*(3), 235-259.

Lundmark, P., & Varna, J. (2006). Crack face sliding effect on stiffness of laminates with ply cracks. *Composites Science and Technology*, *66*(10), 1444-1454.

Loukil, M. S., Varna, J., &Ayadi, Z. (2013). Engineering expressions for thermo-elastic constants of laminates with high density of transverse cracks. *Composites Part A: Applied Science and Manufacturing*, *48*, 37-46.

McCartney, L. N., &Schoeppner, G. A. (2002). Predicting the effect of non-uniform ply cracking on the thermoelastic properties of cross-ply laminates. *Composites Science and Technology*, *62*(14), 1841-1856.

McCartney, L. N., Schoeppner, G. A., & Becker, W. (2000 B). Comparison of models for transverse ply cracks in composite laminates. *Composites Science and Technology*, *60*(12-13), 2347-2359..

McCartney, L. N., Blazquez, A., & Paris, F. (2012). Energy-based delamination theory for biaxial loading in the presence of thermal stresses. *Composites Science and Technology*, *72*(14), 1753-1766.

Nairn, J. A., & Hu, S. (1994). Composite Materials Series: Damage Mechanics of Composite Materials, R. Talreja, Ed.,9, Elsevier, Amsterdam, 187-243.

Nuismer, R. J., & Tan, S. C. (1988). Constitutive relations of a cracked composite lamina. *Journal of Composite Materials*, *22*(4), 306-321.

O'Brien, T. K. (1982). Characterization of delamination onset and growth in a composite laminate. In *Damage in Composite Materials: Basic Mechanisms, Accumulation, Tolerance, and Characterization*. ASTM International, 140-167

Parvizi, A., & Bailey, J. E. (1978). On multiple transverse cracking in glass fibre epoxy cross-ply laminates. *Journal of Materials Science*, *13*(10), 2131-2136.

Pupurs, A., Varna, J., Loukil, M., Kahla, H. B., &Mattsson, D. (2016). Effective stiffness concept in bending modeling of laminates with damage in surface 90-layers. *Composites Part A: Applied Science and Manufacturing*, *82*, 244-252.

Smith, P. A., & Wood, J. R. (1990). Poisson's ratio as a damage parameter in the static tensile loading of simple crossply laminates. *Composites Science and Technology*, *38*(1), 85-93..

Takeda, N., Ogihara, S., & Kobayashi, A. (1995). Microscopic fatigue damage progress in CFRP cross-ply laminates. *Composites*, *26*(12), 859-867.

Varna, J., & Berglund, L. (1991). Multiple transverse cracking and stiffness reduction in cross-ply laminates. *Journal of Composites, Technology and Research*, *13*(2), 97-106.

Varna, J., & Berglund, L. A. (1994). Thermo-elastic properties of composite laminates with transverse cracks. *Journal of Composites, Technology and Research*, *16*(1), 77-87.

Varna, J. (2013). Modelling mechanical performance of damaged laminates. *Journal of composite materials*, *47*(20-21), 2443-2474.

Varna, J. (2015). Strategies for stiffness analysis of laminates with microdamage: combining average stress and crack face displacement based methods. *ZAMM-Journal of Applied Mathematics and Mechanics/ZeitschriftfürAngewandteMathematik und Mechanik*, *95*(10), 1081-1097.

Varna, J., & Loukil, M. S. (2017). Effective transverse modulus of a damaged layer: Potential for predicting symmetric laminate stiffness degradation. *Journal of composite materials*, *51*(14), 1945-1959.

Zhang, J., Fan, J., &Soutis, C. (1992). Analysis of multiple matrix cracking in [±θm/90n] s composite laminates. Part 1: In-plane stiffness properties. *Composites*, *23*(5), 291-298.

# Paper D

# Effective stiffness concept in bending modeling of laminates with damage in surface 90-layers

A. Pupurs[1,2], J. Varna[1*], M. Loukil[2] , H. Ben Kahla[1], D. Mattsson[2]

[1]Composites Centre Sweden, Luleå University of Technology, Luleå, Sweden

[2]Swerea SICOMP, Piteå, Sweden

* Corresponding author (Janis.Varna@LTU.SE)

## Abstract

Simple approach based on Classical Laminate Theory (CLT) and effective stiffness of damaged layer is suggested for bending stiffness determination of laminate with intralaminar cracks in surface 90-layers and delaminations initiated from intralaminar cracks. The effective stiffness of a layer with damage is back-calculated comparing the in-plane stiffness of a symmetric reference cross-ply laminate with and without damage. The in-plane stiffness of the damaged reference cross-ply laminate was calculated in two ways: 1) using FEM model of representative volume element (RVE) and 2) using the analytical GLOB-LOC model. The obtained effective stiffness of a layer at varying crack density and delamination length was used to calculate the *A, B* and *D* matrices in the unsymmetrically damaged laminate. The applicability of the effective stiffness in CLT to solve bending problems was validated analyzing bending of the damaged laminate in 4-point bending test which was also simulated by 3-D FEM.

**Keywords**: Bending stiffness; Transverse cracking; Analytical modeling; Finite element analysis (FEA)

# 1. Introduction

During service life a structural element made of laminated fiber reinforced composites is subjected to various combinations of thermo-mechanical and environmental loads causing microdamage in layers as well as between layers (interlayer delamination). The most typical and earliest damage mode in layers is intralaminar cracking often referred also as matrix cracking, tunneling cracks or transverse cracking, see **Figure.1**. The latter name reflects the fact that the crack plane is usually transverse to the laminate middle-plane. The crack runs parallel to fibers in the layer and often (especially in thick layers) it covers the whole thickness of the layer (arrested at the interface with a layer of different fiber orientation) and the width of the specimen. On microscale these cracks are built by coalescence of many fiber/matrix interface failure events (debonds) via matrix cracks linking them. From macroscopic point of view intralaminar cracking is the first damage mode because the transverse tensile strain and in-plane shear strength to failure of unidirectional polymeric composites are lower than other failure strain and stress components. Realizing that tensile in-plane transverse stress and in-plane shear stress cause similar failure mechanisms we can state that combined action of transverse tensile stress and shear stress cause intralaminar cracking in layers of laminates.

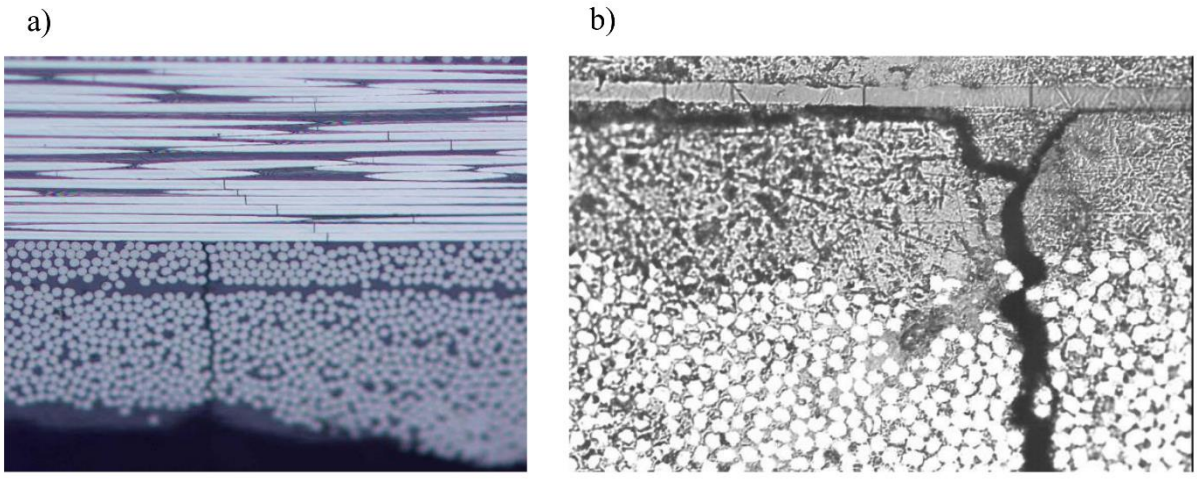



***Figure.1: a) Transverse crack in 90-layer of cross ply laminates; b) local delaminations developing from transverse crack tip.*** ***(For interpretation of the references to colour in this figure legend, the reader is referred to the web version of this article.)***

Due to statistical variation of transverse and shear strength values along the transverse direction of the layer, the first intralaminar crack is created in the weakest position. With increasing applied load (or with increasing number of cycles in cyclic loading) the number of cracks increases.

The number of cracks per unit length in a layer is an average measure of the extent of cracking called crack density, denoted as $\rho_c$. **Figure 2** shows an example of cracking evolution in a 90-layer of glass fiber/epoxy cross-ply laminate. Due to high out-of-plane shear stress concentration and tensile normal out-of-plane stress at the tip of the intralaminar crack where it meets the interface with the next layer, local delaminations are often observed there, see **Figure 1b**. The delamination in **Figure 1b** is from intralaminar crack in the central 90-layer in tensile loading. Due to large tensile out-of-plane normal stress component [1], delaminations initiated in tension from cracks in surface layers or delaminations due to bending are generally larger than from cracks in central layers. As shown in **Figure 1a** the stress concentration can lead to fiber breaks in the neighboring layer. Delaminations are growing during the service life and can be characterized by average delamination length $l_d$. For convenience and for reasons described below the average distance between cracks $2l_c$ which is inversely proportional to the crack density $\rho_c$ in a layer and the delamination length $l_d$ may be normalized with respect to the damaged layer thickness (characteristic dimension of the tunnel).

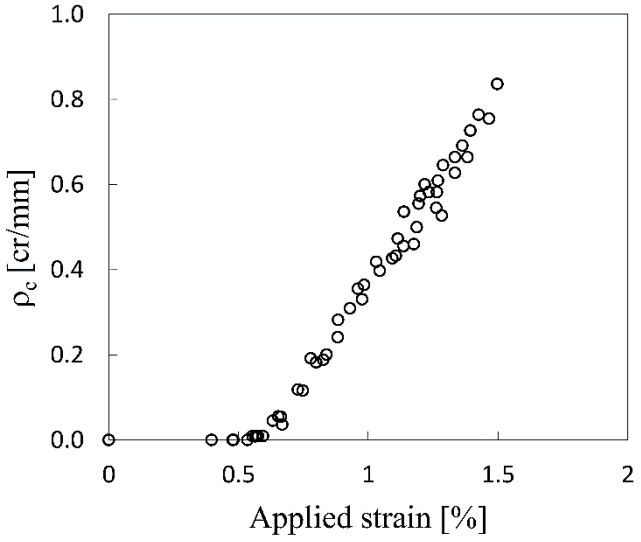



***Figure 2: Crack density as a function of applied strain in glass fiber/epoxy cross-ply laminate.***

An inevitable consequence of microdamage progression is degradation of macroscopic thermo-mechanical properties of the laminate. Constitutive models for in-plane behavior of damaged laminates have been historically developed using two basic approaches, see, for example, reviews in [2,4]: a) continuum damage mechanics approach and b) approach called micromechanics modeling, where stress state in the laminate with cracks is analyzed using analytical and/or numerical methods. The found approximate stress field solution between two cracks is used to determine certain thermo-elastic constants of the damaged laminate. The simplest stress distributions between two cracks are obtained based on shear lag assumption [5] or variational principles [3,6,8]. Most of the analytical solutions are developed for cross-ply type of laminates with cracks in internal 90-layers only, constrained by homogeneous orthotropic material with averaged elastic constants representing the sequence of layers on the top and the bottom of the damaged layer (usually it is balanced sublaminate that has to be considered as symmetrical due to the constraints to being a part of the laminate). Usually the studied properties are laminate axial modulus, Poisson's ratio and in-plane shear modulus. Probably, the most accurate model which is based on Reissner's variational principle was suggested in [9]. It renders very accurate stress distributions comparable with FEM solutions.

Regarding bending stiffness reduction of composite laminates, models based on beam theory in conjunction with shear-lag analysis have been developed in [10,11]. Apart from the used simple one-dimensional analysis, this approach conceptually is similar to the one used in the current paper: the effective elastic modulus of the damaged layer was back-calculated from the in-plane modulus of a reference damaged beam and used to calculate the bending modulus of a similar multilayer beam.

Variational models for stresses in damaged cross-ply laminates [1,12,13,14] and continuum damage mechanics approach [15] have also been previously used for bending stiffness analysis of laminates with damage. In [1] stress analysis in the cracked surface layer of the cross-ply laminate under bending was modeled assuming linear axial stress dependence on the thickness coordinate and using the principle of minimum complementary energy. The assumption is of the same type and approximation as used by Hashin in tensile case [6]. The results are in a reasonable agreement with FEM solution in positions not too close to the crack tip. In [12] this approach was generalized to an arbitrary number of damaged and undamaged layers in a cross-ply laminate under general in-plane and out-of-plane loading, thus, allowing application of ply-

refinement method. In addition, in [12] a comprehensive review of methods and assumptions used in bending modeling can be found.

The ply-refinement technique dividing each ply in several sublayers was used also in the model presented in [13] Stress and displacement distributions in a bended laminate with cracks in 90-plies were obtained assuming quadratic dependence of the out-of-plane stress on the thickness coordinate in each damaged sublayer. In the undamaged layers linear dependence of axial displacements on the thickness coordinate is used. The problem was reduced to solving a high order system of differential equations with constant coefficients. All equilibrium and interface conditions are satisfied except the axial strain-displacement relationship, which is satisfied in average. The model in [13] assumes plane strain condition, thus being limited to cases with one curvature only. This limitation was removed in [14], extending the analysis to orthogonal bending. The latter model was used to solve Test case 9 in the WWFE-III [16]. A drawback of this model and the model in [12] is that rather complex numerical calculations have to be performed to find the stress state for any change of the damage state and/or the geometrical and elastic parameters of layers and the lay-up. The bending stiffness determination routine is exactly the same as it would be using FEM. The approach we are suggesting in this paper is simpler (does not require accurate stress distributions), more flexible and easy to apply. Methods for simulating the intralaminar damage development under bending are presented, for example, in [16,17] where further references can be found.

In [15] extensional, coupling and bending stiffness matrices of the damaged laminate were calculated using the crack face displacement based approach presented in [18]. The expressions used in [15] are linear with respect to crack density, which according to [19] is an approximation with unknown consequences at high crack densities. Also the expressions for face displacements used in [15] are for infinite homogeneous medium and therefore they can lead to rather high inaccuracies when used for cracks constrained by stiff but finite layers [19]. Since damage development is the focus in [15], results for bending stiffness changes are not presented and the only indication of accuracy in bending case is that the nonlinear experimental bending curve and simulations agree well.

In the present paper we suggest a method based on the Classical Laminate Theory (CLT) and the concept of the effective stiffness of the damaged layer to calculate the extensional-, coupling- and bending stiffness matrices (*A, B, D* respectively) for laminate which is unsymmetric due to different intralaminar cracking and delamination state in surface 90-layers.

The effective stiffness of the layer is determined by back-calculation: for a symmetric reference laminate the difference between the undamaged and damaged extensional stiffness matrix is calculated. To find the damaged laminate in-plane stiffness matrix needed in back-calculation, two methods were used in this paper: 1) FEM model of representative volume element (RVE) and 2) analytical GLOB-LOC model which is based on crack opening displacement (COD), which depends on crack density $\rho_c$ and delamination length $l_d$ .

The approach was validated using the calculated *A*, *B* and *D* matrices of the damaged laminate to simulate the applied moment versus curvature relationship in a 4-point bending test and comparing results with 3-D FEM simulations with the same boundary conditions.

## 2. Concept of effective stiffness

The stress perturbation due to damage in one layer may affect the stress state around the damage entity in another layer thus changing its effect on the laminate stiffness. The interaction between different damage modes is especially important for neighboring layers, not so much for layers that do not have common interface. In an approximate way the interaction effect can be accounted for by replacing one of the damaged layers by homogenized (non-damaged) layer with effective elastic properties as it was done, for example, in [20] using modified shear lag model and so called "equivalent constraint model". A routine to determine the effective properties of the damaged layer is necessary for this purpose.

In the present paper we use a similar approach to predict the *A*, *B* and *D* matrix of a laminate with intralaminar cracks in the surface 90-layer, where during bending the local transverse stresses are tensile, and with local delaminations. It is not implied that these cracks are introduced during the bending; they could as well be result of in-plane tensile or thermal loading. Intralaminar cracks in layers under transverse compression are closed and do not affect the stiffness. Crack face sliding in 90-layer is not an issue in four point bending. We suggest using CLT to calculate the $A, B, D$ matrices of the damaged laminate using the so called "effective stiffness" for the layer with intralaminar cracks and delaminations. The effective stiffness decays with increasing crack density in the layer.

The key issue in this approach is the method of calculation of the effective stiffness of a layer with cracks and local delaminations. The most conservative solution called "ply-discount model" is well known: elastic constants of the cracked layer are assumed zero. The

modification of the ply-discount model appropriate for intralaminar cracking assumes zero transverse modulus and in-plane shear modulus of the layer as soon as the layer fails. This assumption leads to zero transverse and shear stress in the damaged layer. This approach does not consider the fact that the crack density increases gradually and the effective stiffness change is progressive. In fact ply-discount model is equal to assumption that an infinite number of cracks develop instantly. This would indeed lead to transverse and in-plane shear stresses in the layer approaching to zero as requested by the ply-discount assumption.

A correct way of determining the effective stiffness of a layer would be by back-calculation: finding the stiffness of the undamaged laminate (experimentally or by calculations knowing the lay-up and layer properties) and also the stiffness of the damaged laminate (experimentally or using FEM). Then the effective stiffness of the damaged layer can be found from the difference by back-calculation using CLT. To avoid this approach of being self-predictive, the back-calculation in order to find the effective stiffness of the layer as a function of crack density and other parameters have to come from a different test (experimental or simulated). We suggest calculating elastic in-plane constants of a symmetric reference cross-ply laminate without cracks and with given crack density to obtain this dependency. In the symmetric reference laminate the damaged layer should have the same thickness ratio and orientation of closest layers as in the bending problem to be solved. The obtained effective stiffness of the damaged layer will be used to predict the damaged laminate *A, B, D* matrices as a function of crack density $\rho_c$ and delamination length $l_d$. Since in in-plane tension the stress in a layer is uniform, whereas in bending it depends on thickness coordinate, the accuracy of the procedure is not known *a priori*. As a matter of fact, even the applicability of the effective stiffness from tensile test in simulating the bending case is not obvious. It may be expected that the accuracy would increase in thick laminate with thin cracked surface layer because the thickness distribution of the transverse stress in this case is rather uniform.

It is easy to realize that in cases where the transverse stress in the damaged layer is compressive, the intralaminar crack faces are in contact and the layer transverse modulus is as it was before cracking (in a more general case not considered in this paper, the crack faces being in contact can still slide with respect to each other and the in-plane shear modulus of the layer is weakened).

The degradation of the laminate elastic properties due to cracks in layers is uniquely related to the relative displacements of the corresponding points on both crack surfaces (opening and in-

plane sliding displacements) [21]. As long as points on both surfaces coincide (relative displacements are zero) the thermo-elastic properties of the laminate are not affected by the presence of crack. The opening and sliding of crack surfaces reduce the average strain and stress in the damaged layer, thus reducing the part of the load carried by this layer. This part of the load is distributed to the rest of the laminate leading to additional deformation which means reduction of laminate thermo-elastic properties. Thus the crack opening displacement (COD) and crack face sliding displacement (CSD) together with the crack density $\rho_c$ in the layer are the micromechanical parameters governing the amount of macroscopic stiffness reduction. In linear elasticity COD and CSD are proportional to the applied load, ply thickness and, therefore, they have to be normalized to be used in stiffness modeling.

A theoretical framework called GLOB-LOC approach expressing the symmetric damaged laminate in-plane thermo-elastic properties via crack density in layers and the microdamage parameters COD and CSD was presented in [21]. It was shown that only the average values of COD and CSD enter the analytical closed form stiffness expressions and the details of the relative displacement profile are not important. Certainly, parameters characterizing the laminate lay-up and elastic properties of layers also enter these exact expressions.

The dependence of the normalized COD on geometrical parameters of the laminate and on the material properties was studied experimentally using optical microscopy and speckle interferometry on damaged specimens in [22,24]. FE studies were performed to analyze which material and geometry parameters affect the COD and CSD at low crack density (non-interactive cracks). Simple empirical relationships ("power laws") based on these studies were proposed in [19,25].

If the crack density is high the stress perturbations of two neighboring cracks interact and the average stress between cracks at the given applied load is lower. It means that the COD and CSD of interacting cracks are smaller than for non-interactive cracks. This effect was found experimentally in [24] and analyzed theoretically in [26,27].

Exact linear relationships between COD, CSD and the average stress perturbations caused by cracks with or without delaminations were derived in [28]. Hence, any stress distribution model (shear lag, Hashin's etc.) can be used in the analytical GLOB-LOC framework to calculate all thermo-elastic constants of a damaged laminate.

Delaminations propagating from the intralaminar crack tip lead to additional laminate stiffness degradation: in the presence of delaminations the COD becomes larger and the average stress between cracks is lower.

In the present paper the effective stiffness of the surface layer with a given crack density $\rho_c$ and delamination length $l_d$ is back-calculated from the difference between in-plane stiffness of the damaged and the undamaged symmetric reference cross-ply laminate. The damaged laminate stiffness is calculated with two different methods: 1) using FEM model of RVE of the symmetric damaged laminate; 2) using the GLOB-LOC model.

For validation purpose the $A, B$ and $D$ matrices calculated using the effective stiffness of the damaged surface 90-layer and CLT are applied to predict behavior of a cross-ply laminate in 4-point bending test and compared with 3-D FEM simulations.

# 3. Bending resistance of the damaged laminate in 4-point bending test

To validate the approach with effective stiffness used in CLT we will analyze initially symmetric $[90_n/0_m]_s$ cross-ply laminate subjected to bending, for example, 4-point bending test, where a region with constant applied moment $M_x$ exists between loading points leading to constant curvature $k_x$. Exactly the same problem will be analyzed also using 3-D FEM. Nevertheless, expressions presented in this section are valid for any laminate with damaged layers. When intralaminar cracks with or without local delaminations are introduced in the surface 90-layers of the laminate the laminate behavior in bending becomes unsymmetrical. Cracks in the surface layer to which the load is applied are closed due to compressive stresses in this layer, whereas cracks in the surface layer under tension are open. The layer with closed cracks behaves like an undamaged layer. Due to the lack of symmetry the B-matrix of the damaged laminate is not zero and some midplane strains $\varepsilon_{x0}$, $\varepsilon_{y0}$ are also present. The laminate *A*, *B* and *D*-matrices, calculated using the effective stiffness, change in a different way with evolving intralaminar cracking and local delamination. In section 7 we will analyze the change of the laminate bending resistance in 4-point bending test with damage development plotting the bending moment to create unit curvature versus the crack density in a layer $(M_x/k_x)\sim\rho_c$. Another damage parameter will be delamination length $l_d$ normalized with respect to the crack

size (damaged ply thickness $t_{90}$). Both these parameters affect the COD, which according to equations in Section 5.2 can be used to calculate the magnitude of stiffness change.
Boundary conditions will be used with applied $k_x$ leading to $M_x$ and, $\gamma_{xy0} = k_{xy} = k_y = 0$ . In this case the relevant CLT equations are

$$0 = A_{11}\varepsilon_{x0} + A_{12}\varepsilon_{y0} + B_{11}k_x$$

$$0 = A_{12}\varepsilon_{x0} + A_{22}\varepsilon_{y0} + B_{12}k_x$$

$$M_x = B_{11}\varepsilon_{x0} + B_{12}\varepsilon_{y0} + D_{11}k_x$$

$$M_y = B_{12}\varepsilon_{x0} + B_{22}\varepsilon_{y0} + D_{12}k_x \quad (1)$$

$$A_{ij} = \sum_{k=1}^{N} \bar{Q}_{ij}^{k} t_k\,, \qquad B_{ij} = \sum_{k=1}^{N} \bar{Q}_{ij}^{k} \frac{z_{k+1}^2 - z_k^2}{2} \qquad D_{ij} = \sum_{k=1}^{N} \bar{Q}_{ij}^{k} \frac{z_{k+1}^3 - z_k^3}{3} \quad (2)$$

In (2) $t_k$, k=1,2..N is the ply thickness; the overbar is used to denote the stiffness of the layer in the global system of coordinates. For damaged layers the effective stiffness is used. Solving the first three equations (1) with respect to $k_x$ we can express the result in form

$$M_x = C_{11}(\rho_c)k_x \quad (3)$$

where the bending stiffness parameter $C_{11}$ is the proportionality coefficient between the applied moment and the curvature in the 4-point bending test with the applied additional constraints on curvatures formulated above. $C_{11}$ is calculated using elements of the *A*, *B* and *D* matrices for the damaged laminate. The dependence of the bending stiffness parameter $C_{11}$ on crack density and delamination length will be investigated in this study.
It has to be emphasized that:

1) $C_{11}$ is not equal to bending stiffness element $D_{11}$ .
2) The boundary conditions in a real experimental test (we present simulations only) could be different, for example, $\gamma_{xy0} = M_{xy} = M_y = 0$.

# 4. Calculation of the effective stiffness in in-plane loading

As discussed in Section 1 the most extreme case of effective stiffness reduction of the damaged layer is obtained using the ply-discount model. With increasing crack density $\rho_c$ and delamination length $l_d$ the effective stiffness of the damaged layer has to approach to this asymptotic value.

In this section we will present expressions for the effective stiffness of the damaged surface layer in a symmetric laminate, assuming the same damage state (crack density $\rho_c$ , delamination length $l_d$ and crack location) in both surface layers. The effective layer stiffness calculated from this reference laminate will be used to calculate the *A*, *B* and *D* matrices of laminates with similar lay-up (the same layer thickness ratio and adjacent layers with the same orientation). In Section 5 the effective stiffness of the surface 90-layer will be calculated from the in-plane stiffness change of the reference $[90_n/0_m]_s$ laminate and used to predict the bending resistance degradation with increasing damage.

The technique is described more in detail in [29] where also parametric analysis is presented. Specifics of the damage state (types of cracks, delaminations, etc) do not change the mathematical treatment presented in this section. Local delaminations change the in-plane stiffness values of the damaged laminate and a different RVE model, see **Figure 3b**, is used in Section 5 for cracks with delaminations. The undamaged and the damaged reference laminate stiffness is denoted $[Q]_0^{LAM}$ and $[Q]^{LAM}$ respectively. The advantage of the assumed symmetry in the damaged state is in the feature that for symmetrical damaged laminate the A matrix represents the stiffness matrix $[Q]^{LAM}$ of the laminate.

When the two equal surface layers with index $i = 1$ and $N$ are damaged their effective stiffness is changing from $[\bar{Q}]_1 = [\bar{Q}]_N$ to $[\bar{Q}]_1^{eff}$.

According to CLT the damaged laminate extensional stiffness matrix of our symmetrical laminate can be written using the effective layer stiffness as

$$[Q]^{LAM} = \frac{t_1}{h}[\bar{Q}]_1^{eff} + \sum_{k=2}^{N-1}\frac{t_k}{h}[\bar{Q}]_k + \frac{t_1}{h}[\bar{Q}]_1^{eff} \quad (4)$$

The undamaged laminate stiffness matrix can be written in a similar form

$$[Q]_0^{LAM} = \frac{t_1}{h}[\bar{Q}]_1 + \sum_{k=2}^{N-1}\frac{t_k}{h}[\bar{Q}]_k + \frac{t_1}{h}[\bar{Q}]_1 \quad (5)$$

Subtracting (4) from (5) we obtain

$$[Q]_0^{LAM} - [Q]^{LAM} = 2\frac{t_1}{h}[\bar{Q}]_1 - 2\frac{t_1}{h}[\bar{Q}]_1^{eff} \quad (6)$$

From (6) the effective stiffness matrix of the damaged k-th layer in global coordinates is found

$$[\bar{Q}]_1^{eff} = [\bar{Q}]_1 - \frac{h}{2t_1}\{[Q]_0^{LAM} - [Q]^{LAM}\} \quad (7)$$

For the analyzed RVE of the cross-ply laminate shown in Fig.3

$$h = 2t_{90} + 2t_0 \quad (8)$$

and $$[\bar{Q}]_{90}^{eff} = [\bar{Q}]_{90} - \frac{h}{2t_{90}}\{[Q]_0^{LAM} - [Q]^{LAM}\} \quad (9)$$

Equation (7) can be transformed to the local coordinate system using expression

$$[Q]_1^{eff} = [T][\bar{Q}]_1^{eff}[T]^T \quad (10)$$

Then the effective compliance matrix of the damaged layer in local axes can be calculated

$$[S]_1^{eff} = \left([Q]_1^{eff}\right)^{-1} \quad (11)$$

From (11) the effective engineering constants of the damaged layer are

$$E_L^{eff} = 1/S_{11}^{eff} \quad , \quad E_T^{eff} = 1/S_{22}^{eff} \quad , \quad \nu_{LT}^{eff} = -E_L^{eff} S_{12}^{eff} \quad , \quad G_{LT}^{eff} = 1/S_{66}^{eff} \quad (12)$$

Parametric analysis for large number of material systems and laminate lay-ups has shown [29] that only the effective transverse modulus $E_T^{eff}$ and the shear modulus $G_{LT}^{eff}$ of the layer are reduced due to intralaminar cracks. The longitudinal modulus $E_L^{eff}$ and $\nu_{LT}^{eff}$ are not changing at all.

# 5. In-plane stiffness of the damaged laminate

## 5.1 FEM RVE model

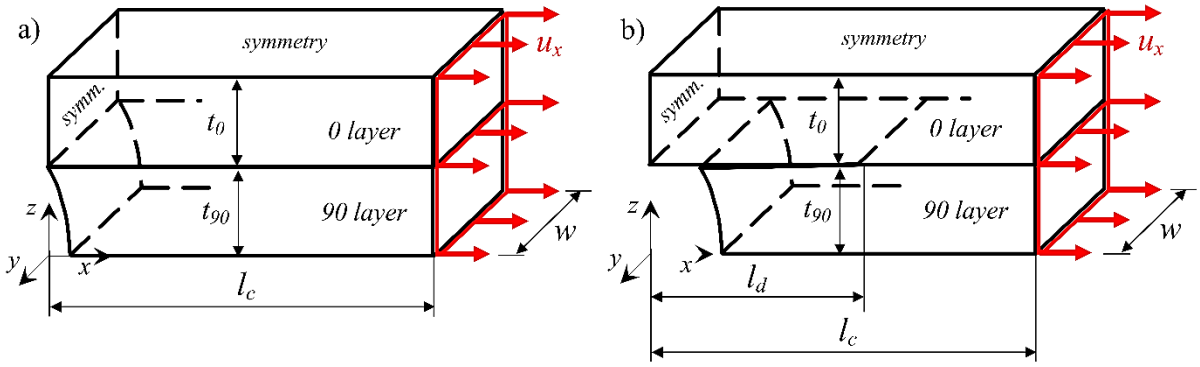



***Figure 3: Representative volume elements (RVE): a) case with transverse crack; b) case with transverse crack and delamination.***

The stiffness matrix of the damaged laminate $[Q]^{LAM}$ is required in order to calculate using (7)-(12) the effective stiffness for the damaged layer. The laminate stiffness matrix $[Q]^{LAM}$ has to be calculated for every crack density value. The used FEM models of the RVE are schematically shown in **Figure 3a** and **b** for cases without and with delaminations respectively. The delaminations (interface cracks) are assumed to grow in both directions from the tip of the intralaminar crack being symmetrical with respect to the crack plane. The 3-D FEM models were generated using FEM software ANSYS [30]. Taking advantage of the symmetry

conditions, the FEM models in **Figure 3** consist of a 90 degree layer of thickness $t_{90}$ and a 0 degree layer of thickness $t_0$ the length of the model is $l_c$, which is the half distance between two transverse cracks in the 90 layer. Thus, parameter $l_c$ defines the crack density ($\rho_c = 1/2l_c$) and was parametrically varied to calculate $[Q]^{LAM}$ for different crack densities. In addition to varying crack density $\rho_c$, for FEM RVE model shown in **Figure 3b** the delamination length $l_d$ was parametrically varied. The width of the FEM model of RVE was in all calculations equal to $w = 0.2 \cdot h$ where $h$ is the total thickness of the laminate. On the top surface of the FEM models ($z = t_0 + t_{90}$) symmetry boundary conditions were used. At $x = 0$, symmetry boundary conditions were applied on the 0 degree layer, while the surface of the 90 degree layer is free representing the transverse crack surface. At $x = l_c$ a uniform displacement in the x axis direction was applied. Separately on each side edge of the model ($y = 0$ and $y = -w$) displacement coupling in the y axis direction was used. With these boundary conditions the stress state does not depend on the y-coordinate.

The elastic modulus $E_x^{LAM}$ and Poisson's ratio $\nu_{xy}^{LAM}$ of the damaged laminate were calculated from post-processing in ANSYS [30] using reaction forces and resulting displacements. The transverse modulus $E_y^{LAM}$ of the damaged laminate was found using the FEM models with the same geometry as in **Figure 3a** and **b** but with different boundary conditions: uniform displacement was applied in the positive $y$ axis direction, symmetry boundary conditions were applied on nodes at $y = -w$, displacement coupling in $x$ axis direction was applied on the nodes with coordinates $x = l_c$.

## 5.2 GLOB-LOC model for cross-ply laminates with cracks in surface 90-layers

The GLOB-LOC model [21] in case of symmetric and balanced laminates with cracks and delaminations in surface 90-layers leads to exact closed form expressions [27]

$$\frac{E_x^{LAM}}{E_{x0}^{LAM}} = \frac{1}{1+2\rho_c t_{90}\frac{t_{90}}{h_0}u_{2an}c_2} \quad \frac{E_y^{LAM}}{E_{y0}^{LAM}} = \frac{1}{1+2\rho_c t_{90}\frac{t_{90}}{h_0}u_{2an}c_4} \tag{13}$$

$$\frac{\nu_{xy}^{LAM}}{\nu_{xy0}^{LAM}} = \frac{1+2\rho_c t_{90}\frac{t_{90}}{h_0}u_{2an}c_1\left(1-\frac{\nu_{LT}}{\nu_{yx0}^{LAM}}\right)}{1+2\rho_c t_{90}\frac{t_{90}}{h_0}u_{2an}c_2} \quad , \quad c_1 = \frac{E_T}{E_{x0}^{LAM}}\frac{1-\nu_{LT}\nu_{xy0}^{LAM}}{(1-\nu_{LT}\nu_{TL})^2} \tag{14}$$

$$c_2 = c_1\left(1-\nu_{LT}\nu_{xy0}^{LAM}\right) \qquad c_4 = \frac{E_T}{E_{yo}^{LAM}}\frac{\left(\nu_{LT}-\nu_{yx0}^{LAM}\right)^2}{(1-\nu_{LT}\nu_{TL})^2} \tag{15}$$

Notation $h_0$ is used for the half thickness of the laminate, in the considered cross-ply case $h_0 = t_{90} + t_0$. Quantities with index "LAM" are laminate constants, quantities with additional lower index 0 are undamaged laminate constants.

Since for the following bending analysis of cross-ply laminates the in-plane shear modulus of the layer is not relevant its degradation is not discussed in this paper.

The only remaining unknown entity in (13)-(15) is the average normalized crack opening displacement $u_{2an}$ . The value of $u_{2an}$ strongly depends on the delamination length $l_d$ and this is how delaminations affect the laminate stiffness. At low crack density intralaminar cracks in absence of delaminations are considered as non-interactive (the stress perturbation zones do not interact) and $u_{2an} = u_{2an}^0$ does not depend on crack density $\rho_c$.

In this paper the $u_{2an}^0$ was calculated using the FEM model shown in **Figure 3a**. As an alternative, analytical expressions for COD (power function from fitting FEM results [21], from average stress in analytical models [28]) could be used. When the crack density is high and there are no delaminations, the $u_{2an}$ depends on crack density [27] and COD of non-interactive cracks, $u_{2an}^0$ by relationship

$$u_{2an} = \lambda(\rho_c) u_{2an}^0 \tag{16}$$

The crack interaction function $\lambda$ is a function of the crack density in the layer. For non-interactive cracks $\lambda = 1$. Detailed analysis of the effect of different parameters on interaction function was performed in [26, 27] using FEM and the following empirical relationship was obtained

$$\lambda = tanh\left(\frac{k}{\rho_n}\right) \tag{17}$$

In (17) $\rho_n = t_{90}\rho_c$ is normalized crack density and

$$k^2 = 0.085 \frac{G_{23}t_0 + t_{90}G_{xz}^s}{G_{23}(t_0 + t_{90})}\left(1 + \frac{t_{90}E_T}{E_x^s t_0}\right) \tag{18}$$

In (18) $G_{23}$ and $E_T$ are elastic constants of the 90-layer, $t_0 = h_0 - t_{90}$ , $E_x^s, G_{xz}^s$ are averaged elastic constants of a sublaminate consisting of all layers except the damaged 90-layer. The interaction function (17), (18) gives a good approximation for $u_{2an}$ if $u_{2an}^0$ is calculated using FEM and not when using approximate expressions.

Expressions for $u_{2an}$ , similar to (16)-(18) do not exist for cracks with delaminations. Therefore, the COD values for all used combinations of crack density and local delamination length were calculated using FEM model shown in Figure.3b.

# 6. FEM simulation of 4-point bending test for cross-ply laminate

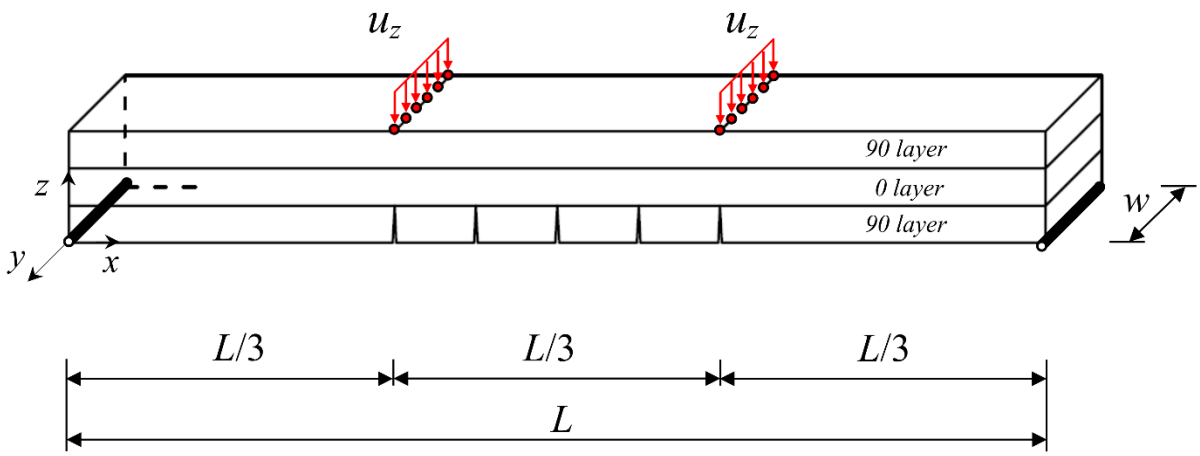



**Figure 4: Schematic representation of 4-point bending FEM model.** ***(For interpretation of the references to colour in this figure legend, the reader is referred to the web version of this article.)***

3-D FEM model schematically shown in **Figure 4** was generated using finite element software ANSYS [30]. The model consists of 3 layers representing the given cross-ply lay-ups $[90_m/0_n]_s$. The total length of the laminate $L$ was 150 mm with the equal distance of 50 mm between the loading points. The width of the laminate beam was 0.8 mm. The laminate was subjected to 4-point bending loading scheme by applying constant displacement $u_z = -3mm$ on the top surface points. Simple supports were added: the nodes corresponding to coordinates $x = 0$, $z = 0$ were constrained against displacement in x and z axis directions; the node at coordinate $x = 0$, $z = 0$, $y = -0.5.w$ was additionally constrained against displacement in the y axis direction; the nodes corresponding to coordinates $x = L$, $z = 0$, were constrained against displacement in the z axis direction and the node corresponding to coordinate $x = L$, $z = 0$ $y = -0.5.w$ was additionally constrained against displacement in y axis direction. Displacement coupling in the y axis direction was applied on the nodes of each edge of the laminate $(y = 0, y = -w)$. These constraints lead to the stress state described in Section 3.

The top 90-layer and the 0-layer were modelled without discontinuities (undamaged). In the bottom 90-layer discontinuities in form of transverse cracks where introduced only in the maximum bending moment zone, i.e., in the region between the displacement application points as shown in **Figure 4**. The number of transverse cracks was parametrically varied from 0 to 33 uniformly spaced cracks leading to reduction of the laminate bending stiffness.

Apart from transverse cracks the effect of delaminations at transverse crack tip on laminate bending stiffness was also investigated. Delamination cracks were introduced between the damaged 90 degree layer and 0 degree layer as shown schematically in **Figure 5**.

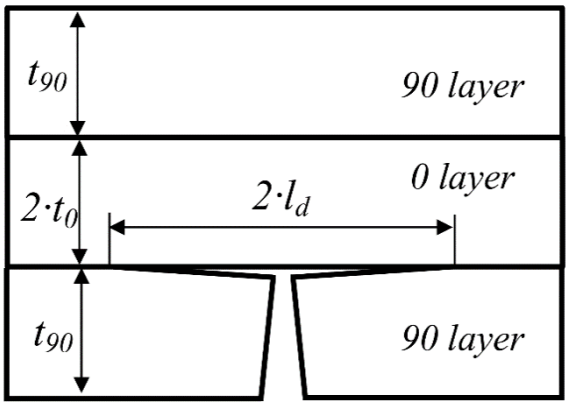



***Figure 5: Schematic representation of delamination crack with total length*** $2l_d$

Delaminations were assumed to be symmetrical with respect to the transverse crack plane. The delamination length $l_d$ was parametrically varied from 0 to $0.5t_{90}$. The bending stiffness parameter was calculated using expression (3) where the bending moment $M_x$ was calculated from the reaction forces and the curvature $k_x$ was calculated from mid-plane displacements $u_z$ in the constant bending moment zone (between the load application points), assuming that the deformed shape follows parabolic line.

# 7. Results and discussion

Carbon fiber/epoxy (denoted CF/EP) and glass fiber/epoxy (GF/EP) laminates with layups $[90/0_2]_s$ , $[90/0]_s$ and $[90_2/0_2]_s$ were studied in this paper. The UD elastic properties of materials are presented in Table 1. The ply thickness was 0.6 mm, the respective 90-layer thickness $t_{90}$ was 0.6 and 1.2 mm.

| Property | $E_1$ | $E_2$ | $\nu_{12}$ | $G_{12}$ | $\nu_{23}$ |
|---|---|---|---|---|---|
| Unit | [GPa] | [GPa] | [-] | [GPa] | [GPa] |
| CF/EP | 104.00 | 6.14 | 0.40 | 5.00 | 0.45 |
| GF/EP | 45.00 | 15.00 | 0.30 | 5.00 | 0.40 |

***Table 1. Elastic constants of UD composites.***

The effective transverse modulus of the damaged 90-layer at different crack densities (no delaminations) calculated using the FEM RVE model (**Figure 3a**) and GLOB-LOC approach

(COD for non-interactive cracks from FEM and expression (16) for interactive cracks) for CF/EP [90/$0_2$] are shown in Figure 6a. The values obtained with the two methods at all crack densities are almost coinciding. As expected only the transverse effective modulus $E_T^{eff}$ of the damaged layer changed with the crack density, while the longitudinal effective modulus $E_L^{eff}$ and the Poisson's ratio $\nu_{LT}^{eff}$ remained unchanged. In **Figure 6a** and in the following figures the CLT results in conjunction with FEM RVE model are denoted as "Eeff-FEM" and the CLT results in conjunction with GLOB-LOC model are denoted as "GLOB-LOC".

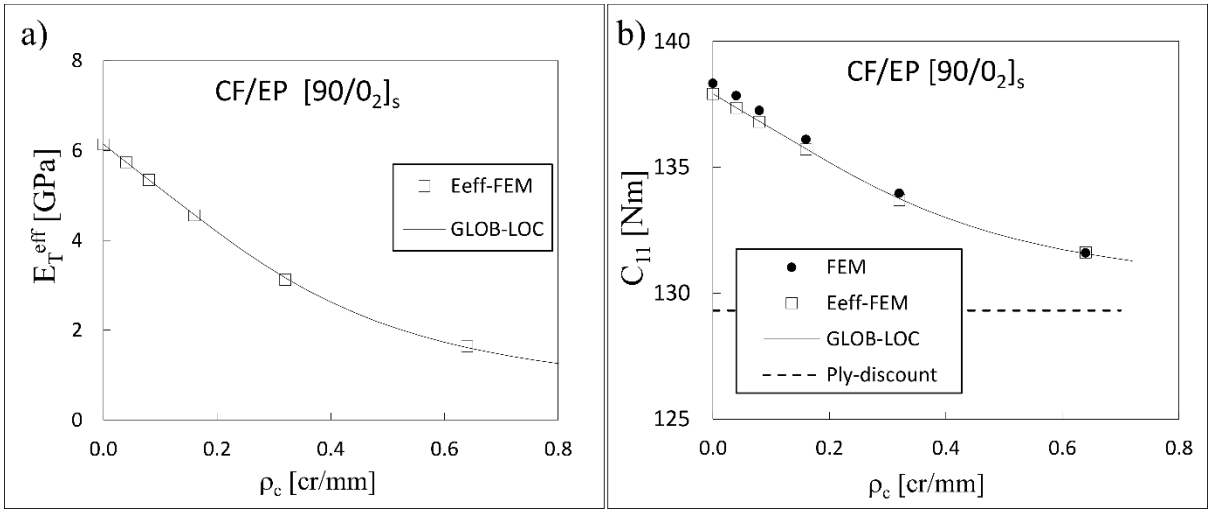



***Figure 6: Simulations for CF/EP [90/$0_2$]$_s$ laminate: a) effective stiffness of damaged 90-layer; b) bending stiffness.***

In **Figure 6b** bending stiffness parameter $C_{11}$ is plotted for CF/EP with lay-up [90/$0_2$]$_s$. In **Figure 6b** and in the following figures the results obtained from 3-D FEM simulations of 4-point bending test are denoted as "FEM", "Eeff-FEM" and "GLOB-LOC" values are obtained first calculating *A*, *B* and *D* matrices using effective stiffness and using expressions in Sections 3 and 4. Notation "Ply-discount" corresponds to ply-discount model, where zero transverse modulus of a damaged layer was assumed.

The dependence of some elements of *A*, *B* and *D* matrices on crack density $\rho_c$ (no delaminations) is shown in **Table 2** Values obtained from back-calculation using RVE and GLOB-LOC (in brackets) models are compared in Table 2 showing very small differences.

| $\rho_c$ [cr/mm] | $A_{11}$ [N/m] | $A_{12}$ [N/m] | $B_{11}$ [N] | $B_{12}$ [N] | $D_{11}$ [N·m] |
|---|---|---|---|---|---|
| 0.00 | $2.594\cdot10^8$ ($2.594\cdot10^8$) | $8.926\cdot10^6$ ($8.926\cdot10^6$) | 0.000 (0.000) | 0.000 (0.000) | $1.379\cdot10^2$ ($1.379\cdot10^2$) |
| 0.04 | $2.592\cdot10^8$ ($2.593\cdot10^8$) | $8.828\cdot10^6$ ($8.830\cdot10^6$) | $-3.655\cdot10^2$ ($-3.617\cdot10^2$) | $-1.462\cdot10^2$ ($-1.447\cdot10^2$) | $1.374\cdot10^2$ ($1.374\cdot10^2$) |
| 0.08 | $2.589\cdot10^8$ ($2.589\cdot10^8$) | $8.732\cdot10^6$ ($8.734\cdot10^6$) | $-7.286\cdot10^2$ ($-7.217\cdot10^2$) | $-2.915\cdot10^2$ ($-2.887\cdot10^2$) | $1.368\cdot10^2$ ($1.368\cdot10^2$) |
| 0.16 | $2.585\cdot10^8$ ($2.585\cdot10^8$) | $8.539\cdot10^6$ ($8.543\cdot10^6$) | $-1.450\cdot10^3$ ($-1.435\cdot10^3$) | $-5.800\cdot10^2$ ($-5.740\cdot10^2$) | $1.357\cdot10^2$ ($1.357\cdot10^2$) |
| 0.32 | $2.576\cdot10^8$ ($2.576\cdot10^8$) | $8.191\cdot10^6$ ($8.202\cdot10^6$) | $-2.756\cdot10^3$ ($-2.714\cdot10^3$) | $-1.103\cdot10^3$ ($-1.086\cdot10^3$) | $1.337\cdot10^2$ ($1.338\cdot10^2$) |
| 0.64 | $2.567\cdot10^8$ ($2.567\cdot10^8$) | $7.833\cdot10^6$ ($7.827\cdot10^6$) | $-4.098\cdot10^3$ ($-4.123\cdot10^3$) | $-1.639\cdot10^3$ ($-1.649\cdot10^3$) | $1.317\cdot10^2$ ($1.316\cdot10^2$) |

***Table 2. A, B, D matrix elements as a function of crack density, back-calculated using RVE and GLOB-LOC (shown in brackets) models.***

In **Figures 7a** and **b** the bending stiffness as a function of crack density $\rho_c$ is plotted for CF/EP lay-up $[90_2/0_2]_s$ and for GF/EP layup $[90/0]_s$ respectively. From **Figures 6** and **7** it can be seen that all models are in very good agreement in the whole range of studied crack densities $\rho_c$. Agreement is excellent for CF/EP laminate with relatively thin damaged surface layer (**Figure 6b**). For laminates with relatively thicker 90-layer shown in **Figure 7** the models based on CLT and effective stiffness slightly overestimate the bending stiffness obtained from 3-D FEM simulations of a bending test. Better agreement for laminates with thinner surface layer (see **Figure 6**) may be because in this case the axial stress distribution across the ply thickness is more uniform and the COD in bending better corresponds to COD in the tensile calculation case used to determine effective constants of the damaged layer.

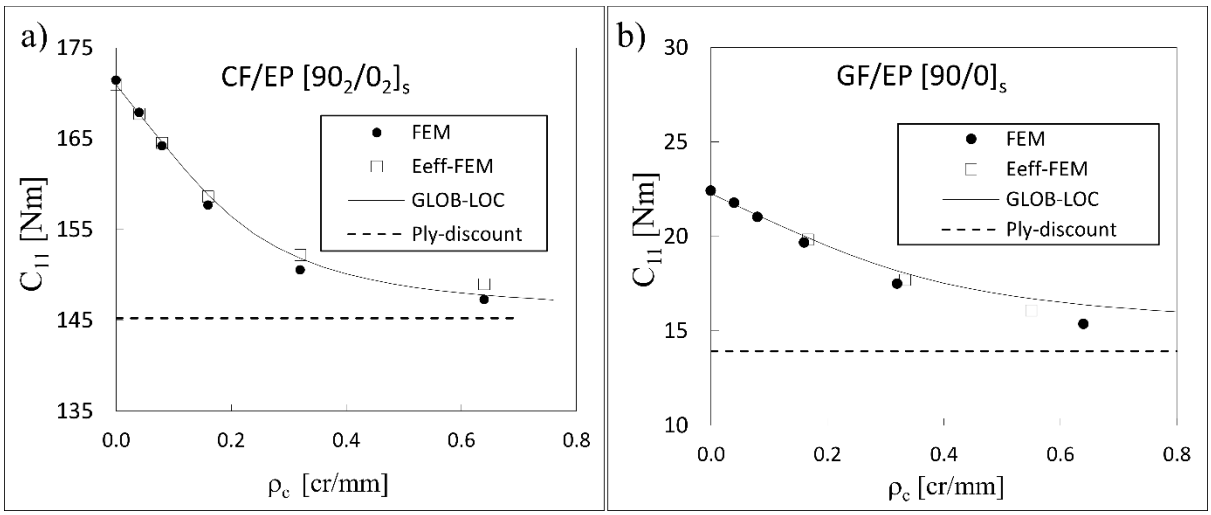



***Figure 7: Bending stiffness of CF/EP and GF/EP cross-ply laminates according to different models.***

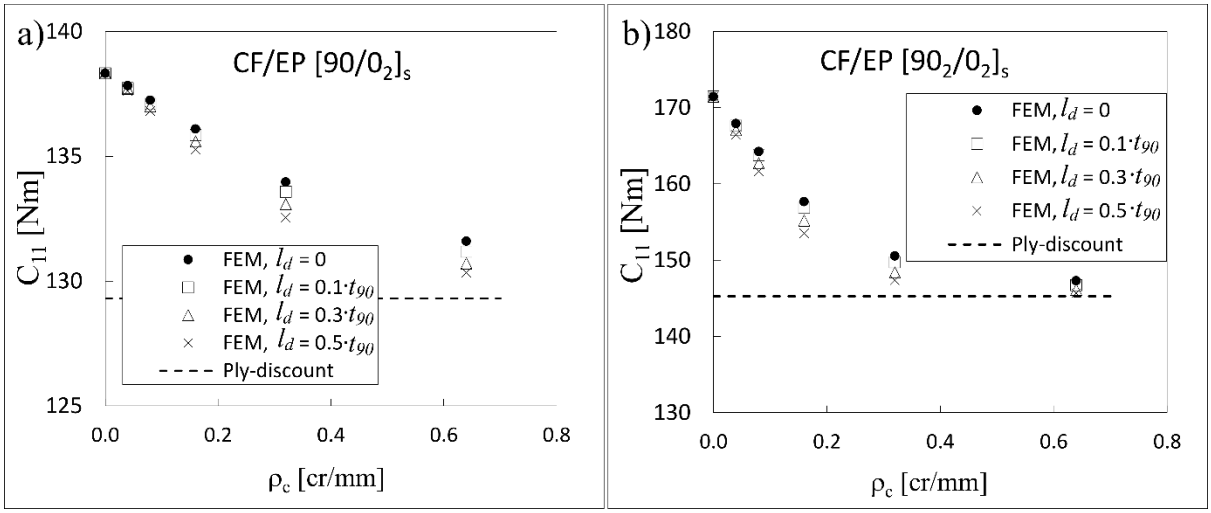



***Figure 8: Delamination effect on bending stiffness of CF/EP laminates with cracks in 90-layer.***

In **Figures 8a** and **b** the influence of delaminations on bending stiffness reduction for CF/EP layups $[90/0_2]_s$ and $[90_2/0_2]_s$ respectively is shown. Results are obtained simulating the 4-point bending test using FEM (**Figures 4** and **5**). As the results in **Figure 8** show the bending resistance of the laminate with cracks is additionally reduced by the presence of delaminations initiating from transverse cracks. As expected, the reduction is larger due to longer delaminations. In the analyzed range the effect of the delamination seems to be relatively smaller (comparing to the cracking effect) for laminates with a relatively thick cracked layer (**Figure 8b**). In all cases the bending stiffness approaches the ply-discount value at high crack density.

Finally, **Figures 9a** and **b** show an excellent agreement between 3-D FEM simulations of a bending test and the CLT results with effective stiffness for the cases of CF/EP $[90,0_2]_s$ laminate with cracks in the bottom 90-layer and with fixed delamination lengths, $l_d = 0.1 \cdot t_{90}$ and $l_d = 0.7 \cdot t_{90}$ respectively. The "Eeff-FEM" values were obtained in conjunction with FEM RVE model shown in **Figure 3b**. The "GLOB-LOC" values were obtained in conjunction with methodology described in Section 5.2.

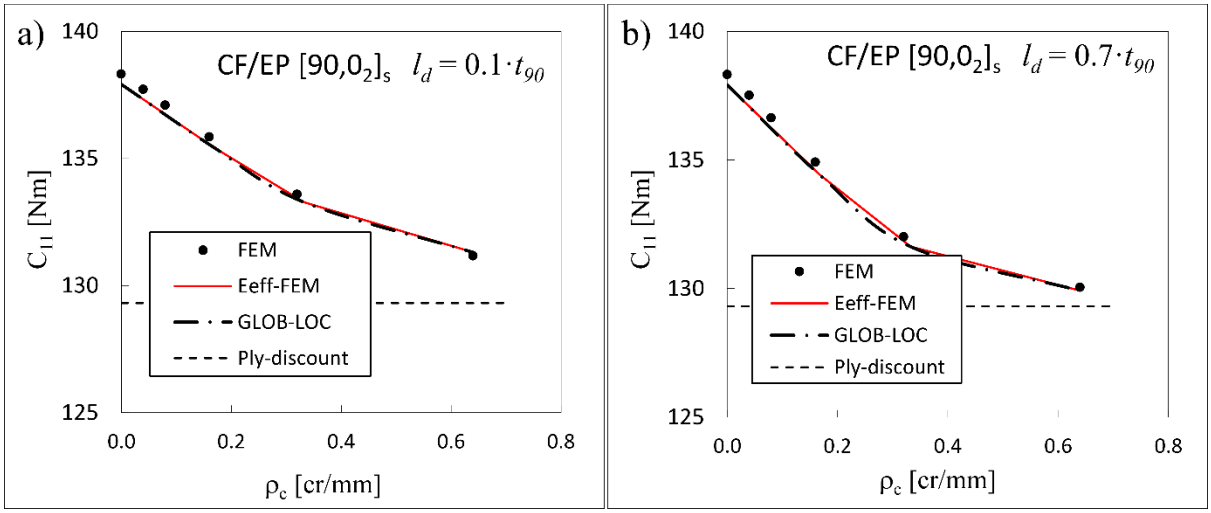



***Figure 9: The effect of delaminations on bending stiffness of CF/EP laminates. Comparison between direct 3-D FEM simulation results and models based on effective stiffness.*** ***(For interpretation of the references to colour in this figure legend, the reader is referred to the web version of this article.)***

# 8. Conclusions

An approach based on effective stiffness of the damaged layer used in the framework of the classical laminate theory (CLT) is suggested to calculate the bending stiffness and coupling stiffness matrices of laminate with intralaminar cracks in surface 90-layers and local delaminations. In this approach the layer with transverse cracks and possibly with interlayer delaminations starting from the crack tip is replaced with undamaged layer with effective stiffness of the damaged layer. The effective stiffness is defined as stiffness which gives the same laminate stiffness as calculations with explicit consideration of each crack.

The effective stiffness is back-calculated by comparing the in-plane stiffness of a symmetric reference cross-ply laminate with and without damage. The effective layer stiffness is used in CLT to calculate A, B and D matrices of laminates with unsymmetrical damage state.

The damaged laminate stiffness was obtained by two methods: 1) using FEM model of representative volume element (RVE) of the laminate between two cracks with or without local delaminations; 2) using the earlier developed analytical GLOB-LOC approach which is exact but the used input values for crack opening displacement (COD) at high crack density in the case without delaminations are approximate. For cracks with delaminations COD was calculated using FEM.

The accuracy of the effective stiffness approach in bending was validated comparing with 3-D FEM simulation of 4-point bending test for laminate with intralaminar cracks and delaminations in tensile surface layer. The effective stiffness approach with effective stiffness from the FEM or GLOB-LOC based calculations gives sufficient accuracy for damaged laminate bending response.

Significant effect of local delamination on bending was found simulating 4-point bending test and confirmed by effective stiffness approach.

# References

[1] Kuriakose S, Talreja R, Variational solutions to stresses in cracked cross-ply laminates under bending,
International Journal of Solids and Structures, Vol. 41(9-10), 2004, pp. 2331-2347

[2] Talreja R. Damage characterization by internal variables. In: Byron Pipes R, Talreja R, editors. Composite

[3] Nairn J, Hu S. Matrix microcracking . In: Byron Pipes R, Talreja R, editors. Composite Material Series, Vol. 9., Damage Mechanics of Composite Materials. Amsterdam: Elsevier, 1994. p. 187-243.

[4] Berthelot JM. Transverse Cracking and Delamination in Cross-ply Glass-fiber and Carbon-fiber Reinforced Plastic Laminates: Static and Fatigue Loading. Appl Mech Rev 2003;56(1):111-147.

[5] Smith PA, Wood JR. Poisson's ratio as a damage parameter in the static tensile loading of simple cross-ply laminates. Compos Sci Tech 1990;38:85-93.

[6] Hashin Z. Analysis of cracked laminates: a variational approach. Mech Mater 1985;4:121-136.

[7] Varna J, Berglund LA. Thermo-Elastic Properties of Composite Laminates with transverse cracks. J Compos Tech Res 1994;16:77-87.

[8] Krasnikovs A, Varna J. Transverse Cracks in Cross-ply Laminates. Part 1. Stress Analysis. Mech Compos Mater 1997;33(6):565-582.

[9] McCartney LN, Schoeppner GA, Becker W. Comparison of models for transverse ply cracks in composite laminates. Compos Sci Tech 2000;60:2347-2359.

[10] Smith PA, Ogin SL. Characterization and Modelling of Matrix Cracking in a (0/90)2s GFRP Laminate Loaded in Flexure. Proc Math Phys Eng Sci 2000;456:2755-2770.

[11] Smith PA, Ogin SL. On transverse matrix cracking in cross-ply laminates loaded in simple bending, Compos Appl Sci Manuf 1999;30:1003-1008.

[12] Hajikazemi M, Sadr M.H, Talreja R, Variational analysis of cracked general cross-ply laminates under bending and biaxial extension, International Journal of Damage Mechanics, Vol. 24(4), 2015, pp. 582-624

[13] McCartney L.N. and Pierse C., Stress transfer mechanics for multiple ply laminates for axial loading and bending, Proc 11th Int. Conf. on Composite Materials, 1997, vol. V, pp. 662-671

[14] McCartney L.N., Stress transfer mechanics for multiple ply cross-ply laminates subjected to bending. Summary in Proceedings of 6th International Conference on Deformation and Fracture of Composites, Manchester, April 2001, pp. 57-66.

[15] Adumitroaie A, Barbero E.J, Intralaminar Damage Model for Laminates Subjected to Membrane and Flexural Deformations, Mechanics of Advanced Materials and Structures, Vol. 22(9), 2015, pp. 705-716

[16] McCartney L.N , Energy methods for modeling damage in laminates, Journal of Composite Materials, 47(20-21), 2613-2640.

[17] McCartney L.N., Physically based damage models for laminated composites, Proc. Instn. Mech. Engrs, Vol. 217, Part L: J. Materials, Design and Applications, 163-169.

[18] E. Adolfsson and P. Gudmundson, Thermoelastic properties in combined bending and extension of thin composite laminates with transverse matrix cracks, Int. J. Solids Struct., vol. 34, no. 16, pp.2035–2060, 1997.

[19] Farge L, Varna J, Ayadi Z. Use of full-field measurements to evaluate analytical models for laminates with intralaminar cracks. J Compos Mater 2012;46(21): 2739-2752.

[20] Zhang J, Fan J, Soutis C. Analysis of multiple matrix cracking in [±θm/90n]s composite laminates. Part 1. In-plane stiffness properties. Composites 1992;23:291-304.

[21] Varna J. Modeling Mechanical Performance of Damaged Laminates, J Compos Mater 2013;47(20-21): 2443-2474.

[22] Varna J, Berglund LA, Talreja R, Jakovics A. A study of the crack opening displacement of transverse cracks in cross ply laminates. Int J Dam Mech 1993;2:272-289.

[23] Loukil MS, Varna J, Ayadi Z. Damage characterization in glass fiber/epoxy laminates using Electronic Speckle Pattern Interferometry. Exp Tech 2015; 39(2):38-45.

[24] Lundmark P, Varna J. Constitutive Relationships for Laminates with Ply Cracks in In-plane Loading. Int J Dam Mech 2005;14(3):235-261.

[25] Lundmark P, Varna J. Crack face sliding effect on stiffness of laminates with ply cracks. Compos Sci Tech 2006;66:1444-1454.

[26] Lundmark P, Varna J. Stiffness reduction in laminates at high intralaminar crack density: effect of crack interaction. Int J Dam Mech 2011;20:279-297.

[27] Loukil MS, Varna J, Ayadi Z. Engineering expressions for thermo-elastic constants of laminates with high density of transverse cracks. Compos Appl Sci Manuf 2013;48(1):37-46.

[28] Varna J, Strategies for stiffness analysis of laminates with microdamage: combining average stress and crack face displacement based methods, J Appl Math Mech Z Angew Math Mech 2015;1–17, In press, DOI 10.1002/zamm.201400296

[29] Varna J. On effective properties of layers in damaged composite laminates. Key Engineering Materials 2012;488-489:490-493.

[30] ANSYS Release 13.0. Canonsburg, PA: ANSYS Academic Research. ANSYS Inc. 2011.